A Machine Learning-Based Approach for Lifting Load Estimation

by

Yuting Ma

A dissertation submitted to the Graduate Faculty of
Auburn University
in partial fulfillment of the
requirements for the Degree of
Doctor of Philosophy

Auburn, Alabama
August 3, 2024

Keywords: Machine Learning, Transformer, BiLSTM, Time-Series, Kinematics, Lifting Weight, IMUs, Cameras

Approved by

Sean Gallagher, Chair, Hal N. and Peggy S. Pennington Professor, Industrial and Systems Engineering
Elvan Ceyhan, Professor, Mathematics and Statistics
Jia (Peter) Liu, Associate Professor, Industrial and Systems Engineering
Konstantinos Mykoniatis, Assistant Professor, Industrial and Systems Engineering
Howard Chen, Assistant Professor, Industrial and Systems Engineering at University of Alabama in Huntsville

Abstract

Lifting weight estimation has gained attention in recent years due to its potential applications in ergonomics, human-robot collaboration systems, and wearable devices. The primary objective of this dissertation was to develop a machine learning based method that can recognize different levels of lifting weight without prior knowledge or measurement of the weight. This research investigated the effects of lifting weights on the upper-body joint kinematics and shoulder-elbow coordination. The results showed that lifting weight level had statistically significant effects on upper extremity kinematics such as velocities and shoulder-elbow coordination.

Building on these results and findings from previous studies, a BiLSTM-Transformer Encoder model was developed using lifting kinematics as input features for lifting weight recognition. This model demonstrated improvements over existing multi-level lifting weight recognition models. Furthermore, with feature importance analysis, we found that the model was able to focus on different features during different phases of the lifting process, highlighting its nuanced understanding of the lifting biomechanics involved.

Further, the dissertation explores the application of the developed model to video data for lifting weight recognition. This approach demonstrated reasonable results in multi-level lifting weight recognition using video footage.

This research demonstrated the potential for improved accuracy in lifting weight recognition tasks. The methods and models developed in this research have promising applications in various areas. The proposed method and findings in this research pave the way for future innovations and developments in lifting weight recognition tasks.

Acknowledgments

I would like to express my deepest gratitude to my advisor, Dr. Sean Gallagher, for his unwavering support, guidance, and invaluable insights throughout the course of my doctoral research. His encouragement and expertise have been instrumental in the completion of this dissertation. I am also grateful to the rest of my dissertation committee, Dr. Howard Chen, Dr. Jia (Peter) Liu, Dr. Konstantinos Mykoniatis, and Dr. Elvan Ceyhan for their insightful feedback and commitment to my academic development.

To my family, words cannot express how grateful I am for your love, patience, and sacrifices. I must thank my parents who have shaped me into the person I am. From a young age my parents taught me the importance of perseverance. Through their own lives, I have witnessed firsthand the power of determination and resilience. To my husband, Kenneth, thank you for believing in me and encouraging me to pursue my dreams.

I acknowledge the funding support from Deep South Center for Occupational Health and Safety PPRT, which made this research possible.

Thank you all for being a part of this journey. This accomplishment would not have been possible without you.

Table of Contents

List of Figures

List of Tables

List of Abbreviations

AI	Artificial Intelligence
BiLSTM	Bidirectional Long Short-Term Memory Network
BLS	Bureau of Labor Statistics
CLN	Convolutional LSTM
CMCs	Coefficient of Multiple Correlations
CNN	Convolutional Neural Network
CPM	Convolutional Pose Machine
CRP	Continuous Relative Phase
CV	Coefficient of Variation
DAFW	Days Away from Work
DNN	Deep Neural Network
DP	Deviation Phase
EAWS	Ergonomic Assessment Worksheet
FNN	Feedforward Neural Network
HAL	Hand Activity Level
HMM	Hidden Markov Model
IG	Integrated Gradients
KNN	K-Nearest Neighbor
LI	Lifting Index
LiFFT	Lifting Fatigue Failure Tool
LSTM	Long Short-Term Memory Network

MARP	Mean Absolute Value of the Ensemble CRP Curve Values
MHT	Maximum Holding Time
MLC	Maximum Lifting Capacity
ML	Machine Learning
MSD	Musculoskeletal Disorder
NIOSH	National Institute for Occupational Safety and Health
OMC	Optical Motion Capture
OWAS	Ovako Working Posture Analysis System
REBA	Rapid Entire Body Assessment
ResNet	Residual Neural Network
RMSE	Root-Mean-Square Error
RNN	Recurrent Neural Network
RULA	Rapid Upper Limb Assessment
RWL	Recommended Weight Limit
SD	Standard Deviation
sEMG	Surface Electromyography
SVM	Support Vector Machine
ToF	Time-of-Flight

Chapter 1

Introduction

While Industry 4.0 has created opportunities for automation and robotization, some manufacturing contexts continue to rely heavily on a human workforce. Assembly lines, known for their intricate nature encompassing multifaceted products comprising hundreds of components and including assembly and handling tasks, necessitate an exceptional degree of adaptability that remains beyond the current capabilities of robots. Tasks and activities that involve navigating complex spaces and performing sophisticated motor skills continue to be carried out manually in logistics. Moreover, humans have cognitive abilities that are very challenging to imitate and replicate (Battini et al., 2022). In such settings, physical ergonomic risk factors can cause injuries like musculoskeletal disorders (MSDs). These factors include awkward working postures, overexertion including manual exertion related to handling objects, and exposure to repetitive motion.

Musculoskeletal disorders are injuries to the body's musculoskeletal system, including tendons, ligaments, muscles, nerves, and discs. MSDs would cause absenteeism and lost productivity and lead to increased health care, disability, and worker's compensation costs. Musculoskeletal injuries are the most common injury among all occupational diseases. According to the European Agency for Safety and Health at Work (EU-OSHA), more than 50% of the EU workforce reported MSDs in 2019 (EU-OSHA, 2019). In the U.S., as of 2018, there were 900,380 cases of days away from work (DAFW) in the private sector, with 30% being MSD cases (U.S. Bureau of Labor Statistics, 2020). Overexertion has been the leading cause of

nonfatal injury or illness involving days away from work. According to the 2021 Liberty Mutual Workplace Safety Index, overexertion related to handling objects continues to rank first among the leading causes of disabling injuries and costs the U.S. $13.3 billion dollars in direct costs(Liberty Mutual, 2021). Therefore, ergonomics is still one of the most important parts of engineering, especially in industrial settings. Findings of scientific research have shown strong associations between physical ergonomic risk factors and the development of MSDs. The measurement of workers' exposure to risk factors has been of vital importance. Subsequently, exposure assessment methods have been developed for physical factors that increase risk.

Traditional exposure assessment methods have been categorized as self-reports, observational methods, and direct measurements. Generally, self-reports from workers can be used to collect data on workplace exposure to physical factors by using worker diaries, interviews, and questionnaires (David, 2005). These methods are straightforward to use and appropriate for a large number of workers at a low cost, but the gathered information (e.g., pain, postural discomfort, and levels of subjective exertion) is imprecise and unreliable (David, 2005). Observational methods are based on direct observation of workers while performing tasks (Diego-Mas et al., 2017). They are usually easy to use and applicable to a wide variety of work situations at a low cost, however, may be subjected to observer biases and are more suitable for the assessment of static jobs (H. Chen, 2017). Direct methods rely on sensors attached directly to the worker for the measurement of exposure variables (Diego-Mas et al., 2017). Although these methods collect accurate data, they are invasive and not suited to be used in real work situations due to the potential for disruption (Diego-Mas et al., 2017).

The so-called 'automated ergonomics assessment system' takes advantage of the advancements in machine learning (ML) and device technologies to assess workplace exposures

to physical risk factors. Recently, the rapid development of machine learning technology has introduced a substantial impact on ergonomics research in manufacturing (S. Lee et al., 2021). Studies have been carried out to apply machine learning algorithms to automatically evaluate worker's posture or quantify the duration of work activity (Lamooki et al., 2022; Lin et al., 2022; Nath et al., 2018). Various machine learning methods, such as neural networks, random forest, and deep learning, have been utilized based on data from sensors and cameras to solve a broad range of ergonomics problems. By focusing on some devices that are commonly used in the manufacturing context, the inertial measurement units (IMUs) and cameras gain higher and higher attention to collect data from workers.

The goal of this research is to monitor external loading on hands by utilizing ML techniques based on data from IMUs and cameras in non-repetitive material handling work. The specific research objectives are to:

1) Investigate the effects of lifting weights on upper limb joint kinematics and shoulder-elbow coordination.
2) Develop a transformer-based model for lifting load recognition and evaluate the model.
3) Examine the potential use of cameras for lifting load recognition.

References

Battini, D., Berti, N., Finco, S., Guidolin, M., Reggiani, M., & Tagliapietra, L. (2022). WEM-Platform: A real-time platform for full-body ergonomic assessment and feedback in manufacturing and logistics systems. *Computers & Industrial Engineering*, *164*, 107881. https://doi.org/10.1016/j.cie.2021.107881

Chen, H. (2017). *The effects of movement speeds and magnetic disturbance on inertial measurement unit accuracy: The implications of sensor fusion algorithms in occupational ergonomics applications*. Iowa Research Online.

David, G. C. (2005). Ergonomic methods for assessing exposure to risk factors for work-related musculoskeletal disorders. *Occupational Medicine*, *55*(3), 190–199. https://doi.org/10.1093/occmed/kqi082

Diego-Mas, J.-A., Alcaide-Marzal, J., & Poveda-Bautista, R. (2017). Errors Using Observational Methods for Ergonomics Assessment in Real Practice. *Human Factors: The Journal of the Human Factors and Ergonomics Society*, *59*(8), 1173–1187. https://doi.org/10.1177/0018720817723496

EU-OSHA. (2019). *Work-related musculoskeletal disorders: Prevalence, costs and demographics in the EU European*. European Agency for Safety and Health at Work (EU-OSHA). https://osha.europa.eu/sites/default/files/Work-related_MSDs_prevalence_costs_and_demographics_in_the_EU_report.pdf

Lamooki, S. R., Hajifar, S., Kang, J., Sun, H., Megahed, F. M., & Cavuoto, L. A. (2022). A data analytic end-to-end framework for the automated quantification of ergonomic risk factors across multiple tasks using a single wearable sensor. *Applied Ergonomics*, *102*, 103732. https://doi.org/10.1016/j.apergo.2022.103732

Lee, S., Liu, L., Radwin, R., & Li, J. (2021). Machine Learning in Manufacturing Ergonomics: Recent Advances, Challenges, and Opportunities. *IEEE Robotics and Automation Letters*, *6*(3), 5745–5752. https://doi.org/10.1109/LRA.2021.3084881

Liberty Mutual. (2021). *Liberty Mutual Workplace Safety Index 2021*. https://business.libertymutual.com/wp-content/uploads/2021/06/2021_WSI_1000_R2.pdf

Lin, P.-C., Chen, Y.-J., Chen, W.-S., & Lee, Y.-J. (2022). Automatic real-time occupational posture evaluation and select corresponding ergonomic assessments. *Scientific Reports*, *12*(1), 2139. https://doi.org/10.1038/s41598-022-05812-9

Nath, N. D., Chaspari, T., & Behzadan, A. H. (2018). Automated ergonomic risk monitoring using body-mounted sensors and machine learning. *Advanced Engineering Informatics*, *38*, 514–526. https://doi.org/10.1016/j.aei.2018.08.020

U.S. Bureau of Labor Statistics. (2020, May 1). *Occupational injuries and illnesses resulting in musculoskeletal disorders (MSDs)*. https://www.bls.gov/iif/factsheets/msds.htm

Chapter 2

Literature Review

2.1 Introduction

The rapidly evolving sensor technologies and artificial intelligence (AI) has permeated numerous aspects of our lives, including workplace environments. One such application is automated ergonomics assessment, which utilizes AI-powered systems, particularly machine learning, to evaluate ergonomic risks. According to the U.S. Bureau of Labor Statistics (BLS), musculoskeletal disorder (MSD) cases accounted for approximately 30% of all reported work-related injuries and illnesses, and the incidence rate of MSD cases was 27.2 per 10,000 full-time workers (U.S. Bureau of Labor Statistics, 2020). Work-related MSDs occur across various industries, with a higher incidence in industries such as healthcare and social assistance, manufacturing, and retail trade (U.S. Bureau of Labor Statistics, 2020). Ergonomics assessment plays a crucial role in identifying and mitigating ergonomic risks in the workplace, ensuring the health and well-being of employees. Traditional ergonomic assessment methods often rely on manual observations and subjective assessments, which can be time-consuming, prone to bias, and limited in scope. Automated ergonomics assessment systems leverage machine learning algorithms and sensor technologies to overcome these limitations, providing objective and comprehensive analyses. In addition, these systems can evaluate and classify ergonomic risk exposure in real time. This allows for immediate feedback to employees and employers, facilitating timely interventions to improve ergonomic conditions. The rapid development in

wearable sensors, computer vision, machine learning and computing power provides solutions that enable automated ergonomic assessment with sufficient reliability and efficiency.

The paradigm shift towards automated ergonomic assessment has opened up a multitude of opportunities for innovative solutions to prevent work-related MSDs. However, these novel advancements have also brought forth new challenges that necessitate a comprehensive understanding of the current state of automated ergonomic assessment. This review seeks to shed light on recent developments, explore potential opportunities, and address the emerging challenges within the domain of automated ergonomic assessment.

2.2 Methods

2.2.1 Search Strategy

A literature review was conducted via Embase, Engineering Village and IEEE Xplore. A search was carried out for journal articles published from January 2007 through June 2022. Our search identified articles that focused on automated quantification of ergonomic risk factors and was limited to studies of ergonomic assessment. The search keywords used to identify studies on automated ergonomics assessment included [‘automat*’ or ‘real-time’] and [‘ergonomics’] and [‘assessment’ or ‘evaluation’ or ‘analysis’ or ‘quantif*’]. Any peer-reviewed journal articles, including the search keywords in the document title, abstract, or keywords, were selected. Only studies written in English were searched. The search process and exclusion criteria are summarized in Figure 2.1.

2.2.2 Exclusion Criteria

The initial search identified 623 studies based on title, abstract, and keyword, with 67 duplicates. After removing duplicates, the selected articles were screened and assessed based on the title abstract, and then the full text. Studies were excluded from further analysis if they: (1)

described a study on ergonomics design. For example, studies used automated ergonomic evaluation to quantify ergonomic comfort in aircraft cockpit design; or (2) focused on rehabilitation ergonomics. For example, studies investigating digital ergonomic evaluation of exoskeleton for upper-limb rehabilitation; or (3) focused on autonomous vehicle ergonomics assessment. For example, studies investigating automated ergonomic evaluation of driver's postures in autonomous and semiautonomous vehicles.

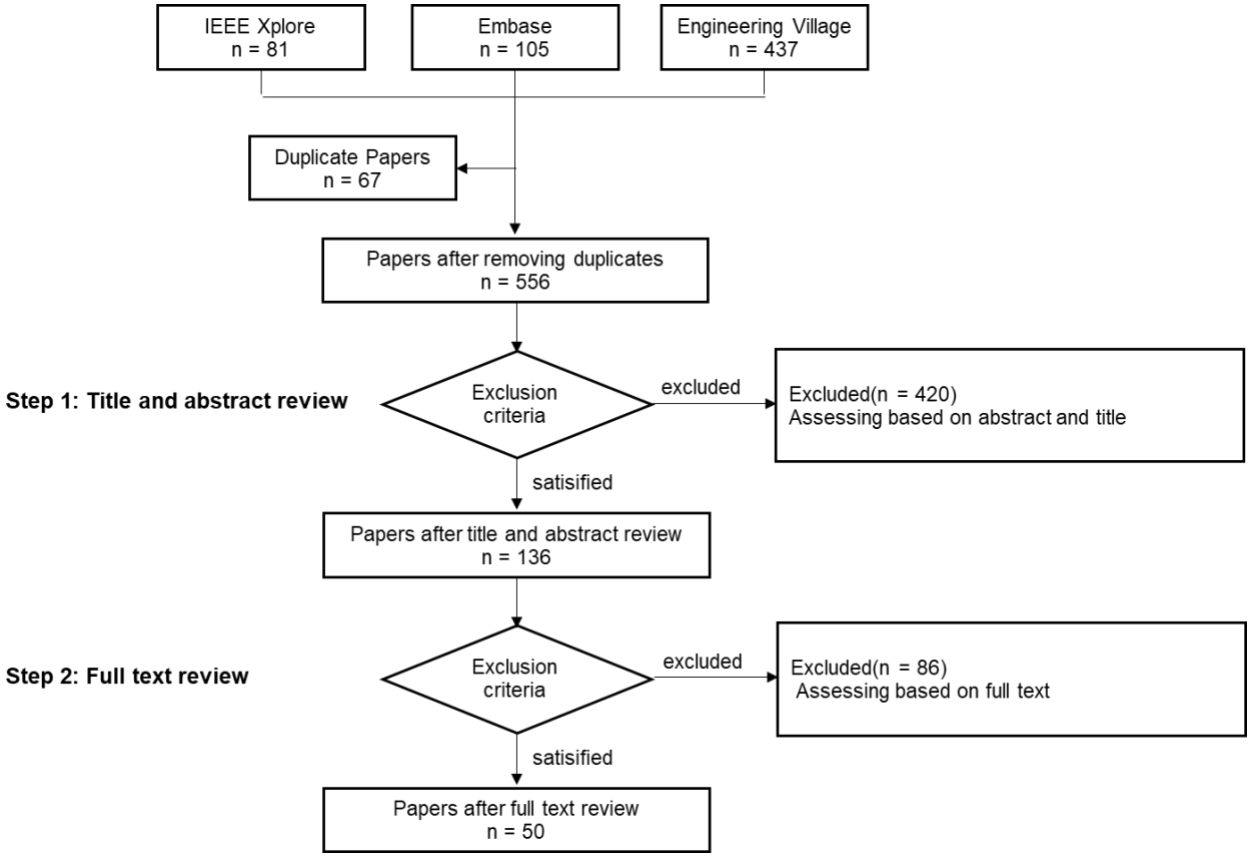

Figure 2.1: Flow-chart according to the different phased of the systematic review as proposed by PRISMA

2.2.3 Assessed Outcomes

A total of 50 studies were retrieved after the full-text review. The following information was extracted from each article:

- general information: authors, year of publication, title, journal, study setting, tasks that were analyzed (i.e., material handling, assembling, stitching), study objective.
- automated assessment of ergonomic risk: ergonomic risk factors (i.e., posture, load/force, movement frequency, repetition, duration, recovery), data acquisition sensors (e.g., surface electromyography, camera, inertial measurement units), data processing and analysis, ergonomic assessment criteria, and real-time feedback.

2.3 Results

Appendix A summarizes extracted information on the 50 studies reviewed. The results indicated that more than half of the studies were published after 2019 (Figure 2.2). Although in the search strategy, the starting year was 2007, the first relevant paper retrieved was published in 2011 by Gong et al., 2011. The number of studies has steadily increased since then, except for the year 2022, for which we only searched studies published from January through June. 40 out of 50 studies examined the applicability of the proposed automated ergonomic assessment system only in laboratory experiments simulating real-field environments. Only 6 studies demonstrated the utility of their method in field-based settings, while the remaining 5 relied on both laboratory and field settings.

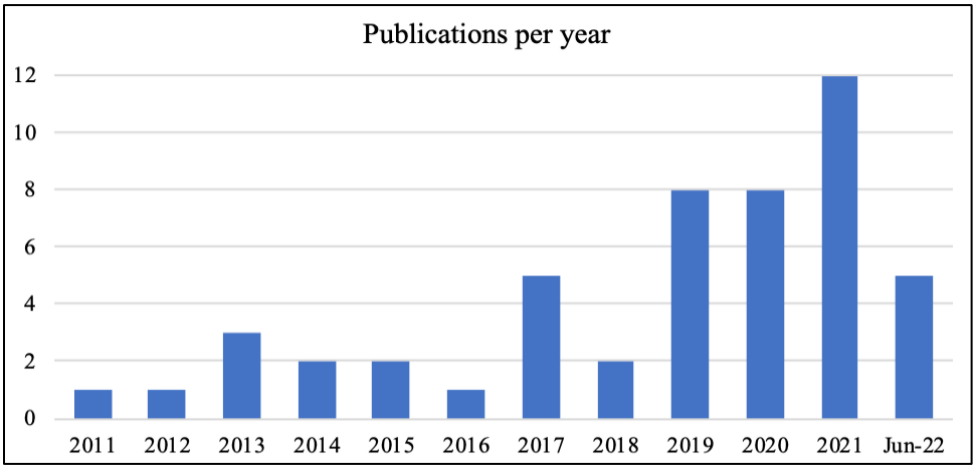

Figure 2.2: Publication per year (n = 50)

Across all studies, various automated ergonomic assessment methods were developed for evaluating risk factors. Figure 2.3 provides a summary of the reviewed studies that reported on risk factors evaluated. The most frequently evaluated ergonomic risk factors were tasks and postures. 32 studies evaluated tasks and postures, with 11 studies assessing upper body ergonomic exposure and the remaining studies assessing the whole body. The upper extremities and low back were the most assessed body segments. 4 studies assessed repetition, frequency, and duration, while 7 studies focused only on forces and moments. Across the retrieved studies, 7 studies evaluated more than one risk factor. In particular, 2 studies assessed different postures and the corresponding duration and frequency (Bortolini et al., 2020; Spector et al., 2014), 1 study evaluated physical intensity as well as frequency and duration (Antwi-Afari et al., 2020), 2 studies evaluated external loads along with postures (Oyekan et al., 2021; Vianello et al., 2022), and 2 studies evaluated all three types of factors (Van Crombrugge et al., 2022).

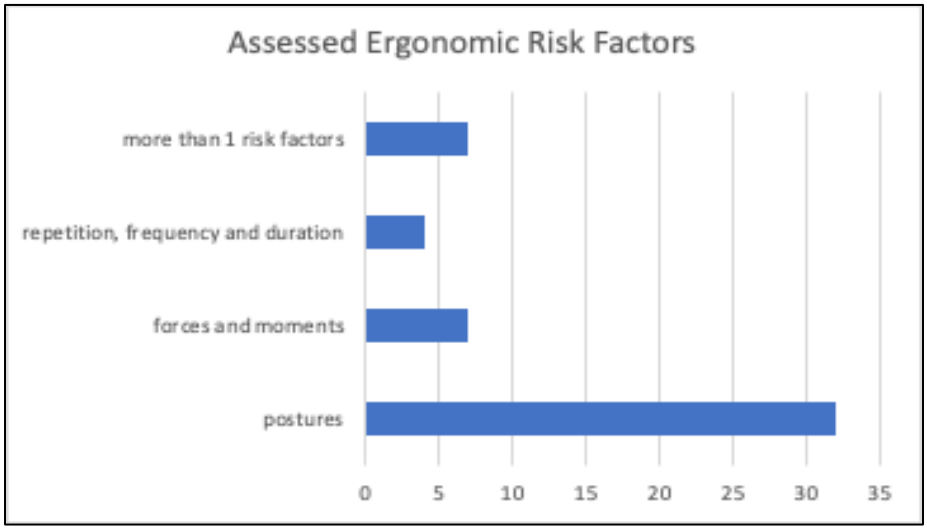

Figure 2.3: The number of studies on each ergonomic risk factor

2.3.1 Data Collection System

Various types of data collection systems were proposed by the retrieved studies for automated ergonomic assessment to gather real-time data on workplaces and evaluate potential risks associated with poor postures, forceful exertions, and prolonged and repetitive motions. These systems often incorporate one or several sensors to capture interested data. Based on sensor placement or location, we categorized data collection systems into two main types, including vision-based system and wearable sensor system.

2.3.1.1 Vision-Based System

Across the retrieved studies, 28 of them used vision-based system for data collection, with 14 studies using Depth camera/depth images, 13 studies using RGB camera/images, and 1 study using optical motion capture system. Depth cameras, also known as 3D camera, capture depth information. Each pixel in a depth image represents the depth or distance information for a specific point in the scene. We categorized them into three categories based on the technologies they used: stereo camera (e.g., RealSense D455' and RealSense D435), time-of-flight (ToF) camera (e.g., PMD CamCube 2.0, Kinect for Xbox One, Kinect for Windows v2, Azure Kinect DK), and structured light camera (e.g., Kinect for Xbox 360). Stereo cameras use two or more cameras to capture images from a slightly different perspective. Depth information can be calculated by comparing the disparities between corresponding points in the images. Stereo cameras are low-cost and generally work well in indoor environments with controlled lighting. While it can work outdoors, it may encounter challenges in direct sunlight or scenes with highly reflective surfaces. It is also sensitive to calibration errors and requires multiple calibrations. To automatically calculate Rapid Entire Body Assessment (REBA) scores, Van Crombrugge et al., 2022 estimated 3D joint angles from depth data captured by a RealSense camera. Their results showed that the accuracy of the 3D joint angles from a RealSense was limited when compared to

the ground truth of VICON measurements (Van Crombrugge et al., 2022a). ToF cameras and structured light cameras are also known as range cameras. Compared to stereo cameras, range cameras generally offer higher accuracy and can cover a wider range of distances. ToF cameras measure the distance from the camera to a subject by measuring the time it takes for light to travel forth and back between them. It provides depth information in real-time and can work both indoors and outdoors. But it can be less accurate in extremely bright sunlight. Structured light cameras calculate depth by analyzing the deformation of the pattern of the light that is projected onto the scene. This type of camera can provide highly accurate depth measurements. But they are generally used indoors and require consistent lighting. Across the studies, the most widely used depth cameras were Kinect sensors. They have built-in skeletal joint tracking algorithms and are capable of tracking joint positions in real-time. However, the accuracy of the 3D skeleton estimation was limited when using Kinect in an industrial environment due to complex human motions and occlusions. To overcome this limitation and calculate more accurate Rapid Upper Limb Assessment (RULA) scores in real work conditions, Plantard et al., 2017 proposed using Filtered Pose Graph to reconstruct poses. Most studies used a single depth camera which was usually placed in front of the subject. Depth data were usually collected at 10 - 30 fps (frames per second), and the tracking distance was from 1.4 to 5 meters.

Another imaging device used was RGB cameras that capture color images or video frames in color. Each pixel has three channels (red, green, and blue) representing its color. RGB cameras are widely available and cost-effective. They can be used in indoor and outdoor settings. In industrial cases, RGB cameras can be easily integrated into existing monitoring systems, minimizing the need for additional hardware. With a single RGB camera, it typically provides 2D information rather than 3D information. For example, Greene et al., 2019 proposed a method

that automatically classified lifting postures (e.g., squatting, stooping and standing) using 2D information from video frames captured by a side view camera. However, using multiple RGB cameras, it is possible to estimate 3D information by combining information from different camera views. In Van Crombrugge et al., 2022, three cameras were positioned at different angles around the capture area where a subject performed work. 3D joint angles were obtained by triangulating 2D information from two and three cameras, respectively. Their results suggested the accuracy could be improved by using more cameras as it provides larger overlapping coverage and minimizes occlusion (Van Crombrugge et al., 2022a). Of 13 RGB camera-based studies, 9 studies reported sampling frequency varying from 7 to 30 fps, and only 4 studies reported the capture distance of the camera(s) which ranged from 2 to 3.3 meters from the subject.

Optical motion capture (OMC) system is another vision-based technique for obtaining 3D information of subjects. With multiple cameras positioned around the capture area, optical motion capture system records video frames that contain information about the positions of reflective markers attached to subject's body. By estimating tracked marker positions, it allows for detailed and accurate 3D kinematic measurements related to subject's motion. Maruyama et al. used OMC system to estimate and track 3D joint positions for ergonomics assessment (Maruyama et al., 2021).

2.3.1.2 Wearable Sensor System

Wearable sensors, such as smart gloves, pressure insoles or inertial measurement units (IMUs), were also used to collect data on workers' physiological responses, joint forces and moments, and body movements and postures for ergonomic assessment. IMUs consist of multiple sensors, typically accelerometers, gyroscopes, and magnetometers, that work together to

provide information about a subject's motion and orientation. To capture movements of different segments simultaneously, multiple IMUs are usually placed at various subject's body parts. Then 3D kinematic data of body segments or joints can be estimated either by commercially available software or custom-made scripts. The number of inertial sensors used in the reviewed literature varied from 1 to 17. Matijevich et al., 2021 evaluated the feasibility of using a reduced number of inertial sensors, with the number varying from 2 to 8 (Matijevich et al., 2021). IMU is also used in smartphones for motion tracking. Nath et al., 2018 used smartphones for manual work activity detection in addition to activity duration and frequency estimation (Nath et al., 2018). Pressure insoles, also known as plantar pressure measurement systems or foot pressure sensors, are devices designed to measure the distribution of pressure and force exerted on the foot soles. The use of pressure insoles measures the vertical ground reaction force (vGRF), which also provides an estimate of the external forces applied to the subject (Antwi-Afari et al., 2020; Lorenzini et al., 2018; Matijevich et al., 2021; Yu, Li, Umer, et al., 2019; Yu, Li, Yang, et al., 2019). By combining the external forces measured from pressure insoles with joint kinematics from motion capture systems, inverse dynamics analysis can compute the internal joint forces and moments (Yu, Li, Umer, et al., 2019; Yu, Li, Yang, et al., 2019). Smart glove, often embedded with flexion sensors and pressure sensors, captures hand movements and finger motions. Malaise et al. used an e-glove to automatically track workers' hand activities (Malaise et al., 2019). In the retrieved studies, surface electromyography (sEMG) was used to evaluate muscle effort during various work tasks. By combining sEMG and IMC system, Oyekan et al. and Peppoloni et al. developed frameworks for automatic ergonomic assessment concerning muscle effort intensity and work postures (Oyekan et al., 2021; Peppoloni et al., 2016).

2.3.2 Data Processing and Analysis

Automated ergonomic assessment requires efficient, sometimes real-time, data analysis and modeling. Data characterizing ergonomic risks are high-dimensional, complex, and big in volume with various sources; often, advanced data processing and analytic techniques are used to extract from these data informative features that describe risk factors including postures, force exertion, and task duration and repetition. Depending on specific ergonomic assessment needs, technical expertise and resources, different data processing and analysis methods were used. These methods are categorized into two main categories: commercially available software-based, and machine learning-based.

2.3.2.1 Commercially Available Software-Based

Some studies used commercially available software packages for processing data from IMU sensors. Commercially available software packages often offer data visualization, analysis, and even real-time processing capabilities. Some of them are provided by sensor manufacturers, while others are from third-party developers. For example, Xsens (Technologies B.V., Enschede, Netherlands) offers manufacturer-developed software packages such as MVN Animate/Analyze, which can process motion data and estimate joint and segment kinematic parameters, such as orientation, position, angle, velocity, and acceleration. In a few studies, depth images captured by Kinect were processed by Kinect SDK, a commercial software developed by Microsoft. The software estimated the 3D coordinates of joints by built-in algorithms. The joint positions were then used for calculating joint angles which were used for risk posture assessment (E. Rocha-Ibarra et al., 2021; Manghisi et al., 2017; Plantard et al., 2015).

2.3.2.2 Machine Learning-Based

Depending on the type of data collection sensors and specific ergonomic risks being assessed, different machine learning methods are applied to perform ergonomic evaluation.

These methods can be summarized into traditional machine learning methods and deep learning methods. Traditional machine learning refers to a subset of machine learning methods that rely on handcrafted features and mathematical models to make predictions. Deep learning is based on deep neural networks (DNNs) and can automatically learn hierarchical features from the data, eliminating the need for extensive manual feature engineering.

1. Traditional Machine Learning

1) Feature Engineering and Selection

Feature engineering is the process of creating and transforming new features from raw data (e.g., wearable sensor data, images and videos), while feature selection involves selecting the most relevant ones from available features. The choice of feature engineering techniques depends on specific machine-learning tasks and data sources. Due to their distinct characteristics, different features were engineered for sensor data and vision-based data. Sensor data feature engineering involved summarizing temporal and frequency aspects and incorporating domain-specific knowledge, while vision-based data feature engineering focused on spatial and temporal relationships, colors, and textures.

Wearable Sensor-Based Data

Traditional machine learning models were trained on IMU data for work posture and task recognition. Data from pressure sensors and sEMG were used for joint force and moment estimation, and muscle force estimation. Relevant features were most commonly engineered from sensor data using domain knowledge. Domain knowledge was used to extract key kinematic and kinetic features, such as range of motion, orientation of segments, position of joints, and foot plantar center of pressure (COP), containing meaningful information with respect to the target variable. Time domain statistical features, such as mean, minimum, maximum, root

mean square (RMS), and standard deviation (SD), were also extracted from time-series sensor data. Frequency domain features were derived from frequency domain data which were converted from time domain data by applying mathematical transformations (e.g., Fast Fourier Transform, FFT). Before feeding these features to a machine learning model, some studies implemented feature selection to choose a subset of the most relevant features from the whole set of features(Antwi-Afari et al., 2020; H. Jeong & W. Park, 2021; Malaise et al., 2019). Feature selection approaches included filter methods, wrapper methods, and hybrid methods.

Vision-Based Data

Vision-based data were mainly used to train traditional machine learning models for recognizing work tasks and detecting risk postures based on ergonomic assessment tools, including Ergonomic Assessment Worksheet (EAWS) and Ovako Working Posture Analysis System (OWAS). Relevant features were extracted from images and videos by different methods. The most straightforward features were kinematic features computed from body joint positions, which were detected and estimated by pose estimation techniques. For example, Kruger & Nguyen, 2015 extracted body angle features from joint positions to recognize 16 postures. We will discuss pose estimation with deep learning methods in section 2.3.2.2.2. The position of certain body parts can also be tracked and features were extracted. Azari et al., 2019 tracked hand motion and extracted from hand trajectories a set of features describing hand kinematics. Some studies extracted features from human body silhouettes. Ray & Teizer, 2012 extracted a human body silhouettes feature vector representing work postures. In Greene et al., 2019, the height and width of a bounding box around the body silhouettes were used as features. Seo & Lee, 2021 derived features from a bounding box and an ellipse around the body silhouettes. Silhouette features were used to train models for classifying different working

postures, such as twisting, crawling, stooping, etc. However, features from silhouettes are sensitive to camera location, occlusion, and subject appearance. The bag-of-vision-words approach was used to extract spatiotemporal features from video sequences of different actions (Gong et al., 2011). Bag-of-vison-words approach represents features as a collection of tokens and retains the information about feature occurrence for each action class. This technique is often used in classification tasks with Naïve Bayes which we will discuss in the next section.

2) Learning Algorithms

A variety of algorithms were used for ergonomic assessment. Support vector machine (SVM) was used for recognizing ergonomic condition vs. unergonomic condition, such as squat lifting vs. stoop lifting, LI (lifting index) < 1 vs. LI > 1 (Conforti et al., 2020; Donisi et al., 2021). SVM is initially designed for binary classification tasks, but it can be extended to handle multi-class classification problems through methods like one-vs-all or one-vs-one classification. Seo & Lee, 2021 used a one-vs-one SVM model to recognize multiple work postures, including back bending, arm raising, and knee bending. SVM was also used to recognize work activities, such as loading, carrying, pushing/pulling, lifting/lowering (Antwi-Afari et al., 2020; Nath et al., 2018). Some studies classified multiple work postures using a decision tree (Azari et al., 2019; Greene et al., 2019). A decision tree partitions dataset into subsets based on simple rules (e.g., the values of input features) and creates a tree-like structure of decisions, where each internal node represents a feature, each branch represents a possible feature value, and each leaf node represents a prediction. However, decision trees can easily overfit the training data and are sensitive to changes in data where small changes in data can result in significantly different tree structures. Besides, single decision trees may not capture complex relationships in the data. Therefore random forest, an ensemble method that used multiple decision trees, was also used by

studies for posture and activity recognition (Antwi-Afari et al., 2020; Azari et al., 2019; Donisi et al., 2021; Kruger & Nguyen, 2015). Random forest combines the predictions of multiple individual decision trees to make more accurate and robust predictions. Both decision tree and random forest can provide measures of feature importance, which helps identify the most influential features in the dataset. As mentioned above, decision trees split data based on values of input features, while K-nearest neighbor (KNN) classifies data points based on their proximity to other data points. H. Jeong & W. Park, 2021 used a KNN classifier to classify eleven sitting postures. KNN can be computationally expensive, especially for large dataset, as it requires calculating distances to all data points. Naïve Bayes is a classification algorithm based on Bayes' theorem. It assumes that each feature is independent of every other feature, which aligns with the idea the order of "words" is not considered in the bag-of-vision-words feature representation. Gong et al., 2011 used Naïve Bayes with bag-of-vision-words feature representation to classify three classes - relocating, excavating and swing. In order to model time-series data and retain temporal state information, Hidden Markov Models (HMMs) were used to recognize work activities (Azari et al., 2019; Malaise et al., 2019). Each work activity often consists of several actions. When performing a specific work activity, the next action should be expected based on the current state of action. HMM can be useful for understanding the sequential patterns and temporal dependencies for each activity class, and the extracted information can be used to determine which activity class is most probable. Another commonly used algorithm was Feedforward Neural Network (FNN), which outputs the probability for each class. Donisi et al., 2021 used an FNN with a single hidden layer to recognize LI < 1 and LI > 1 during lifting.

Although the algorithms mentioned above were used for classification tasks, most of them can be adapted for regression. That said, there are variations of them that are well-suited for

predicting continuous numerical values. For example, there are support vector regression and random forest regression. Similarly as random forest, gradient boosting decision tree algorithm also uses decision trees as fundamental building blocks. It builds decision trees sequentially and can be used for both classification and regression tasks. Matijevich et al., 2021 used a gradient boosted decision tree model to estimate lumbar moments. When using a single output neuron and a regression loss, FNN can be used for regression. In Lorenzini et al., 2018, an FNN with a single hidden layer was used for the estimation of feet ground reaction forces (GRFs) and centers of pressure (CoP).

2. Deep Learning

Wearable Sensor-Based Data

Deep learning models such as Convolutional Neural Networks (CNNs) or Recurrent Neural Networks (RNNs) were applied to wearable sensor data to evaluate ergonomic risk factors. CNN was used to process and extract features from multi-channel data. For example, Lamooki et al., 2022 applied a 2D CNN on data from three accelerometer channels to extract spatial features representing different work tasks (e.g., lifting, pushing, typing, etc.). CNNs are designed for processing grid data and can be used to extract spatial information from sensor data, while RNNs are well-suited for handling sequential data such as time-series data. However, traditional RNNs have limitations on their ability to capture long-range dependencies in sequences due to the vanishing gradient problem. Sensor measurements used for ergonomic assessment could span a work shift, potentially containing thousands or millions of data points. Long Short-Term Memory (LSTM) networks (Hochreiter & Schmidhuber, 1997) are a specific type of RNN and are designed to handle long sequences and mitigate the vanishing gradient

problem. Zhao et al., 2021 integrated a 2D CNN and LSTM as a convolutional LSTM (CLN) and applied it to data from 5 IMUs for detecting risk postures based on OWAS.

Vision-Based Data

Most vision-based studies applied deep learning methods for single-person 2D work pose estimation from which joint angles were calculated and used for risk postures assessment or inverse dynamic analysis. The models used for 2D pose estimation mainly included DeepPose (Toshev & Szegedy, 2014), stacked hourglass network (Newell et al., 2016), and convolutional pose machine (CPM) (Wei et al., 2016). A few studies also used computer vision libraries and toolkits, such as OpenPose (Cao et al., 2018) and Detectron2 (Wu et al., 2019), for pose estimation. In 2D pose estimation, the goal is to estimate the pixel coordinates (X, Y) of key body joints in a 2D image or video frame. Typically, key body joints include head, neck, shoulders, elbows, wrists, hips, knees, and ankles. The X and Y coordinates represent the positions of these joints in the image, with the origin (0,0) located at the top-left corner of the image, and X and Y corresponding to the horizontal and vertical axes. The angles (θ) between body segments can be calculated with the formula $\theta = \arccos(\mathbf{a}\cdot\mathbf{b}) / (\|\mathbf{a}\| \|\mathbf{b}\|)$, where vectors **a** and **b** represent body segments and can be obtained from 2D pose. For example, Pan et al., 2022 and Z. Li et al., 2020 used CPM (Wei et al., 2016) with images from a side view camera to estimate 2D pose from which 2D joint angles in the sagittal plane and postures of neck/trunk twisting and side-bending were obtained for the calculation of REBA scores. However, 3D joint angles enable the assessment of complex, three-dimensional postures and movements, which is essential for jobs involving tasks, such as twisting, bending, reaching, crouching, etc. Some studies estimated 3D angles based on 3D pose estimation from multi-view images (Kim et al., 2021; Van Crombrugge et al., 2022a). Multiple synchronized cameras recorded from different

angles, and 3D pose estimation was obtained by combining 2D pose estimation from each camera. For example, Kim et al., 2021 used OpenPose (Cao et al., 2018) to estimate whole-body 2D poses from images of three different camera views, respectively. They then calculated 3D joint angles from 3D pose which was obtained by triangulating the estimated 2D pose. Fewer studies estimated 3D pose from a single image. For example, Yu, Yang, Li, et al., 2019 adopted a weakly-supervised approach proposed by Zhou et al., 2017 to estimate 3D pose estimation from a single image. In the study, 2D pose was first estimated by a stacked hourglass network (Newell et al., 2016), and then 3D pose was recovered from the 2D pose estimation by a depth regression network. But minor errors in the locations of the 2D body joints can have large consequences in the 3D space when recovering 3D from a single image (Sarafianos et al., 2016). Besides it requires additional steps to convert 3D coordinates of joint positions into joint angles. Abobakr et al., 2019 proposed a skeleton-free holistic posture analysis method to estimate 3D joint angles directly from a depth image. They used a deep residual network (ResNet) model (He et al., 2015) to map an input depth image to 15 joint angles.

2.3.3 Ergonomic Assessment Criteria

Different ergonomic assessment criteria were used to evaluate interested risk factors for various work tasks. In particular, 15 studies assessed upper body postures on the basis of RULA, while 10 studies applied REBA which is developed on the basis of the RULA and appropriate for whole body posture assessment. RULA and REBA identify harmful postures by evaluating postural angles of six different body positions, forceful exertions/load, static posture duration, action repetition, and coupling. In the studies, body position angles were derived automatically from motion data by commercially available software or machine learning methods, while other factors such as duration and repetition, force/load score, and coupling score were added

manually. Some studies applied OWAS, which identifies four postures for the back, three for the arms, and seven for the lower extremity, and has three weight categories for the load handled. Similar to RULA/REBA-based studies, work postures, such as back bending and rotation, arm elevation, and knee bending and kneeling, were recognized automatically by the use of machine learning method, while handled load were added manually. A few studies proposed automatic procedure for recognizing awkward postures based on EAWS. While these studies successfully demonstrated the use of machine learning methods to screen and identify awkward postures, other risk factors evaluated in EAWS, including action forces of whole-body and hand-finger, load conditions in manual material handling, and upper limb load in repetitive tasks, were not considered. NIOSH lifting equation is a tool to determine the recommended weight limit (RWL) for manual lifting tasks. The equation can be written: RWL = LC*HM*VM*DM*AM*FM*CM, where LC is the load constant, HM is the horizontal multiplier, VM is the vertical multiplier, DM is the distance multiplier, AM is the asymmetry multiplier, FM is the frequency multiplier, and CM is the coupling multiplier. Spector et al., 2014 automatically estimated the values of HM, VM, DM, AM and FM for the lifting equation. Another widely used tool for assessing lifting tasks is Lifting Fatigue Failure Tool (LiFFT). LiFFT estimates cumulative loading damage for the low back by taking into account the moment exerted on the low back from load, and the corresponding repetitions. Matijevich et al., 2021 estimated automatically lumbar moments that can be input into LiFFT. Another tool that is applicable to assess cumulative loading damage is the Shoulder Tool. Shoulder Tool takes into account types of manual tasks, the moment exerted on the shoulder from load, and the corresponding repetitions. Lamooki et al., 2022 demonstrated the use of machine learning methods to automatically recognize different manual tasks and the corresponding repetition and duration for the Shoulder Tool. Greene et al., 2017 and C.-H. Chen

et al., 2013 also presented a method for the automated estimation of frequency and duty cycle that can be used in hand activity level (HAL) analysis. To identify tasks that require excessive forceful exertion, some studies calculated joint torques with inverse dynamic analysis, where joint angles were automatically estimated from motion data, while external loads were manually added (Maruyama et al., 2021; Plantard et al., 2017), obtained from pressure insoles (Yu, Li, Umer, et al., 2019; Yu, Li, Yang, et al., 2019), or measured by torque sensors (Vianello et al., 2022).

2.3.4 Real-Time Ergonomic Assessment Feedback

Real-time feedback is an approach to identifying and addressing ergonomic issues as they occur, often using real-time data. It requires continuously monitoring workers' activity, posture, force exertion, and duration and frequency of tasks. When specific ergonomic thresholds are reached, feedback is activated and sent out. Different types of feedback were used in the literature. Some studies used visual cues as feedback. Real-time posture angles or joint force/moments were visualized through a human body model or time-series graphs, and the level of ergonomic risk was color-coded. Cumulative ergonomic exposures in a work shift were also visualized and displayed in a few studies. Other studies also used visual cues with haptic or auditory cues, where visual cues were used for real-time, continuous risk factor monitoring and the vibration or auditory alert was sent out for ergonomic threshold breaching. For example, in Yan et al., 2017, real-time posture angle was visualized and displayed on a smartphone screen, and an auditory alert was sent out from the smartphone if an awkward posture was held for a period longer than the maximum holding time (MHT). In a few studies, immediate action was required if risk was detected. In Yan et al., 2017, an auditory alert would only be silenced until the detected prolonged awkward posture was adjusted to an acceptable one.

2.4 Discussion

The use of automated assessment approaches in ergonomic research is on the rise. From work posture monitoring to predicting overload joint torques, the range of applications where advanced sensing systems and analytics can improve ergonomic research will continue to expand, particularly as machine learning methods are capable of learning from vast amounts of data. The aim of this review is to bring to light automated assessment approaches in ergonomic research and find research gaps that will inform future research in this area.

2.4.1 Sensor Selection

Choosing which type of sensor to collect data is a critical decision when considering the use of sensors for automated ergonomic risk assessment. In the reviewed studies, advanced sensing systems were used for motion capture and exerted force measurement with automated tools. Pressure insoles were mostly used to measure exerted force data in the literature due to its minimal influence on worker's comfort and productivity. However, the type of sensors used for motion capture differed across the reviewed studies. Inertial sensors were capable of capturing accurate and reliable 3D motion data. It relied on direct measurements from sensors attached to worker's body, which may not be feasible in long-time applications due to its intrusiveness. The number and anatomical locations of the sensors were dependent on the study's research question and segments, or joints interested. For example, Lamooki et al., 2022 developed an effective method using just one IMU for activity recognition, while to capture whole-body kinematic data the studies used up to 17 IMUs on different body segments. Vision-based motion capture methods such as depth cameras and RGB cameras provided a non-intrusive and whole-body assessment. Depth camera was proved to be an effective tool for 3D motion capture. Biomechanically meaningful 3D motion data were also extracted from RGB images with the

help of computer vision algorithms. But the accuracy of these sensors was subject to illumination changes, viewpoint variation, background clutter and occlusions. Overall, this review identified a need for motion capture methods that are capable of capturing subtle movement and providing stable data and are robust to varying environments. These methods should also require minimal intrusiveness and disturbance.

2.4.2 Analysis

In the literature, working postures were assessed by a set of detailed segment kinematics that were derived from inertial data, depth images/video or RGB images/video. Different angle ranges corresponded different levels of risk on the basis of ergonomic criteria. But such methods didn't provide contextual information for a given job (e.g., task type, duration, repetition). To extract task information, some studies used machine learning algorithms to classify different postures or tasks, using extracted features that represented different tasks. For example, Azari et al., 2019 calculated a feature set of 1213 predictor variables describing hands' postures for surgical maneuver classification. Deep learning algorithms were also used for activity classification in three studies and were able to take raw data as input (Parsa et al., 2019; Roberts et al., 2020; Zhao, Obonyo, & G Bilén, 2021), skipping the feature extraction step. Six studies extracted activity repetition and duration based on counting activity types which were recognized by machine learning (or deep learning) algorithms. While posture, repetition and duration are important risk factors, overexertion injuries also result from accumulative microdamage caused by repetitive loading to musculoskeletal tissues, which is consistent with a fatigue failure process (Gallagher & Schall Jr., 2017). In reviewed studies, loadings were estimated based on posture data and exerted force data. Force data were either from prior knowledge of external load or derived from data from sensors such as pressure insole and sEMG.

2.4.3 Risk Factors and Ergonomic Criteria

Motion capture sensors along with predictive modeling techniques have shown strong potential for extracting information representing posture risks. Most commonly used methods for posture evaluation are RULA, REBA, and EAWS. These methods require the estimation of segment angles and evaluate posture risk levels by some certain thresholds of segment angles, characterizing risk as low-risk level, medium-risk level and high-risk level. RULA only specifies angles in the sagittal plane, paying little attention to the movements in the coronal plane. LiFFT and Shoulder Tool investigate repetition and loading. LiFFT evaluates the risk of low back loading during lifting tasks where the low back tissues are exposed to cumulative damage. Shoulder Tool estimates cumulative damage to shoulder tissues during pulling and pushing. Joint torques and forces are also important to estimate the biomechanical constraints of working tasks in ergonomics. Multiple studies used data from motion sensors and pressure sensors for the estimation of joint torques. Messeri et al., 2022 trained a DNN model to predict muscle activation on the basis of motion data. This study shows potential for combining motion data with a deep learning model for estimating muscle activation and further predicting muscle force.

2.4.4 Feedback

Visual feedback often uses graphical icons, changing colors on a display or on-screen messages. It is highly effective for conveying information. But it may not be suitable in situations where workers' visual attention is already engaged elsewhere, because looking at display could distract workers and increase the risk of accidents. However, it can be useful for ergonomists to observe trends and patterns of ergonomic risk from past and current data, potentially identifying improvements or deteriorations in workplace ergonomics. Besides, visual representations of risk factors are often accessible to non-expert audiences, which is important

when presenting findings to stakeholders. Haptic cues can use vibration alerts on wearable devices and allow workers to receive feedback without having to constantly look at a screen. It can be more immediate and attention-grabbing, which makes it suitable for real-time alerts where quick responses are necessary. But haptic cues can convey a limited amount of information due to the relatively simple nature of tactile feedback. It may not be as intuitive as visual cues, and its interpretation can be subjective. Similar to haptic cues, auditory cues are also effective for immediate attention and allow workers to receive feedback without having to divert their visual attention. But auditory cues can lack privacy, as they are audible to others nearby. In general, the choice of feedback type depends on the specific application context and the preferences and needs of the workers. Often, a combination of these feedback types can be used to ensure that ergonomic assessment feedback is communicated and acted upon effectively.

2.4.5 Limitations

The current review was limited to the assessment of physical risk factors. Exposure to job-related psychosocial stress and organizational factor have also been implicated in the development of work-related injuries. The study intentionally focused on data acquisition sensors, ergonomic risk factors, data modeling and ergonomic risk assessment criteria. Aspects related to feedback and intervention though being a step of the automated ergonomic assessment loop were outside of the scope of this study. This review also didn't evaluate or rate the quality of individual studies. We only included journal papers available in three electronic databases. Therefore, we may have overlooked potential interesting studies if published in conferences, or not indexed in the selected electronic databases.

2.5 Conclusion

This paper reviewed the current state of the method and system for automated ergonomic assessment. Findings suggest a growing number of studies pertaining to automating risk assessment in ergonomics. The main advantage of this trending research in ergonomics is its ability to evaluate ergonomic risk exposures continuously, automatically and in real-time. More than half of the studies relied on RULA and REBA that evaluate a single risk factor to assess the risk of work-related MSDs. New methods and systems are needed that are capable of automating ergonomic assessment criteria such as LiFFT and Shoulder tool which consider multiple risk factors. Additionally, analysis of joint loadings was largely limited to estimating external loads. Developing a modeling framework that has the ability to predict external loads would also be a direction for future research.

2.6 References

Abobakr, A., Nahavandi, D., Hossny, M., Iskander, J., Attia, M., Nahavandi, S., & Smets, M. (2019). RGB-D ergonomic assessment system of adopted working postures. *Applied Ergonomics*, *80*, 75–88. https://doi.org/10.1016/j.apergo.2019.05.004

Antwi-Afari, M. F., Li, H., Umer, W., Yu, Y., & Xing, X. (2020). Construction Activity Recognition and Ergonomic Risk Assessment Using a Wearable Insole Pressure System. *Journal of Construction Engineering and Management*, *146*(7), 04020077. https://doi.org/10.1061/(ASCE)CO.1943-7862.0001849

Azari, D. P., Hu, Y. H., Miller, B. L., Le, B. V., & Radwin, R. G. (2019). Using Surgeon Hand Motions to Predict Surgical Maneuvers. *Human Factors: The Journal of the Human Factors and Ergonomics Society*, *61*(8), 1326–1339. https://doi.org/10.1177/0018720819838901

Bortolini, M., Faccio, M., Gamberi, M., & Pilati, F. (2020). Motion Analysis System (MAS) for production and ergonomics assessment in the manufacturing processes. *Computers & Industrial Engineering*, *139*, 105485. https://doi.org/10.1016/j.cie.2018.10.046

Cao, Z., Hidalgo, G., Simon, T., Wei, S.-E., & Sheikh, Y. (2018). *OpenPose: Realtime Multi-Person 2D Pose Estimation using Part Affinity Fields* (Version 2). arXiv. https://doi.org/10.48550/ARXIV.1812.08008

Chen, C.-H., Hu, Y. H., Yen, T. Y., & Radwin, R. G. (2013). Automated Video Exposure Assessment of Repetitive Hand Activity Level for a Load Transfer Task. *Human Factors: The Journal of the Human Factors and Ergonomics Society*, *55*(2), 298–308. https://doi.org/10.1177/0018720812458121

Conforti, I., Mileti, I., Del Prete, Z., & Palermo, E. (2020). Measuring Biomechanical Risk in Lifting Load Tasks Through Wearable System and Machine-Learning Approach. *Sensors*, *20*(6), 1557. https://doi.org/10.3390/s20061557

Donisi, L., Cesarelli, G., Coccia, A., Panigazzi, M., Capodaglio, E. M., & D'Addio, G. (2021). Work-Related Risk Assessment According to the Revised NIOSH Lifting Equation: A Preliminary Study Using a Wearable Inertial Sensor and Machine Learning. *Sensors*, *21*(8), 2593. https://doi.org/10.3390/s21082593

Gallagher, S., & Schall Jr., M. C. (2017). Musculoskeletal disorders as a fatigue failure process: Evidence, implications and research needs. *Ergonomics*, *60*(2), 255–269. https://doi.org/10.1080/00140139.2016.1208848

Gong, J., Caldas, C. H., & Gordon, C. (2011). Learning and classifying actions of construction workers and equipment using Bag-of-Video-Feature-Words and Bayesian network models. *Advanced Engineering Informatics*, *25*(4), 771–782. https://doi.org/10.1016/j.aei.2011.06.002

Greene, R. L., Azari, D. P., Hu, Y. H., & Radwin, R. G. (2017). Visualizing stressful aspects of repetitive motion tasks and opportunities for ergonomic improvements using computer vision. *Applied Ergonomics*, *65*, 461–472. https://doi.org/10.1016/j.apergo.2017.02.020

Greene, R. L., Hu, Y. H., Difranco, N., Wang, X., Lu, M.-L., Bao, S., Lin, J.-H., & Radwin, R. G. (2019). Predicting Sagittal Plane Lifting Postures From Image Bounding Box Dimensions. *Human Factors: The Journal of the Human Factors and Ergonomics Society*, *61*(1), 64–77. https://doi.org/10.1177/0018720818791367

He, K., Zhang, X., Ren, S., & Sun, J. (2015). *Deep Residual Learning for Image Recognition* (Version 1). arXiv. https://doi.org/10.48550/ARXIV.1512.03385

Hochreiter, S., & Schmidhuber, J. (1997). Long Short-Term Memory. *Neural Computation*, *9*(8), 1735–1780. https://doi.org/10.1162/neco.1997.9.8.1735

Jeong, H., & Park, W. (2021). Developing and Evaluating a Mixed Sensor Smart Chair System for Real-Time Posture Classification: Combining Pressure and Distance Sensors. *IEEE Journal of Biomedical and Health Informatics*, *25*(5), 1805–1813. https://doi.org/10.1109/JBHI.2020.3030096

Kim, W., Sung, J., Saakes, D., Huang, C., & Xiong, S. (2021). Ergonomic postural assessment using a new open-source human pose estimation technology (OpenPose). *International Journal of Industrial Ergonomics*, *84*, 103164. https://doi.org/10.1016/j.ergon.2021.103164

Krüger, J., & Nguyen, T. D. (2015). Automated vision-based live ergonomics analysis in assembly operations. *CIRP Annals*, *64*(1), 9–12. https://doi.org/10.1016/j.cirp.2015.04.046

Lamooki, S. R., Hajifar, S., Kang, J., Sun, H., Megahed, F. M., & Cavuoto, L. A. (2022). A data analytic end-to-end framework for the automated quantification of ergonomic risk factors across multiple tasks using a single wearable sensor. *Applied Ergonomics*, *102*, 103732. https://doi.org/10.1016/j.apergo.2022.103732

Li, Y., Greene, R. L., Mu, F., Hu, Y. H., & Radwin, R. G. (2020). Towards Video-Based Automatic Lifting Load Prediction. *Proceedings of the Human Factors and Ergonomics Society Annual Meeting*, *64*(1), 962–963. https://doi.org/10.1177/1071181320641230

Li, Z., Zhang, R., Lee, C.-H., & Lee, Y.-C. (2020). An Evaluation of Posture Recognition Based on Intelligent Rapid Entire Body Assessment System for Determining Musculoskeletal Disorders. *Sensors*, *20*(16), 4414. https://doi.org/10.3390/s20164414

Lorenzini, M., Kim, W., De Momi, E., & Ajoudani, A. (2018). A Synergistic Approach to the Real-Time Estimation of the Feet Ground Reaction Forces and Centers of Pressure in Humans With Application to Human–Robot Collaboration. *IEEE Robotics and Automation Letters*, *3*(4), 3654–3661. https://doi.org/10.1109/LRA.2018.2855802

Malaise, A., Maurice, P., Colas, F., & Ivaldi, S. (2019). Activity Recognition for Ergonomics Assessment of Industrial Tasks With Automatic Feature Selection. *IEEE Robotics and Automation Letters*, *4*(2), 1132–1139. https://doi.org/10.1109/LRA.2019.2894389

Manghisi, V. M., Uva, A. E., Fiorentino, M., Bevilacqua, V., Trotta, G. F., & Monno, G. (2017). Real time RULA assessment using Kinect v2 sensor. *Applied Ergonomics*, *65*, 481–491. https://doi.org/10.1016/j.apergo.2017.02.015

Maruyama, T., Ueshiba, T., Tada, M., Toda, H., Endo, Y., Domae, Y., Nakabo, Y., Mori, T., & Suita, K. (2021). Digital Twin-Driven Human Robot Collaboration Using a Digital Human. *Sensors*, *21*(24), 8266. https://doi.org/10.3390/s21248266

Matijevich, E. S., Volgyesi, P., & Zelik, K. E. (2021). A Promising Wearable Solution for the Practical and Accurate Monitoring of Low Back Loading in Manual Material Handling. *Sensors*, *21*(2), 340. https://doi.org/10.3390/s21020340

Messeri, C., Bicchi, A., Zanchettin, A. M., & Rocco, P. (2022). A Dynamic Task Allocation Strategy to Mitigate the Human Physical Fatigue in Collaborative Robotics. *IEEE Robotics and Automation Letters*, *7*(2), 2178–2185. https://doi.org/10.1109/LRA.2022.3143520

Nath, N. D., Chaspari, T., & Behzadan, A. H. (2018). Automated ergonomic risk monitoring using body-mounted sensors and machine learning. *Advanced Engineering Informatics*, *38*, 514–526. https://doi.org/10.1016/j.aei.2018.08.020

Newell, A., Yang, K., & Deng, J. (2016). Stacked Hourglass Networks for Human Pose Estimation. In B. Leibe, J. Matas, N. Sebe, & M. Welling (Eds.), *Computer Vision – ECCV 2016* (Vol. 9912, pp. 483–499). Springer International Publishing. https://doi.org/10.1007/978-3-319-46484-8_29

Oyekan, J., Chen, Y., Turner, C., & Tiwari, A. (2021). Applying a fusion of wearable sensors and a cognitive inspired architecture to real-time ergonomics analysis of manual assembly tasks. *Journal of Manufacturing Systems*, *61*, 391–405. https://doi.org/10.1016/j.jmsy.2021.09.015

Pan, T., Wang, Z., & Fan, Y. (2022). Optimized convolutional pose machine for 2D hand pose estimation. *Journal of Visual Communication and Image Representation*, *83*, 103461. https://doi.org/10.1016/j.jvcir.2022.103461

Parsa, B., Samani, E. U., Hendrix, R., Devine, C., Singh, S. M., Devasia, S., & Banerjee, A. G. (2019). Toward Ergonomic Risk Prediction via Segmentation of Indoor Object Manipulation Actions Using Spatiotemporal Convolutional Networks. *IEEE Robotics and Automation Letters*, *4*(4), 3153–3160. https://doi.org/10.1109/LRA.2019.2925305

Peppoloni, L., Filippeschi, A., Ruffaldi, E., & Avizzano, C. A. (2016). A novel wearable system for the online assessment of risk for biomechanical load in repetitive efforts. *International Journal of Industrial Ergonomics*, *52*, 1–11. https://doi.org/10.1016/j.ergon.2015.07.002

Plantard, P., Auvinet, E., Pierres, A.-S., & Multon, F. (2015). Pose Estimation with a Kinect for Ergonomic Studies: Evaluation of the Accuracy Using a Virtual Mannequin. *Sensors*, *15*(1), 1785–1803. https://doi.org/10.3390/s150101785

Plantard, P., Muller, A., Pontonnier, C., Dumont, G., Shum, H. P. H., & Multon, F. (2017). Inverse dynamics based on occlusion-resistant Kinect data: Is it usable for ergonomics? *International Journal of Industrial Ergonomics*, *61*, 71–80. https://doi.org/10.1016/j.ergon.2017.05.010

Ray, S. J., & Teizer, J. (2012). Real-time construction worker posture analysis for ergonomics training. *Advanced Engineering Informatics*, *26*(2), 439–455. https://doi.org/10.1016/j.aei.2012.02.011

Roberts, D., Torres Calderon, W., Tang, S., & Golparvar-Fard, M. (2020). Vision-Based Construction Worker Activity Analysis Informed by Body Posture. *Journal of Computing in Civil Engineering*, *34*(4), 04020017. https://doi.org/10.1061/(ASCE)CP.1943-5487.0000898

Rocha-Ibarra, E., Oros-Flores, M.-I., Almanza-Ojeda, D.-L., Lugo-Bustillo, G.-A., Rosales-Castellanos, A., Ibarra-Manzano, M.-A., & Gomez, J. C. (2021). Kinect Validation of Ergonomics in Human Pick and Place Activities Through Lateral Automatic Posture Detection. *IEEE Access*, *9*, 109067–109079. https://doi.org/10.1109/ACCESS.2021.3101964

Sarafianos, N., Boteanu, B., Ionescu, B., & Kakadiaris, I. A. (2016). 3D Human pose estimation: A review of the literature and analysis of covariates. *Computer Vision and Image Understanding*, *152*, 1–20. https://doi.org/10.1016/j.cviu.2016.09.002

Seo, J., & Lee, S. (2021). Automated postural ergonomic risk assessment using vision-based posture classification. *Automation in Construction*, *128*, 103725. https://doi.org/10.1016/j.autcon.2021.103725

Spector, J. T., Lieblich, M., Bao, S., McQuade, K., & Hughes, M. (2014). Automation of Workplace Lifting Hazard Assessment for Musculoskeletal Injury Prevention. *Annals of Occupational and Environmental Medicine*, *26*(1), 15. https://doi.org/10.1186/2052-4374-26-15

Toshev, A., & Szegedy, C. (2014). DeepPose: Human Pose Estimation via Deep Neural Networks. *2014 IEEE Conference on Computer Vision and Pattern Recognition*, 1653–1660. https://doi.org/10.1109/CVPR.2014.214

U.S. Bureau of Labor Statistics. (2020, May 1). *Occupational injuries and illnesses resulting in musculoskeletal disorders (MSDs)*. https://www.bls.gov/iif/factsheets/msds.htm

Van Crombrugge, I., Sels, S., Ribbens, B., Steenackers, G., Penne, R., & Vanlanduit, S. (2022). Accuracy Assessment of Joint Angles Estimated from 2D and 3D Camera Measurements. *Sensors*, *22*(5), 1729. https://doi.org/10.3390/s22051729

Vianello, L., Gomes, W., Stulp, F., Aubry, A., Maurice, P., & Ivaldi, S. (2022). Latent Ergonomics Maps: Real-Time Visualization of Estimated Ergonomics of Human Movements. *Sensors*, *22*(11), 3981. https://doi.org/10.3390/s22113981

Wei, S.-E., Ramakrishna, V., Kanade, T., & Sheikh, Y. (2016). Convolutional Pose Machines. *2016 IEEE Conference on Computer Vision and Pattern Recognition (CVPR)*, 4724–4732. https://doi.org/10.1109/CVPR.2016.511

Wu, Y., Kirillov, A., Massa, F., Lo, W.-Y., & Girshick, R. (2019). *Detectron2*. https://github.com/facebookresearch/detectron2

Yan, X., Li, H., Li, A. R., & Zhang, H. (2017). Wearable IMU-based real-time motion warning system for construction workers' musculoskeletal disorders prevention. *Automation in Construction*, *74*, 2–11. https://doi.org/10.1016/j.autcon.2016.11.007

Yu, Y., Li, H., Umer, W., Dong, C., Yang, X., Skitmore, M., & Wong, A. Y. L. (2019). Automatic Biomechanical Workload Estimation for Construction Workers by Computer Vision and Smart Insoles. *Journal of Computing in Civil Engineering*, *33*(3), 04019010. https://doi.org/10.1061/(ASCE)CP.1943-5487.0000827

Yu, Y., Li, H., Yang, X., Kong, L., Luo, X., & Wong, A. Y. L. (2019). An automatic and non-invasive physical fatigue assessment method for construction workers. *Automation in Construction*, *103*, 1–12. https://doi.org/10.1016/j.autcon.2019.02.020

Yu, Y., Yang, X., Li, H., Luo, X., Guo, H., & Fang, Q. (2019). Joint-Level Vision-Based Ergonomic Assessment Tool for Construction Workers. *Journal of Construction Engineering and Management*, *145*(5), 04019025. https://doi.org/10.1061/(ASCE)CO.1943-7862.0001647

Zhao, J., Obonyo, E., & G. Bilén, S. (2021). Wearable Inertial Measurement Unit Sensing System for Musculoskeletal Disorders Prevention in Construction. *Sensors*, *21*(4), 1324. https://doi.org/10.3390/s21041324

Chapter 3

Assessment of the Effects of Lifting Weight on Upper Limb Joint Kinematics

3.1 Introduction

Musculoskeletal disorders (MSDs), encompassing conditions like low back pain, neck pain, and shoulder pain, are pervasive in the workforce. These MSDs not only lead to personal suffering but also impose substantial economic burdens on society through healthcare costs and reduced work productivity. Lifting objects is a common job demand in various industries, and it is frequently associated with increased risk for MSDs since lifting heavy weights places considerable mechanical demands on the human body. These demands manifest as changes in lifting kinematics and kinetics (Davis & Marras, 2000; T.-H. Lee, 2015; Norasi et al., 2019; Plamondon et al., 2017; Song & Qu, 2014).

Previous studies have assessed the relationship between lifting weight and trunk kinematics and kinetics. Plamondon et al., 2017 reported significantly increased peak and cumulative low back moments with higher lifting weight. Similarly, Song & Qu, 2014 studied the effects of lifting weight on the low back moment and the sagittal plane kinematics. Their results showed that both peak and average low back moments increased with heavier lifting weight. Davis & Marras, 2000 investigated trunk peak kinematics of lifting 9.1 kg – 41.8 kg, and showed that there was an overall decrease in sagittal velocity and acceleration. Their result also indicated that there was no difference in spinal loads with small increases (3-9 kg) in box weights due to an offset by the sagittal velocity. In Norasi et al., 2019, they studied the effects of lifting weight on the variance in the ground reaction force (e.g., peak vertical ground reaction force, peak horizontal shear force), and the sagittal and transverse trunk kinematics (e.g., range of motion, average velocity, peak velocity, and peak acceleration). The results indicated that

there was no significant effect of lifting weight on the variance of trunk kinematic variables, while the lifting load had a significant effect on the variance of the peak shear ground reaction force. These studies demonstrated that changes of lifting weight generally led to changes of trunk kinematic and kinetic variables during lifting.

However, these studies failed to consider the effects of lifting weight on whole body kinematics. Lifting is enabled by coordinated movements of a complex biomechanical system consisting of multiple body joints, mostly by those of the ankle, knee, hip, lumbar, shoulder and elbow. It is a process in which different joints interact and coordinate with each other to produce smooth and effective movements. When lifting different weights, the body instinctively adjusts the angles of joints to maximize mechanical advantage by aligning the limbs and joints in a way that allows the body to execute actions efficiently. Thus, the changes of lifting weight may influence not only trunk kinematics but also kinematics of other joints as well as the coordination between these joints within the whole-body biomechanical system. One study reported decreases were found in the peak trunk sagittal angular velocity and peak hip sagittal angular acceleration when lifting weight increased (Song & Qu, 2014). The limitation with this study is that they didn't report upper limb kinematics which is a crucial body part during lifting. Furthermore, the gender of an individual may also affect joint kinematics and coordination, which could be a confounding factor when studying the effects of lifting weight on these variables. Previous studies found that females used different lifting techniques from males(Davis et al., 2003; K. Li & Zhang, 2009; Marras et al., 2003).

The measurement of joint kinematics can be captured by optical motion capture systems (OMC), which are the most used and considered the benchmark in kinematics analysis. But OMC typically require controlled environment and are conducted inside laboratories. An

alternative is inertial measurement units (IMUs), which are portable, easy to set up, and able to be used in field settings. Previous studies have found good agreement in quantifying motion kinematics with IMUs (El-Gohary & McNames, 2012; Lee et al., 2003; Picerno et al., 2008; Robert-Lachaine et al., 2017; Schall et al., 2016). Schall et al., 2016 showed that the estimates of mean angular displacement and angular displacement variation for trunk and upper arm were to change < 1.5° on average in the field. In Lee et al., 2003, coefficient of multiple correlations (CMCs) for were found to range from 0.972 to 0.991 for trunk angular movement. El-Gohary & McNames, 2012 reported root-mean-square error (RMSE) < 8° for shoulder and elbow angles and correlation coefficient > 0.95. Robert-Lachaine et al., 2017 reported accurate estimates of whole-body joint angles with CMCs > 0.92 and RMSE < 5°.

The objective of this study was to investigate the effects of lifting weight on the upper body joint kinematics, considering gender difference. The study hypothesized that changes in lifting weight would affect lifting kinematics of upper limbs, and the effects varies between females and males.

3.2 Methods

3.2.1 Experiment Design

The participants in this study were 9 male and 9 female who were college students and had a mean age, height, and weight of 30.0 (SD = 9.23) years, 173.7 (SD = 6.8) cm, and 67.1 (SD =9.5) kg, respectively. The study was approved by Auburn University's institutional review board. Prior to participation, each participant provided written informed consent and were screened for chronic pain, pre-existing disease, injury or surgery in the low back, neck/shoulder, or upper extremity.

To better simulate a realistic manual material handling task, participants lifted a weighted box and placed it on a shelf at three different heights set by individual anthropometry, including floor to knee height ($H_{floor\text{-}knee}$), floor to elbow height ($H_{floor\text{-}elbow}$) and knee to elbow height ($H_{knee\text{-}elbow}$) (Figure A1 in Appendix A). The weights evaluated in this study were 0.5, 2.3, 4.6, 6.9, 9.2, 11.5, and 13.8 kg. For weight 0.5 kg, the dimension of the box was 41.2 × 27.1 × 14.2 cm (length × width × height). While for the other weights, the box dimension was 46.3 × 31.3 × 11.2 cm (length × width × height). The participants performed free-style liftings at a self-selected pace. A two-factor completely randomized design was used in the experiment. Each participant performed all combinations of lifting height and weight levels. The representation order of the combinations was randomized with three replications.

3.2.2 Data Acquisition and Processing

Whole-body kinematics were measured using a commercial IMU system (MVN Awinda, Xsens Technologies B.V., Enschede, Netherlands) with 17 inertial sensors positioned on the head, sternum and pelvis; and bilaterally on the scapulae, the upper and lower arms, hands, thighs, shanks and feet (Figure A2 in Appendix A). Before the measurements, anatomical measurements and calibration were performed according to the procedure provided by Xsens. The 17 inertial sensors synchronously recorded triaxial accelerometer, gyroscope, and magnetometer data at a sampling frequency of 60 Hz. Joint angles were computed using the segments' orientations from Xsens .MVNX files with medio-lateral, anteroposterior, axial Cardan sequence (Grood & Suntay, 1983). Joint angular velocities were further obtained for the shoulder (humerus vs. thorax) and elbow. The continuous relative phase (CRP) was also calculated to quantify shoulder-elbow coordination using methods described by previous studies (Hamill et al., 1999). To calculate CRP, a phase plot of each lifting cycle was calculated for the

shoulder and elbow. In phase plots, sagittal angles and velocities were normalized to [-1, 1]. The normalized angles were then plotted versus normalized angular velocity. This was illustrated by Figure 3.1. The lift started at far right of the lower part (i.e. at the end of grasping the box), proceeded clockwise to left, and then proceeded upward and to the end (i.e. at the beginning of placing the box). Phase angles φ were calculated for both joints at each data point through the lifting cycle. CRP was obtained for shoulder-elbow coordination from the difference between phase angles ($\varphi_{shoulder}$- φ_{elbow}). Each CRP profile of shoulder-elbow was interpolated to 100 data points using cubic spline (Hamill et al., 1999). Ensemble CRP curves were calculated at each combination of lifting height and weight for each subject as the mean from three repetition CRP curves.

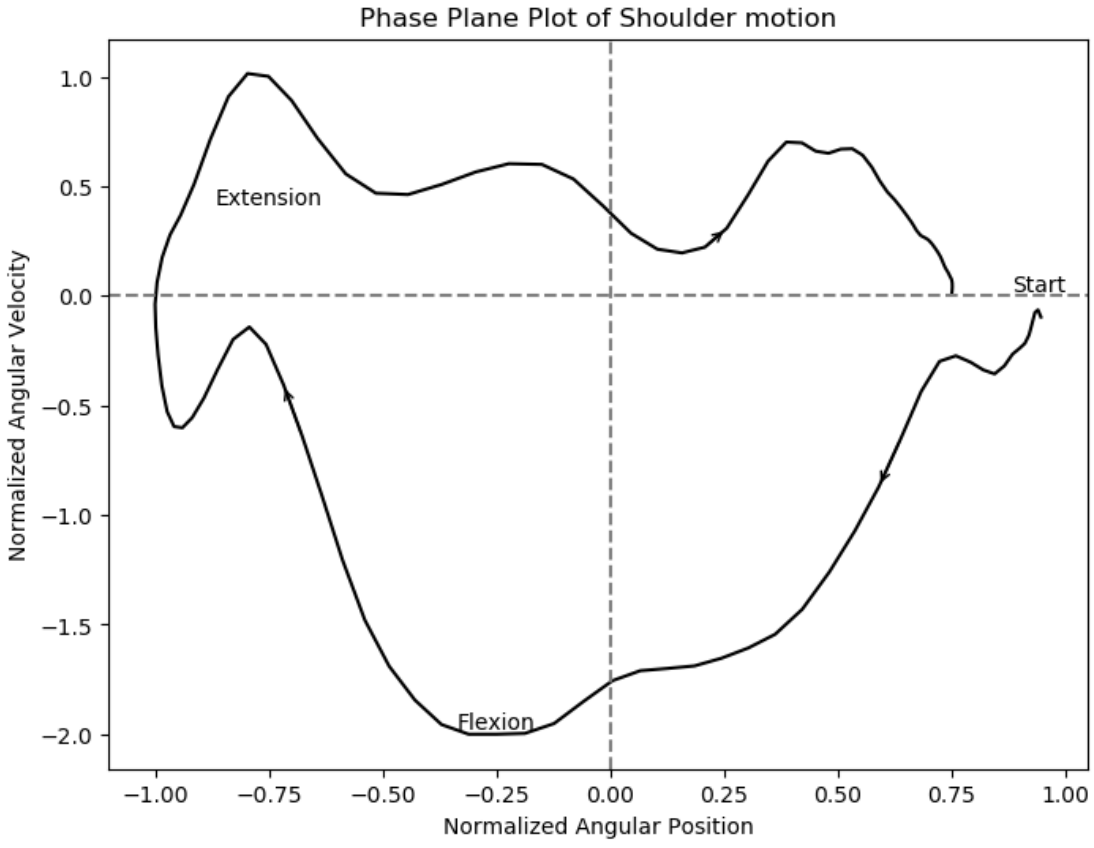

Figure 3.1: A typical normalized phase plane plot of shoulder motion for one lifting cycle

3.2.3 Variables

The independent variables in this experiment were gender (e.g., F and M), the height of lifting (Floor-Knee, Floor-Elbow and Knee-Elbow) and the weight of the box. The kinematics analysis was performed based on three-dimensional shoulder motion and sagittal elbow motion. Because the handles of the boxes did not rotate or change its orientation, a consistent grip and forearm posture were consistent throughout a lift cycle; thus, elbow pronation/supination were highly constrained and excluded from analysis. Peak and average joint velocities of the following motion were obtained: shoulder flexion and extension, shoulder abduction and adduction, shoulder external and internal rotation, and elbow flexion and extension. Since velocity is a vector quantity, positive and negative values of the velocity vector only denote direction, thus, for the purposes of analysis, only the magnitude was considered. We assumed that lifting was symmetric and there was no difference between the right and left side of the lifting kinematics. The dependent variables in this experiment were peak and average angular velocities on the right side during the lift phase. To quantify shoulder-elbow coordination, the mean absolute value of the ensemble CRP curve values (MARP) and the deviation phase (DP) were computed from the ensemble CRP curves (Stergiou et al., 2001).

3.2.4 Statistical Analysis

Data from one female participant was removed due to equipment failure. Mixed-factor analyses of variance (ANOVA) models were used in which lifting height and lifting weight were within-subjects factors and gender was between-subjects factor. In this study, the main focus was on lifting weight. Therefore, Bonferroni post hoc tests were conducted on lifting weight, interaction of lifting weight and gender, and interaction between lifting weight and lifting height if they showed significant effects ($p<0.05$). The coefficient of variation (CV) which was

calculated as the standard deviation divided by the mean was used to study the variations within subjects as well as between subjects (Kjellberg et al., 1998). To obtain within-subject CV, the CV was first calculated for each combination of lifting weight and height over the three repetitions for each subject. The within-subject CV was then calculated by taking the mean of CVs across all subjects for each combination of lifting weight and height. The between-subject CV was calculated for the 17 means of repetitions across subjects for each combination of lifting weight and height (Kjellberg et al., 1998).

3.3 Results

The ANOVA results showed that the main effects of lifting weight, lifting height and gender, and the two-way interactions of lifting weight and two other factors were significant (i.e., $p < 0.05$). The main and interaction effects of lifting weight on each dependent variable are presented below.

3.3.1 Peak Angular Velocity

The peak shoulder flexion velocity was significantly affected by the main effects of gender, lifting height, lifting weight and the interaction of gender and lifting height (Table 3.1). Peak shoulder flexion velocity had an overall decreased trend as lifting weight increased (Figure 3.2). The results of the post-hoc comparisons indicated that the majority of significant differences between pairs were found when the lifting weight differences were greater than 4 kg, while there was no significance found between the three highest weights (9.1, 11.3, 13.6 kg) (Figure 3.2). Peak shoulder external rotation velocity was significantly affected by the main effects of gender, lifting height, lifting weight, the interaction of gender and lifting weight, the interaction of gender and lifting height, and the interaction of lifting height and weight (Table 3.1). When investigating the effect of lifting weight within each gender group, it was found that

peak shoulder external rotation velocity decreased overall with increased lifting weight for both female and male subjects (Figure 3.3). The results of the post-hoc comparisons indicated that most of significant differences occurred between the two lowest levels and the higher levels (Figure 3.3). For the gender-related difference at each lifting weight level, significant gender effects were found on the peak shoulder external rotation velocity for all lifting weights (Table 3.2). In particular, female subjects had significantly higher peak shoulder external rotation velocity at each lifting weight level comparing with male subjects. When examining the effect of lifting weight at each lifting height level, the peak shoulder external rotation velocity had an overall decreasing trend with increased lifting weight at each lifting height level (Figure 3.4). The post-hoc comparison results revealed that at each lifting height level most significant differences were only found between 2.3 kg and the higher levels, which were 4 kg greater (Figure 3.4). Peak shoulder abduction velocity was significantly affected by the main effects of gender, lifting height, lifting weight, the interaction of gender and lifting weight, and the interaction of gender and lifting height (Table 3.1). For the effect of lifting weight within each gender group, it was found that peak shoulder abduction velocity decreased overall with increased lifting weight in both gender groups (Figure 3.5). The post-hoc comparison results indicated that most significant differences occurred between the two lowest levels and the other higher levels (Figure 3.5). Significant gender effects were observed at each lifting weight level when examining the differences in peak shoulder abduction velocity related to gender (Table 3.3), in which female subjects had a significantly higher value at each lifting weight level.

The peak shoulder internal rotation velocity was significantly affected by the main effects of gender, lifting height and lifting weight (Table 3.1). However, there was not a noticeable increasing or decreasing trend observed for peak shoulder internal rotation velocity as lifting

weight increased (Figure 3.6). The post-hoc comparison results indicated that significant differences occurred only between the lowest weight (0.5 kg) and all the other levels (Figure 3.6). Peak elbow extension velocity was also significantly affected by the main effects of gender, lifting height and lifting weight (Table 3.1). An overall decreased trend was observed for peak elbow extension velocity as lifting weight increased (Figure 3.7). The post-hoc comparison results indicated that most of significant differences between pairs were found when the lifting weight differences were greater than 4 kg (Figure 3.7).

3.3.2 Average Angular Velocity

The average shoulder flexion velocity was significantly affected by the main effects of lifting height, lifting weight, the interaction of gender and lifting weight, and the interaction of gender and lifting height (Table 3.4). For the effect of lifting weight within each gender group, an increase in lifting weight was associated with an overall decreased in the average shoulder flexion velocity in both gender groups (Figure 3.8). For both genders, most of significant differences between pairs were found when the lifting weight differences exceeded 4 kg (Figure 3.8). However, there was no significant gender effects at each lifting weight level when examining the differences in average shoulder flexion velocity related to gender. Average shoulder external rotation velocity was significantly affected by the main effects of gender, lifting height, lifting weight, the interaction of gender and lifting weight, and the interaction of gender and lifting height (Table 3.4). When investigating the effect of lifting weight within each gender group, an increase in lifting weight was associated with an overall decreased in the average shoulder external rotation velocity in both gender groups (Figure 3.9). Most of significant differences occurred between pairs of which weight differences exceeded 4 kg (Figure 3.9). For the gender-related difference at each lifting weight level, significant gender

effects were found on the average shoulder external rotation velocity for most of lifting weights (Table 3.5), in which female subjects had a significantly higher value at each lifting weight level. Average shoulder Abduction velocity was significantly affected by the main effects of gender, lifting height, lifting weight, and the interaction of gender and lifting height (Table 3.4). For the effect of lifting weight, however, there was not a noticeable increasing or decreasing trend observed for the average shoulder abduction velocity as lifting weight increased (Figure 3.10). Post-hoc comparisons indicated significant differences were only found between the lowest weight (0.5 kg) and the other higher weights (Figure 3.10). Average elbow flexion velocity was significantly affected by the main effects of lifting height, lifting weight, the interaction between gender and lifting weight, the interaction between gender and lifting height, and the interaction between lifting height and lifting weight (Table 3.4). For the effect of lifting weight within each gender group, average elbow flexion velocity decreased overall with increased lifting weight for both female and male subjects (Figure 3.11). However, most of significant differences occurred only between the two lowest levels and the other higher levels (Figure 3.11). For the effect of lifting weight at each lifting height level, although the average elbow flexion velocity had an overall decreasing trend with increased lifting weight at each lifting height level (Figure 3.12), most of significant differences were only found between the two lowest weights and the other higher weights (Figure 3.12).

Average shoulder extension velocity was significantly affected by the main effects of gender, lifting height, lifting weight, the interaction of gender and lifting weight, and the interaction of gender and lifting height (Table 3.4). For the effect of lifting weight within each gender group, an interesting trend was observed for both female and male subjects, in that the average shoulder extension velocity increased as lifting weights increased from 0.5 kg to 6.8 kg

whereas a downward trend was observed as the weights increased from 6.8 kg to 13.6 kg (Figure 3.13). However, the magnitude of velocity was statistically equivalent between 2.3, 4.5, 6.8 and 9.12 kg. Significant differences were only found between these lower weights and the two highest weights (11.3 and 13.6 kg) that had the lowest magnitude of velocity (Figure 3.13). For the gender-related differences at each lifting weight level, although female subjects had higher average shoulder extension velocity at each lifting weight level comparing with male subjects, significant gender effects were only found at lifting weights from 0.5 kg to 6.8 kg (Table 3.6). Average shoulder internal rotation velocity was significantly affected by the main effects of gender, lifting height, and lifting weight (Table 3.4). The average shoulder internal rotation velocity had an upward trend when weights increased from 0.5 kg to 6.8 kg, but a downward trend was observed as the weights increased from 6.8 kg to 13.6 kg (Figure 3.14). However, the post-hoc comparisons indicated that significant differences occurred only between the lowest weight (0.5 kg) and all the other levels, and between the highest weight (13.6 kg) and weights that were $\leq$ 6.8 kg (Figure 3.14). Average elbow extension velocity was significantly affected by the main effects of gender, lifting height, and lifting weight (Table 3.4). The average elbow extension velocity decreased overall with increased weights (Figure 3.15). Post-hoc tests revealed that velocities of between 2.3, 4.5, 6.8 and 9.12 kg were equivalent, there were no significant differences between them. Significant differences occurred between the lowest weight (0.5 kg) and the other higher levels, and between the two highest weights (11.3 and 13.6 kg) and the other lower weights (Figure 3.15).

Table 3.1: Results of mixed-factor ANOVA for peak angular velocities. Cells entries are *F* values (*p* values).

Dependent Variable	Gender (G)	Lifting Height (LH)	Lifting Weight (LW)	G x LW	G x LH	LH x LW	G x LH x LW
Shoulder Flexion	**33.178 (0.001)**	**855.427 (<.001)**	**36.326 (0.001)**	1.959 (0.151)	**16.502 (<.001)**	0.913 (0.562)	0.405 (0.962)
Shoulder Extension	**291.351 (<.001)**	**26.486 (<.001)**	20.757 (0.062)	0.341 (0.902)	3.624 (0.059)	1.32 (0.319)	1.623 (0.08)
Shoulder External Rotation	**81.853 (<.001)**	**346.169 (<.001)**	**14.076 (<.001)**	**5.186 (0.008)**	**37.002 (<.001)**	**3.035 (0.033)**	0.201 (0.998)
Shoulder Internal Rotation	**339.297 (<.001)**	**23.421 (<.001)**	**22.88 (0.006)**	0.51 (0.79)	3.858 (0.051)	1.622 (0.207)	1.256 (0.239)
Shoulder Abduction	**80.262 (<.001)**	**421.833 (<.001)**	**14.721 (<.001)**	**3.658 (0.027)**	**30.094 (<.001)**	1.752 (0.172)	0.274 (0.993)
Shoulder Adduction	**478.836 (<.001)**	**35.817 (<.001)**	39.369 (0.059)	0.353 (0.895)	3.397 (0.068)	1.219 (0.369)	1.289 (0.219)
Elbow Flexion	15.213 (0.008)	**1351.82 (<.001)**	256.642 (0.122)	1.373 (0.301)	1.955 (0.184)	0.138 (0.999)	0.67 (0.781)
Elbow Extension	**23.409 (0.003)**	**34.111 (<.001)**	**29.037 (<.001)**	1.35 (0.309)	1.225 (0.328)	2.503 (0.063)	0.926 (0.52)

Table 3.2: Results of post-hoc comparison between genders at each lifting weight for peak shoulder external rotation velocity. Note that * denotes a significant difference between females and males.

Weight (kg)	Gender	Mean	SD
0.5	F	96.87 *	18.53
	M	85.78 *	12.55
2.3	F	103.46 *	19.83
	M	94.48 *	15.92
4.5	F	94.24 *	15.79
	M	87.90 *	14.06
6.8	F	92.92 *	15.10
	M	85.89 *	13.95
9.1	F	90.07 *	14.10
	M	84.21 *	13.77
11.3	F	89.65 *	16.90
	M	85.11 *	13.59
13.6	F	87.69 *	15.96
	M	80.41 *	13.12

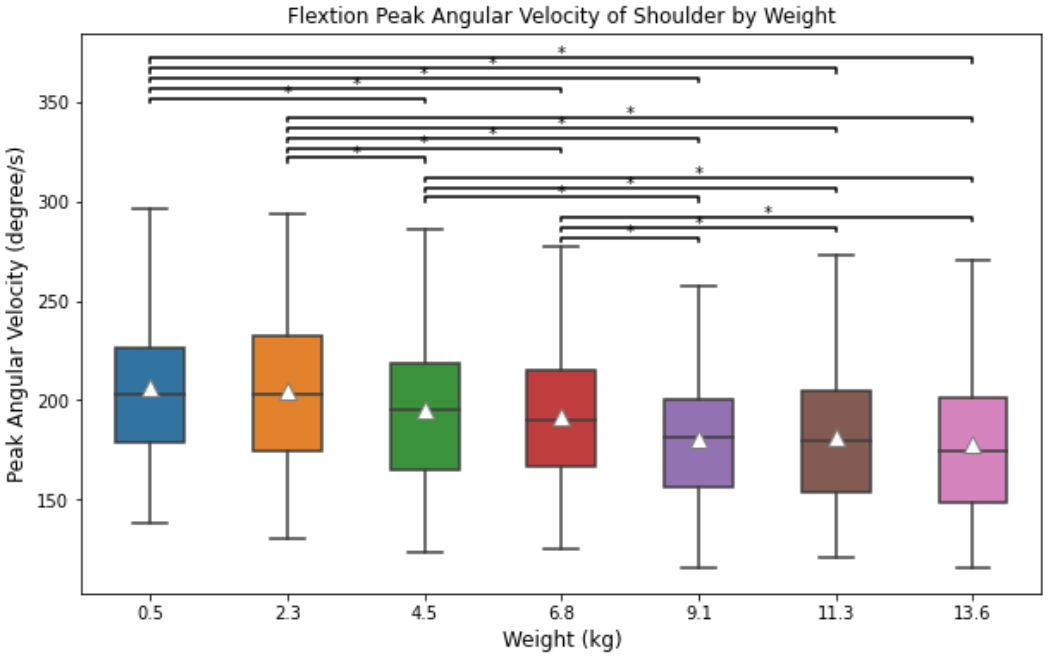

Figure 3.2: Peak shoulder flexion velocity at different lifting weights. (Note that * denotes a significant difference between two weights.)

(a)

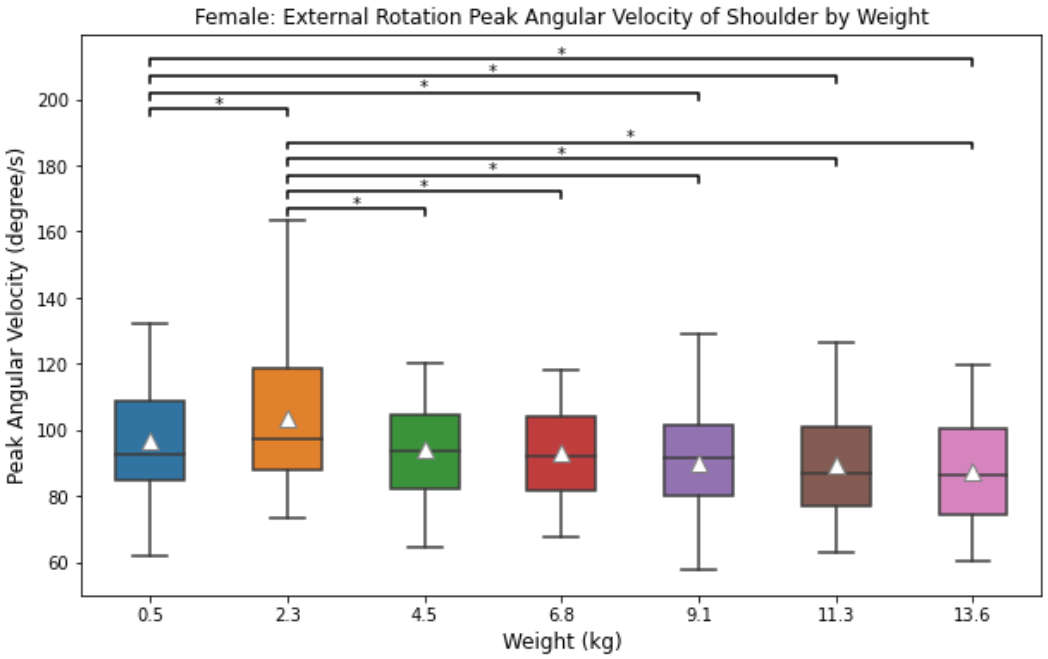

(b)

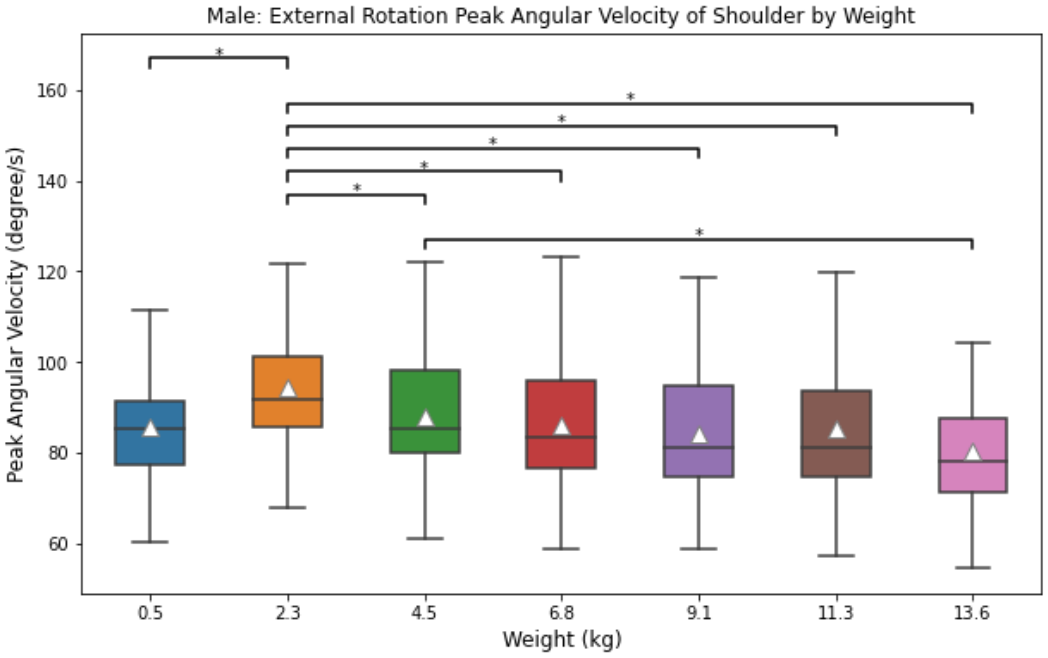

Figure 3.3: Peak shoulder external rotation velocity at different lifting weights for (a) female and (b) male. (Note that * denotes a significant difference between two weights.)

(a)

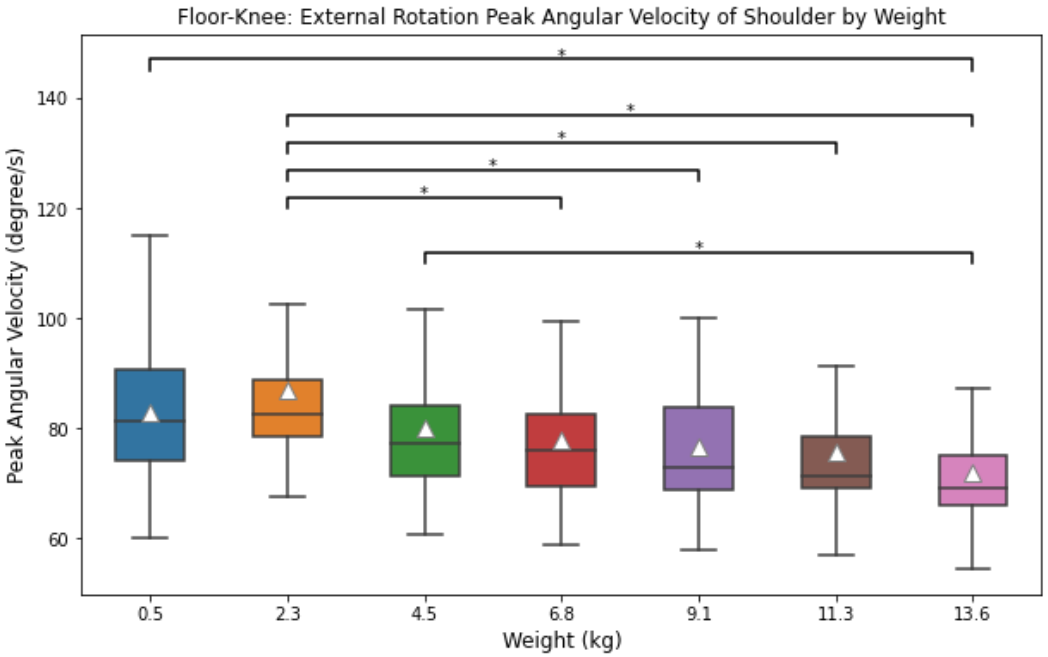
Floor-Knee: External Rotation Peak Angular Velocity of Shoulder by Weight
Peak Angular Velocity (degree/s)
140
120
100
80
60
0.5
2.3
4.5
6.8
9.1
11.3
13.6
Weight (kg)

(b)

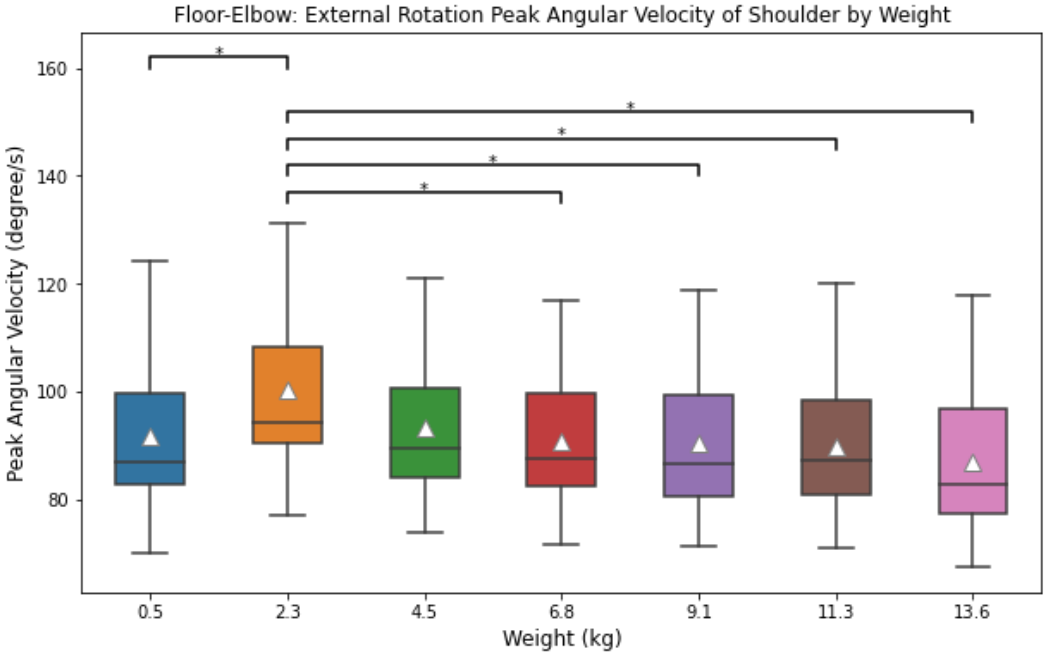
Floor-Elbow: External Rotation Peak Angular Velocity of Shoulder by Weight
Peak Angular Velocity (degree/s)
160
140
120
100
80
0.5
2.3
4.5
6.8
9.1
11.3
13.6
Weight (kg)

(c)

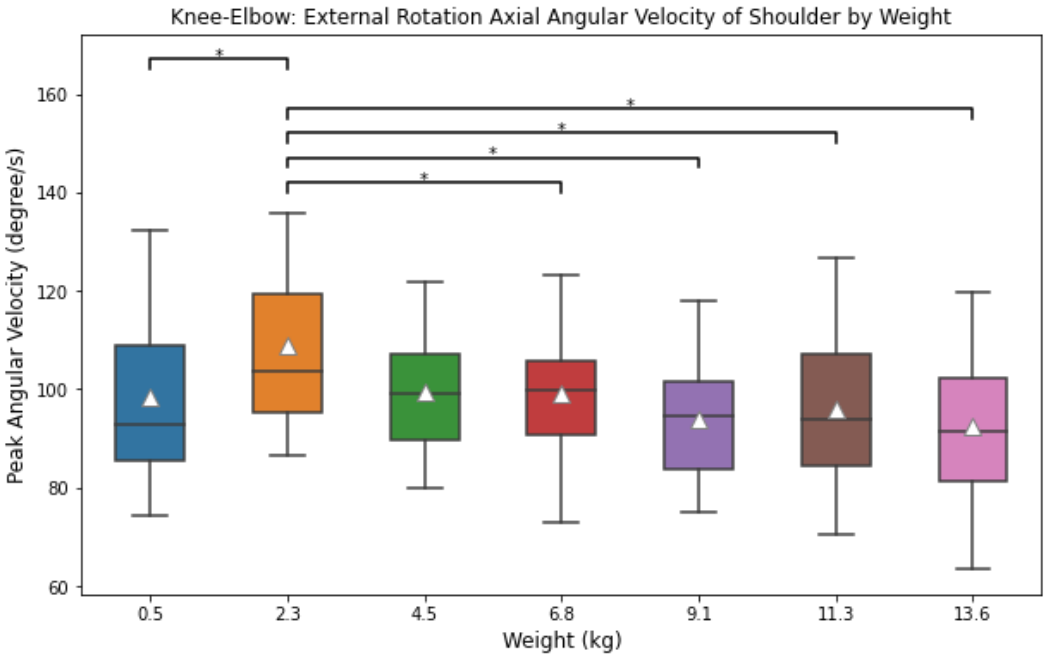

Figure 3.4: Peak shoulder external rotation velocity at different lifting weights for lifting height (a) floor-knee, (b) floor-elbow, and (c) knee-elbow. (Note that * denotes a significant difference between two weights.)

(a)

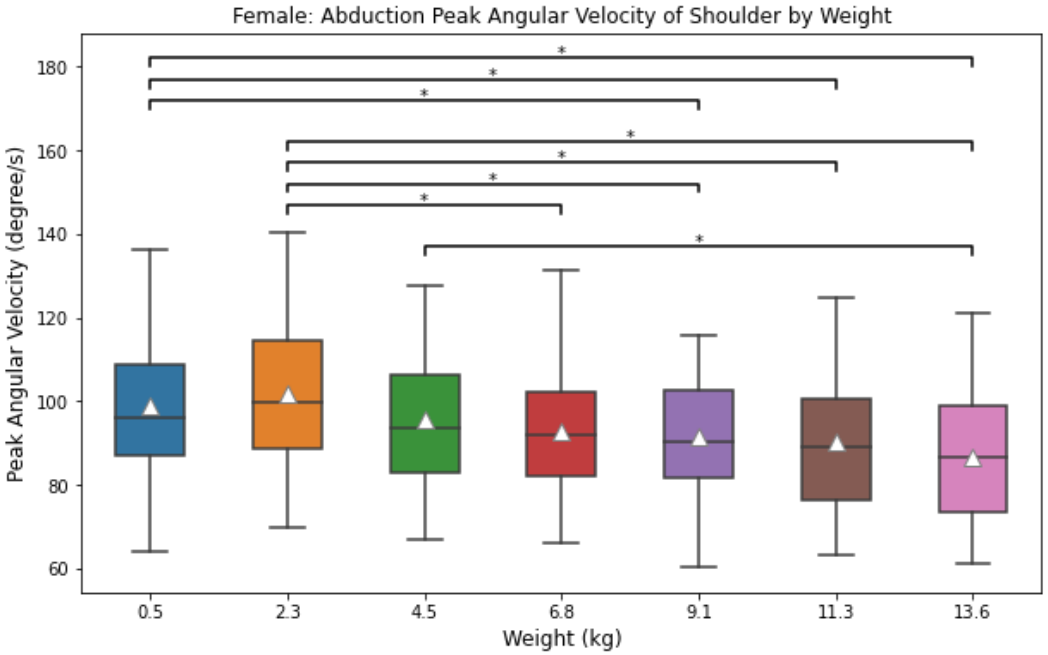

(b)

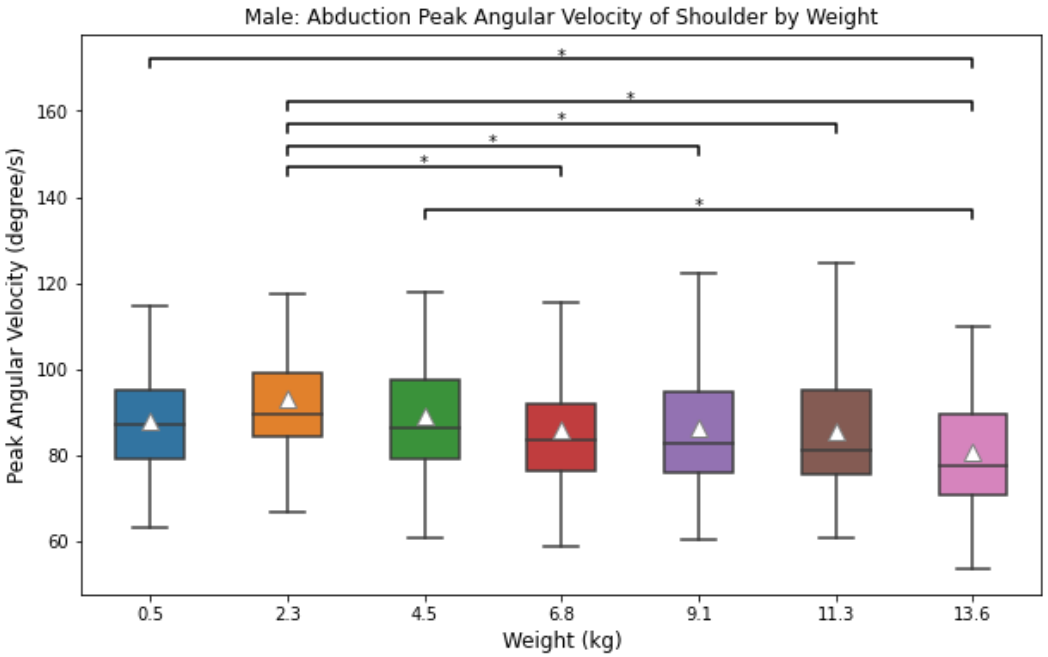

Figure 3.5: Peak shoulder abduction velocity at different lifting weights for (a) female and (b) male. (Note that * denotes a significant difference between two weights.)

Table 3.3: Results of post-hoc comparison between genders at each lifting weight for peak shoulder abduction velocity. Note that * denotes a significant difference between females and males.

Weight (kg)	Gender	Mean	SD
0.5	F	98.80 *	17.24
	M	87.88 *	12.90
2.3	F	101.82 *	17.85
	M	92.92 *	14.54
4.5	F	95.77 *	17.15
	M	88.87 *	14.27
6.8	F	92.90 *	15.21
	M	86.02 *	14.57
9.1	F	91.61 *	13.52
	M	86.09 *	14.87
11.3	F	90.18 *	16.57
	M	85.51 *	14.60
13.6	F	86.57 *	15.80
	M	80.47 *	14.54

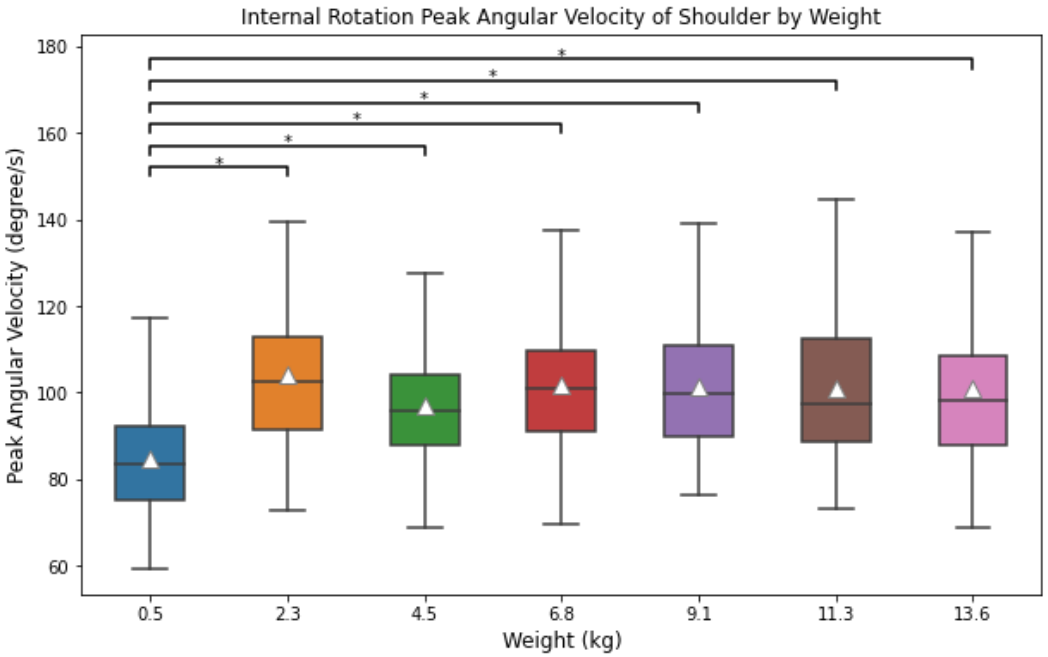

Figure 3.6: Peak shoulder internal rotation velocity at different lifting weights. (Note that * denotes a significant difference between two weights.)

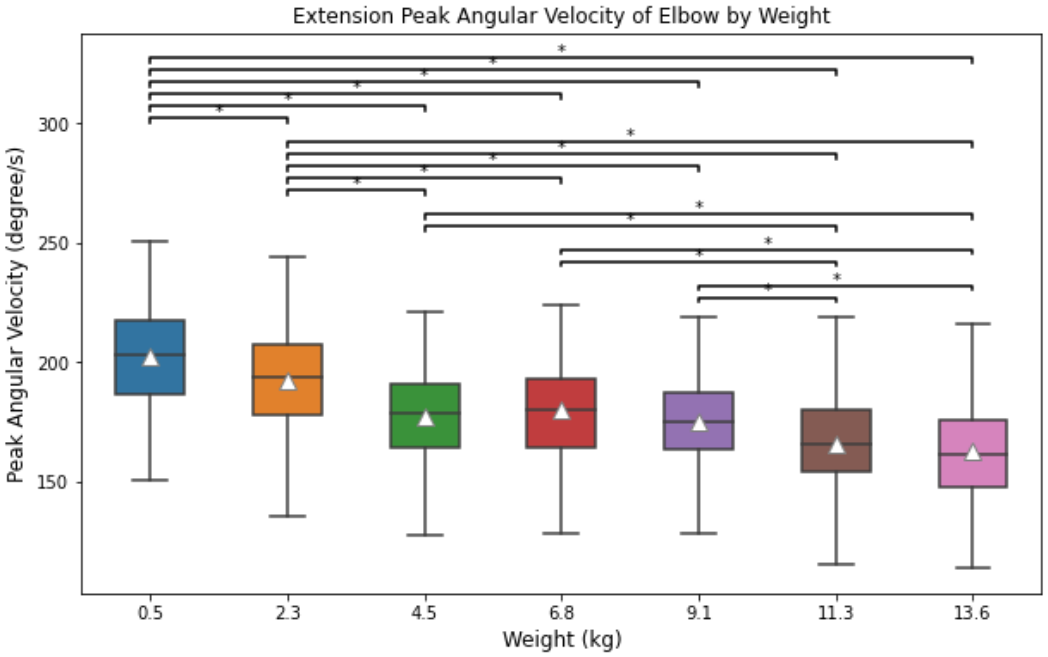

Figure 3.7: Peak elbow extension velocity at different lifting weights. (Note that * denotes a significant difference between two weights.)

Table 3.4: Results of mixed-factor ANOVA for average angular velocities. Cells entries are *F* values (*p* values).

Dependent Variable	Gender (G)	Lifting Height (LH)	Lifting Weight (LW)	G x LW	G x LH	LH x LW	G x LH x LW
Shoulder Flexion	1.296 (0.298)	**1128.301 (<.001)**	**84.399 (<.001)**	**3.55 (0.029)**	**4.726 (0.031)**	1.552 (0.229)	0.255 (0.995)
Shoulder Extension	**27.955 (0.002)**	**24.238 (<.001)**	**26.83 (<.001)**	**3.326 (0.036)**	**4.089 (0.044)**	1.459 (0.261)	0.466 (0.935)
Shoulder External Rotation	**46.8 (<.001)**	**795.559 (<.001)**	**34.772 (<.001)**	**4.663 (0.011)**	**63.284 (<.001)**	1.799 (0.161)	0.204 (0.998)
Shoulder Internal Rotation	**293.803 (<.001)**	**10.027 (0.003)**	**25.717 (<.001)**	1.003 (0.467)	1.756 (0.214)	2.293 (0.082)	0.8 (0.651)
Shoulder Abduction	**69.437 (<.001)**	**14.036 (<.001)**	**10.086 (0.016)**	2.496 (0.084)	**12.986 (<.001)**	0.781 (0.662)	0.543 (0.887)
Shoulder Adduction	**195.421 (<.001)**	**22.884 (<.001)**	31.315 (0.55)	0.257 (0.947)	**5.029 (0.026)**	0.938 (0.543)	0.997 (0.449)
Elbow Flexion	5.174 (0.063)	**46.176 (<.001)**	**47.031 (<.001)**	**10.855 (<.001)**	**10.947 (0.002)**	**5.882 (0.002)**	0.127 (1)
Elbow Extension	**64.337 (<.001)**	**7.967 (0.006)**	**29.763 (<.001)**	0.65 (0.69)	1.599 (0.242)	1.951 (0.131)	0.748 (0.705)

(a)

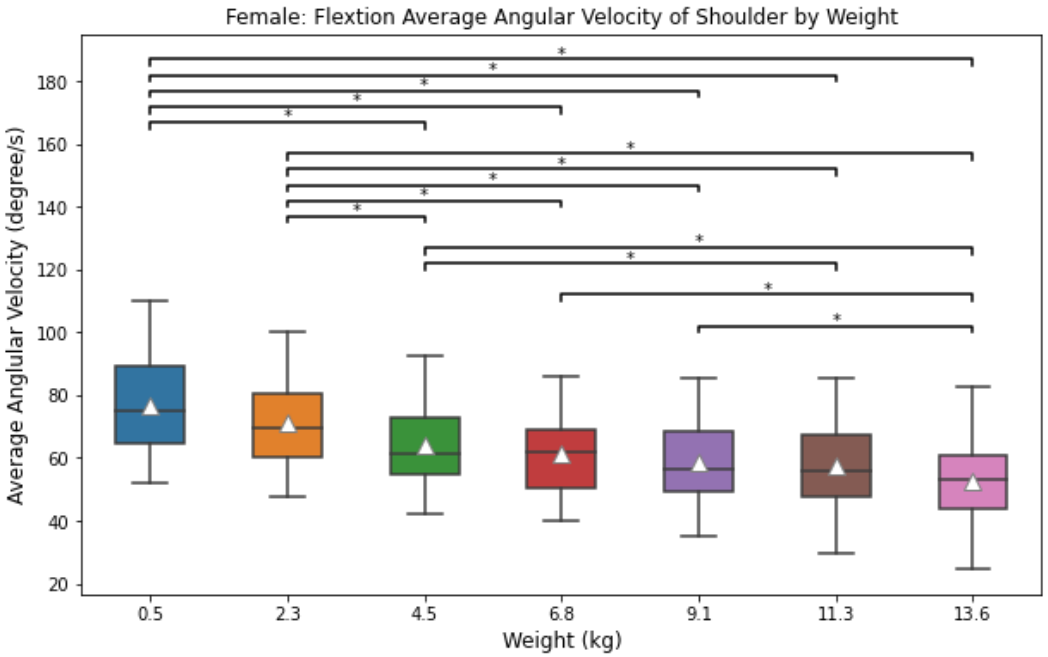

(b)

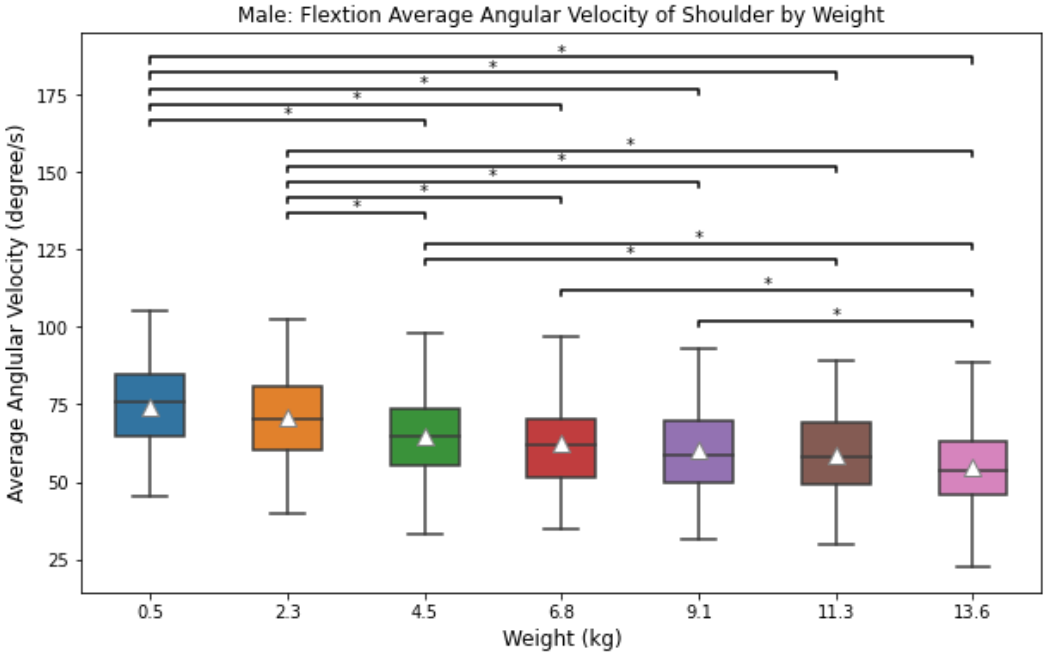

Figure 3.8: Average shoulder flexion velocity at different lifting weights for (a) female and (b) male. (Note that * denotes a significant difference between two weights.)

(a)

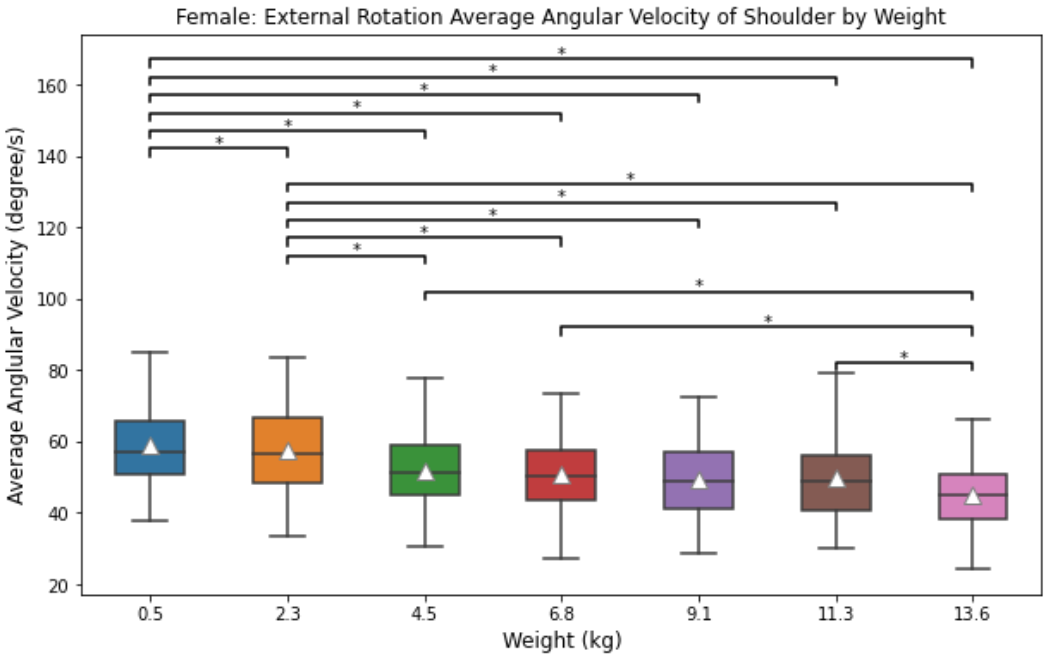

(b)

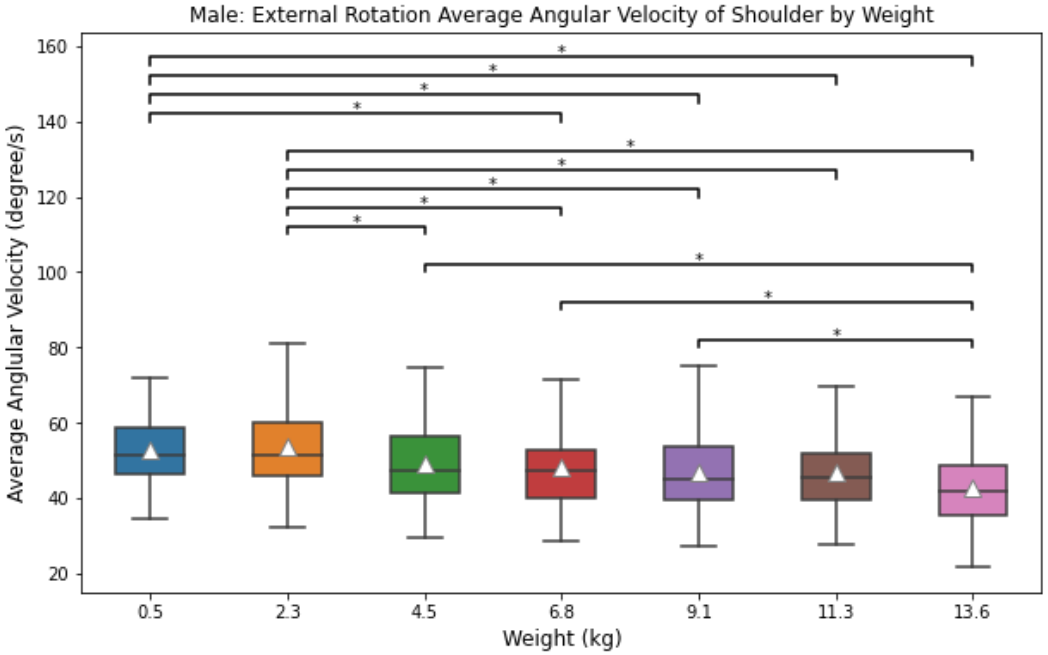

Figure 3.9: Average shoulder external rotation velocity at different lifting weights for (a) female and (b) male. (Note that * denotes a significant difference between two weights.)

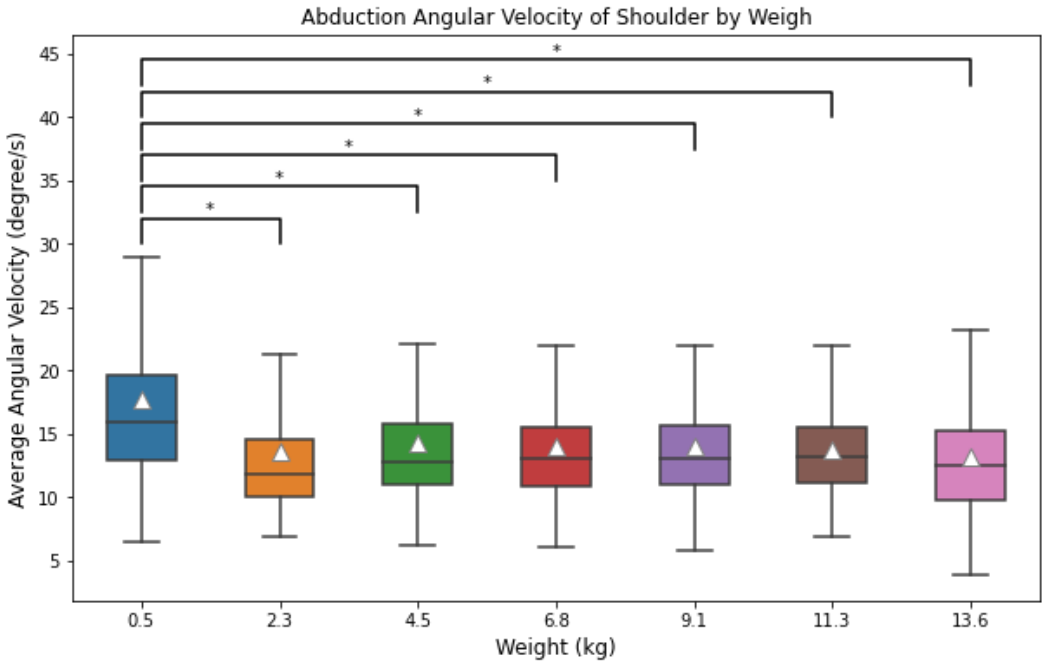

Figure 3.10: Average shoulder abduction velocity at different lifting weights. (Note that * denotes a significant difference between two weights.)

(a)

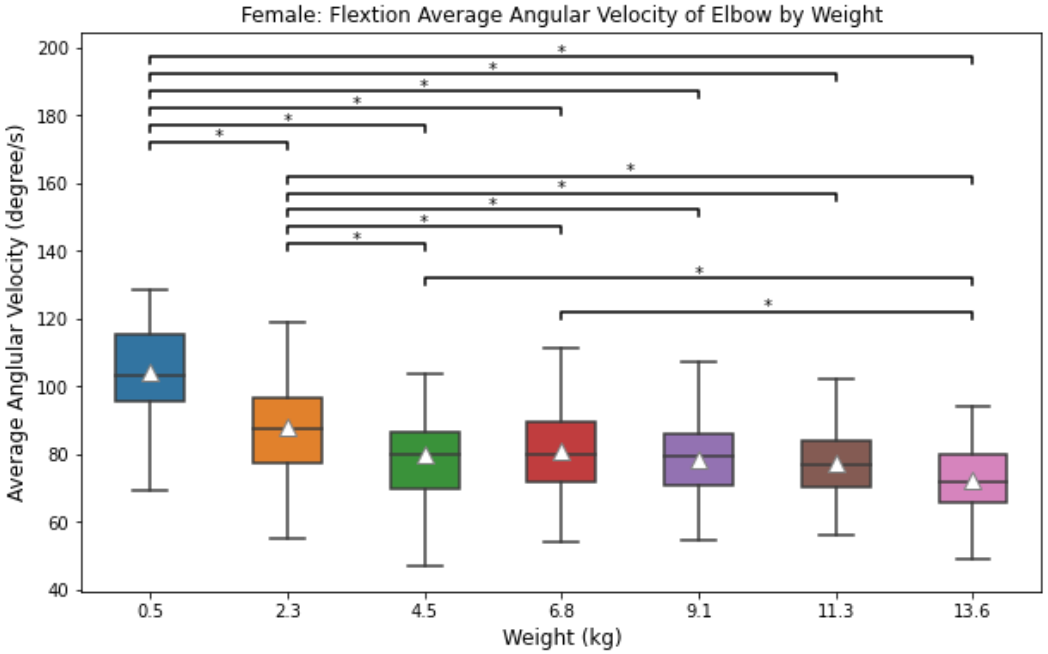

(b)

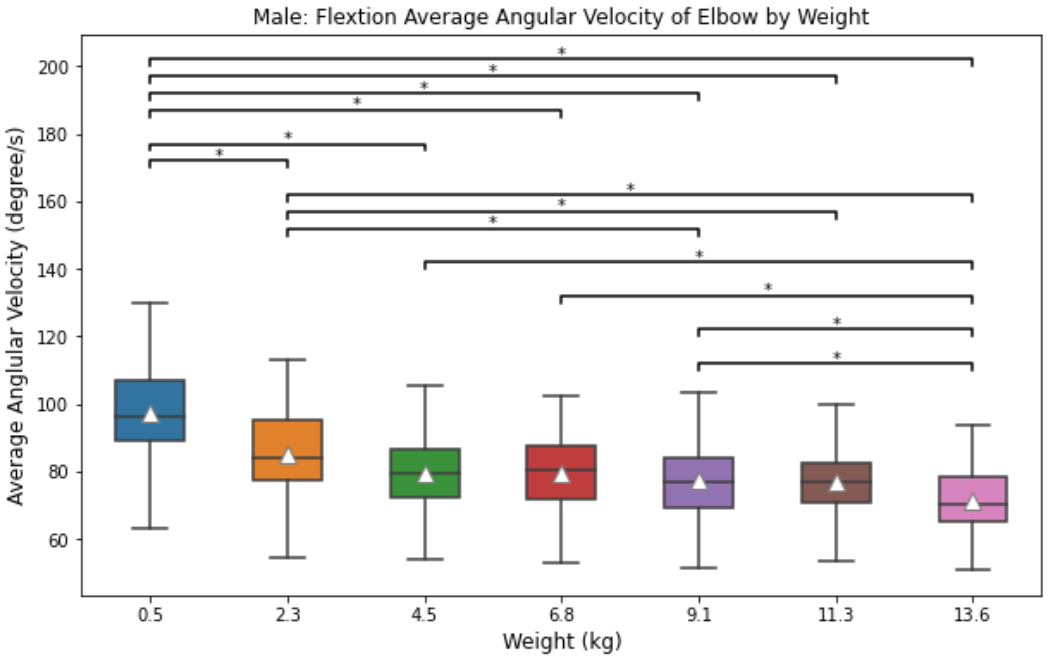

Figure 3.11: Average elbow flexion velocity at different lifting weights for (a) female and (b) male. (Note that * denotes a significant difference between two weights.)

(a)

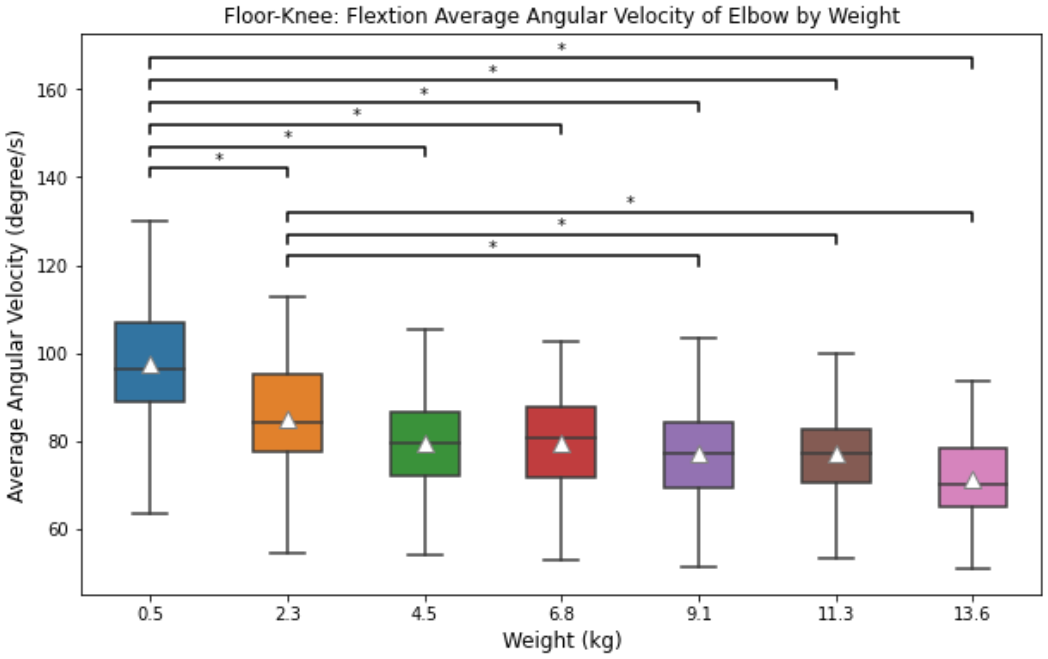

(b)

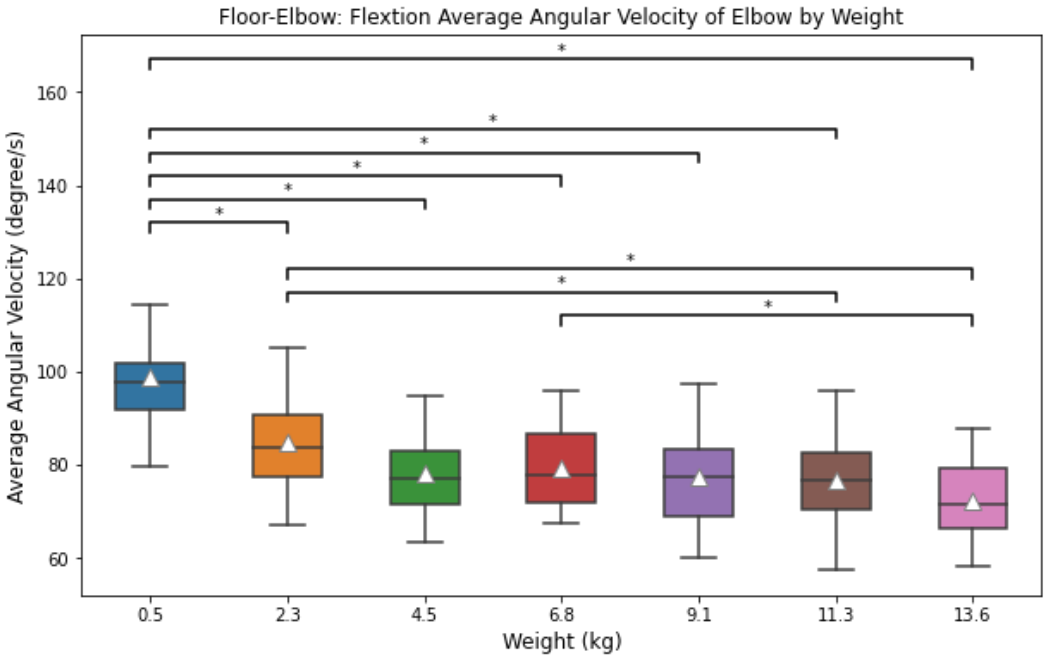

(c)

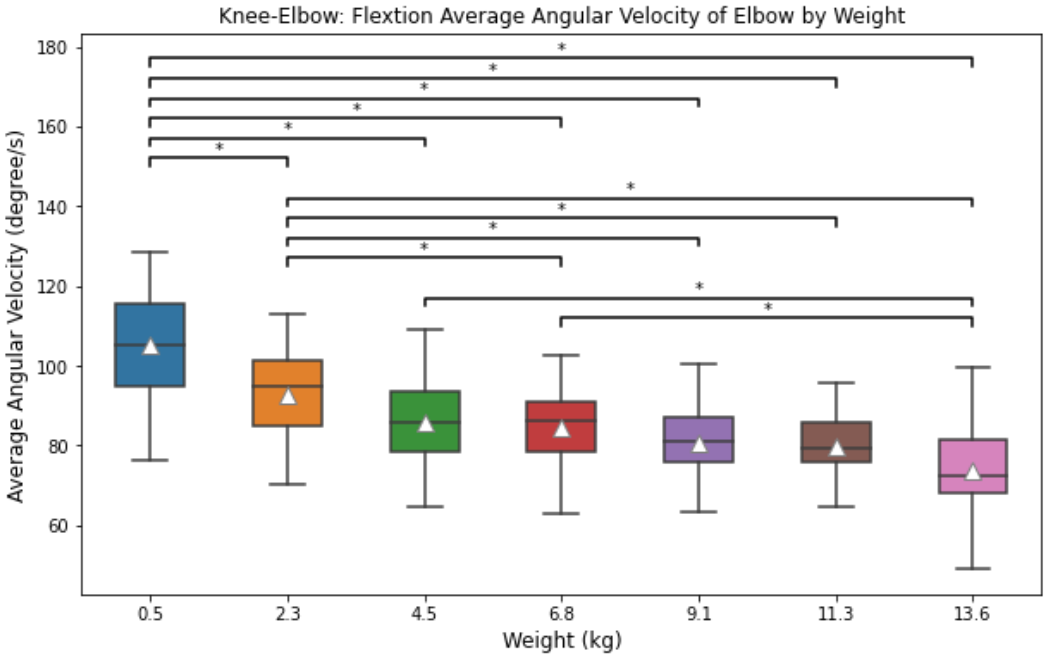

Figure 3.12: Average elbow flexion velocity at different lifting weights for lifting height (a) floor-knee, (b) floor-elbow, and (c) knee-elbow. (Note that * denotes a significant difference between two weights.)

(a)

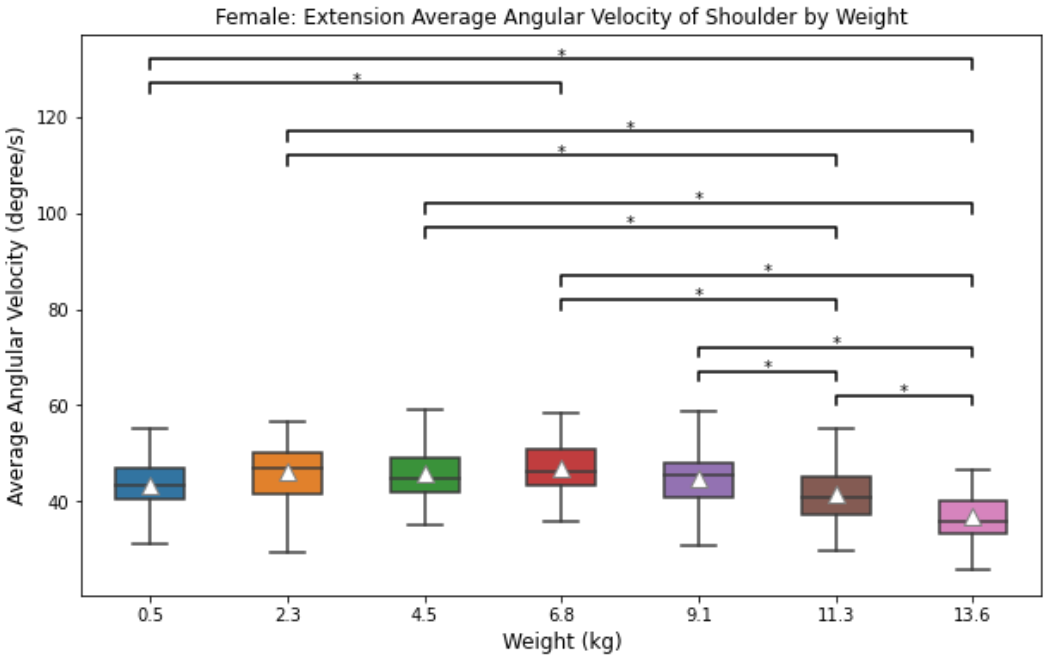

(b)

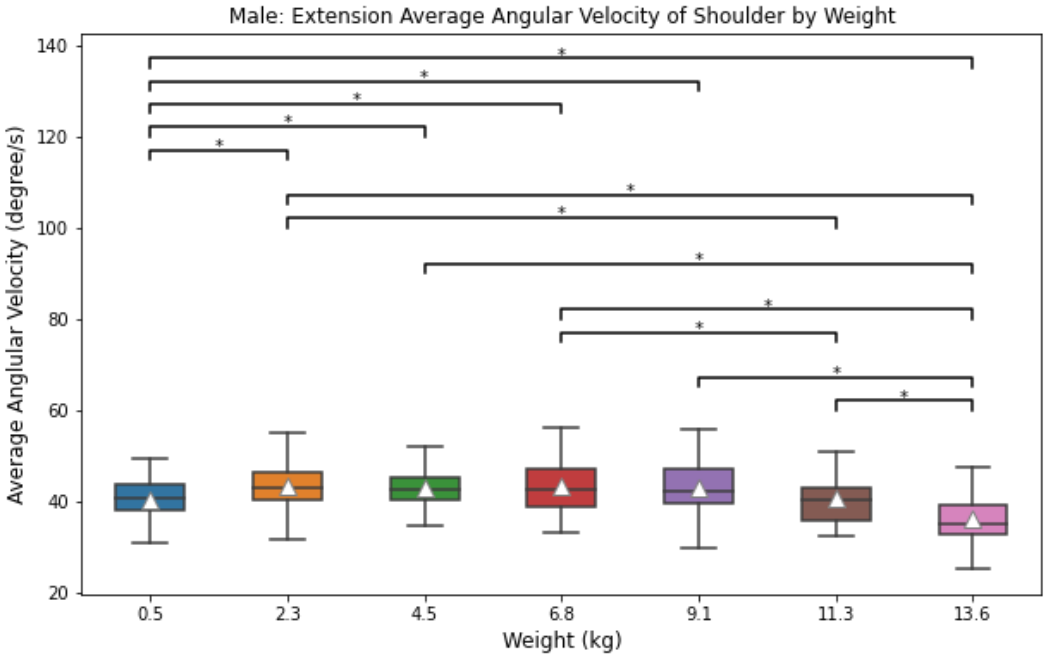

Figure 3.13: Average shoulder extension velocity at different lifting weights for (a) female and (b) male. (Note that * denotes a significant difference between two weights.)

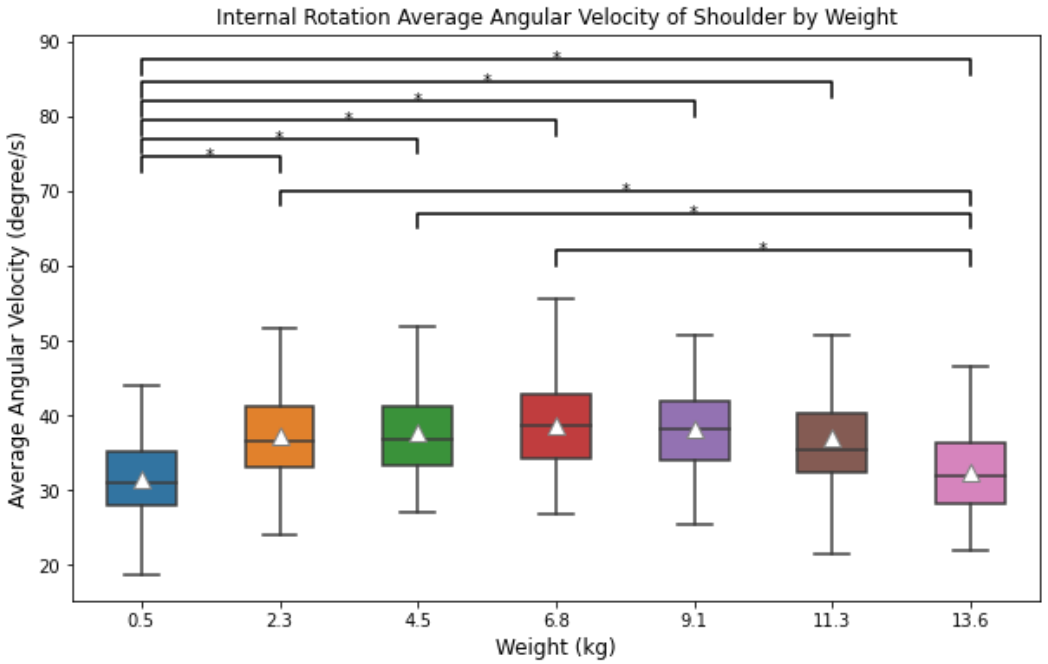

Figure 3.14: Average shoulder internal rotation velocity at different lifting weights. (Note that * denotes a significant difference between two weights.)

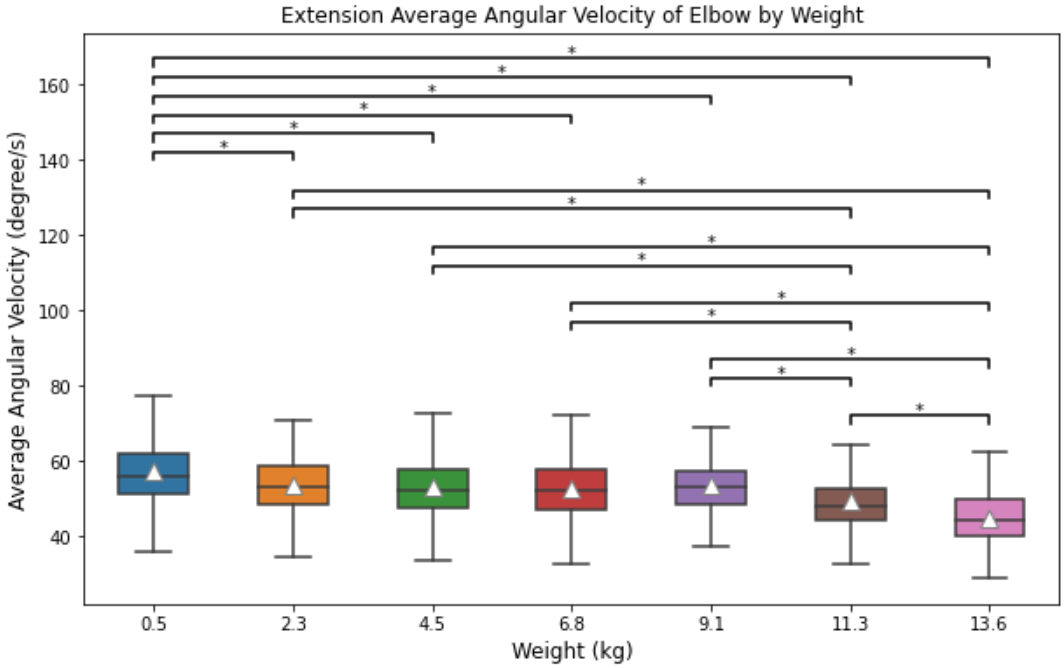

Figure 3.15: Average elbow extension velocity at different lifting weights. (Note that * denotes a significant difference between two weights.)

Table 3.5: Results of post-hoc comparison between genders at each lifting weight for average shoulder external rotation velocity. Note that * denotes a significant difference between females and males.

Weight (kg)	Gender	Mean	SD
0.5	F	59.17 *	12.09
	M	52.82*	9.62
2.3	F	57.56*	11.27
	M	53.62*	10.71
4.5	F	51.89*	10.97
	M	49.17*	10.86
6.8	F	50.78*	10.53
	M	47.97*	10.61
9.1	F	49.38*	9.76
	M	46.84*	10.97
11.3	F	49.98*	11.16
	M	46.66*	10.17
13.6	F	45.23*	9.50
	M	42.66*	10.11

Table 3.6: Results of post-hoc comparison between genders at each lifting weight for average shoulder extension velocity. Note that * denotes a significant difference between females and males.

Weight (kg)	Gender	Mean	SD
0.5	F	43.37*	5.66
	M	40.34*	5.47
2.3	F	46.10*	5.43
	M	43.36*	5.36
4.5	F	45.76*	5.79
	M	43.08*	4.74
6.8	F	46.91*	5.77
	M	43.17*	5.50
9.1	F	44.83	5.32
	M	43.10	5.92
11.3	F	41.32	5.96
	M	40.48	6.12
13.6	F	36.83	5.50
	M	36.01	5.55

3.3.3 Shoulder-Elbow Coordination

MARP was significantly affected by the main effect of lifting height, weight, and the interaction of gender and lifting height (Table 3.7). Pairwise comparisons were used to further study the significant differences in MARP caused by the main effect of lifting weight. An overall increased trend in MARP was observed as lifting weight increased (Figure 3.16), which indicated that the shoulder-elbow coordination was less synchronized overall, and their movement was less efficient as lifting weight increased. Furthermore, the results of pairwise comparisons indicated that the MARPs of the three lowest weights (0.5, 2.3, 4.5 kg) were significantly smaller than that of two highest weights (11.3, 13.6 kg) (Figure 3.16). To better illustrate the effect of lifting weight on the shoulder-elbow coordination pattern throughout the lifting cycle, we plotted an average curve of ensemble curves which was computed by aligning ensemble curves in time and then taking the mean value at each time point for each weight across all subjects (Figure 3.17). Comparing the CRP curves of the three lowest and two highest weights, all began with shoulder leading, with higher weights having higher CRP values indicating a less synchronized movement between shoulder and elbow. While progressing through the middle stage, elbow and shoulder were relatively synchronized for the three lowest weights. For the two highest weights, first the elbow was leading and then the relationship was reversed with shoulder leading. Toward the ending stage elbow was leading for all weights, with higher weights having higher absolute CRP values indicating a less synchronized movement between shoulder and elbow.

DP was significantly affected by the interaction of gender and lifting height and the interaction of gender and lifting weight (Table 3.7). For both female and male, increased lifting weights were generally associated with increased DP (Figure 3.18), indicating an overall less

consistent and more variable pattern of coordination with increased weights. The results of pairwise comparisons indicated the absence of any significant difference for male. For female, DPs of the two lowest weights (0.5, 2.3 kg) were significantly smaller than those of the two highest weights (11.3, 13.6 kg) (Figure 3.18). An average curve of ensemble curves was used to illustrate the interaction effects on the consistency pattern throughout the lifting cycle (Figure 3.19). Comparing the fluctuation of CRP curves for different weights, a wider range of fluctuation was observed throughout the lifting cycle with higher weights for female. The fluctuation ranges were relatively similar during the majority of the cycle between different weights for male.

Table 3.7: Results of mixed-factor ANOVA for MARP and DP. Cells entries are *F* values (*p* values).

Dependent Variable	Gender (G)	Lifting Height (LH)	Lifting Weight (LW)	G x LW	G x LH	LH x LW	G x LH x LW
MAPR	2.738 (0.149)	**82.351 (<.001)**	**6.942 (0.05)**	1.881 (0.166)	**4.215 (0.041)**	0.729 (0.704)	1.012 (0.437)
DP	4.369 (0.082)	**100.052 (<.001)**	3.469 (0.054)	**4.199 (0.017)**	**8.635 (0.005)**	1.997 (0.123)	0.5 (0.914)

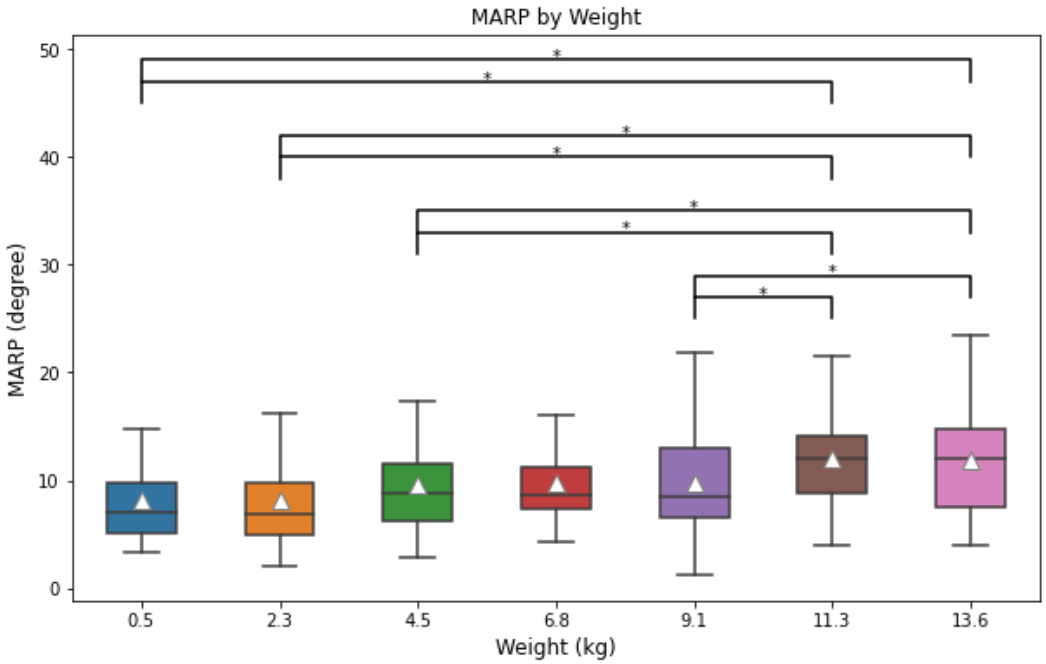

Figure 3.16: MARP at different lifting weights. (Note that * denotes a significant difference between two weights.)

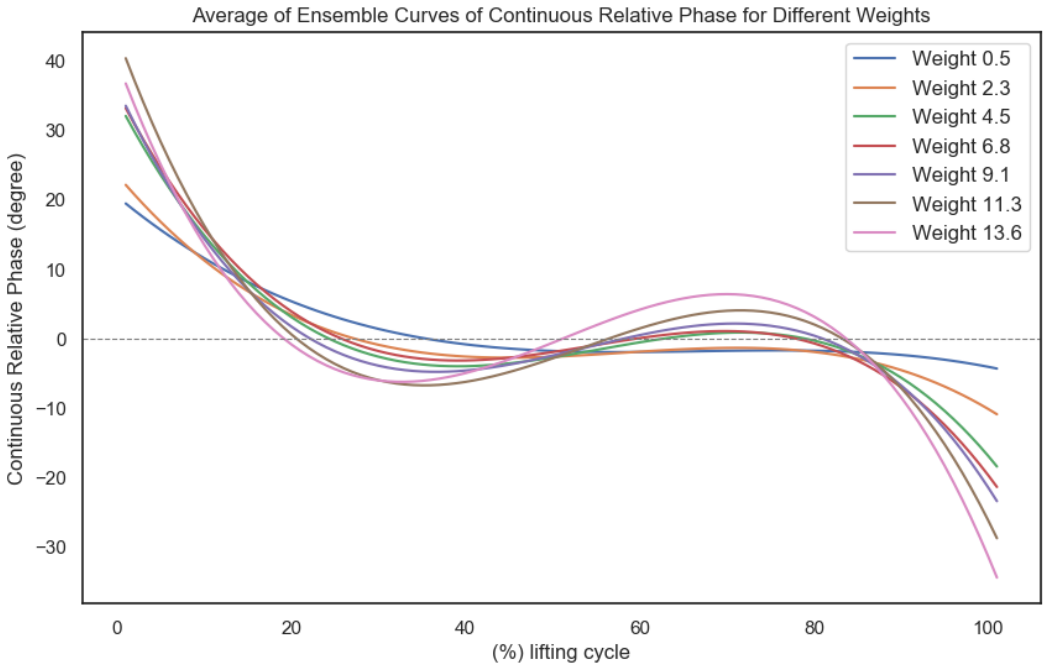

Figure 3.17: Average of ensemble curves of continuous relative phase for different weights. (Note that * denotes a significant difference between two weights.)

(a)

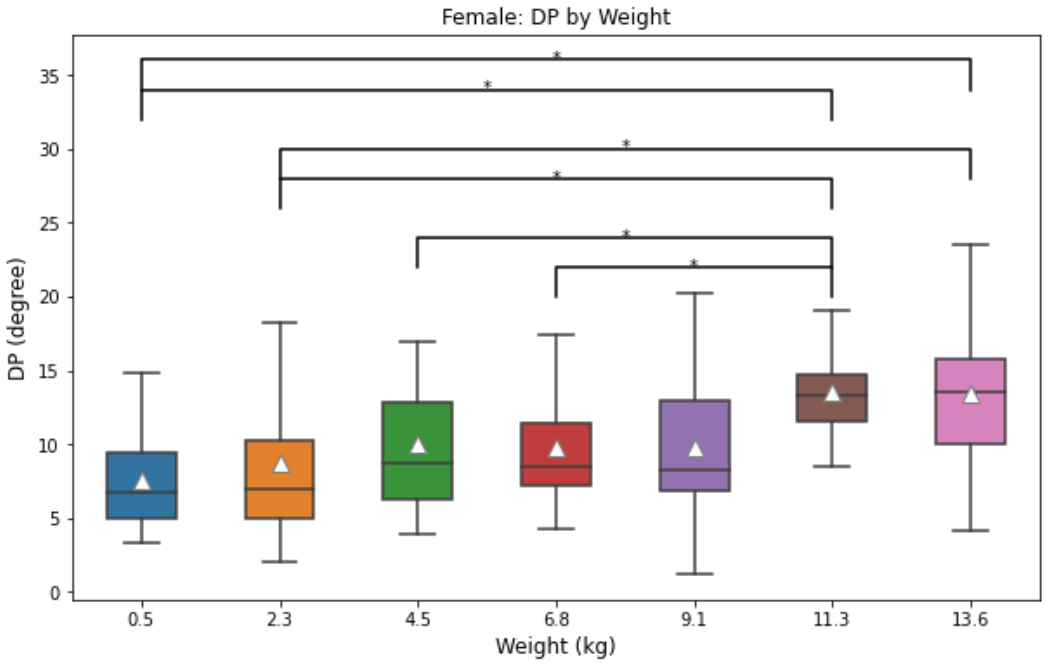

(b)

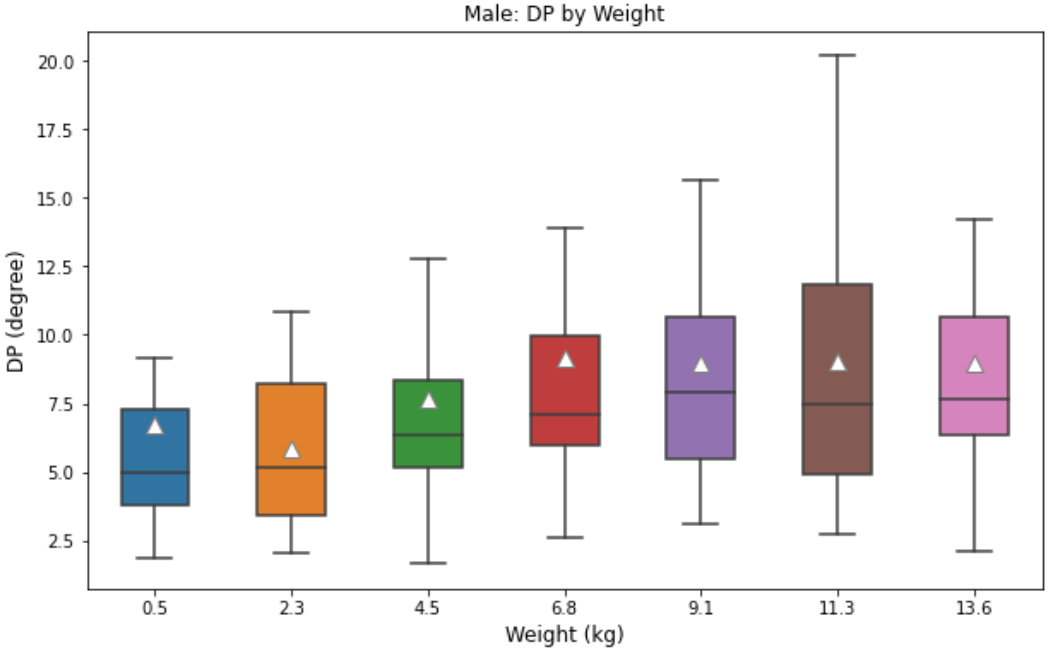

Figure 3.18: DP at different lifting weights for (a) female and (b) male. (Note that * denotes a significant difference between two weights.)

(a)

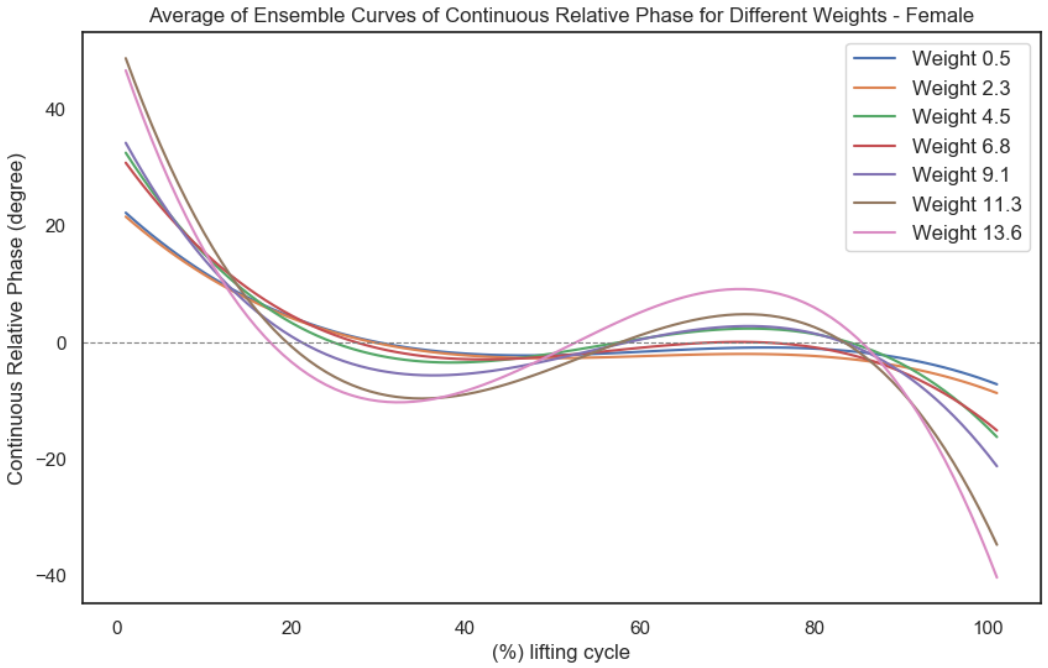

(b)

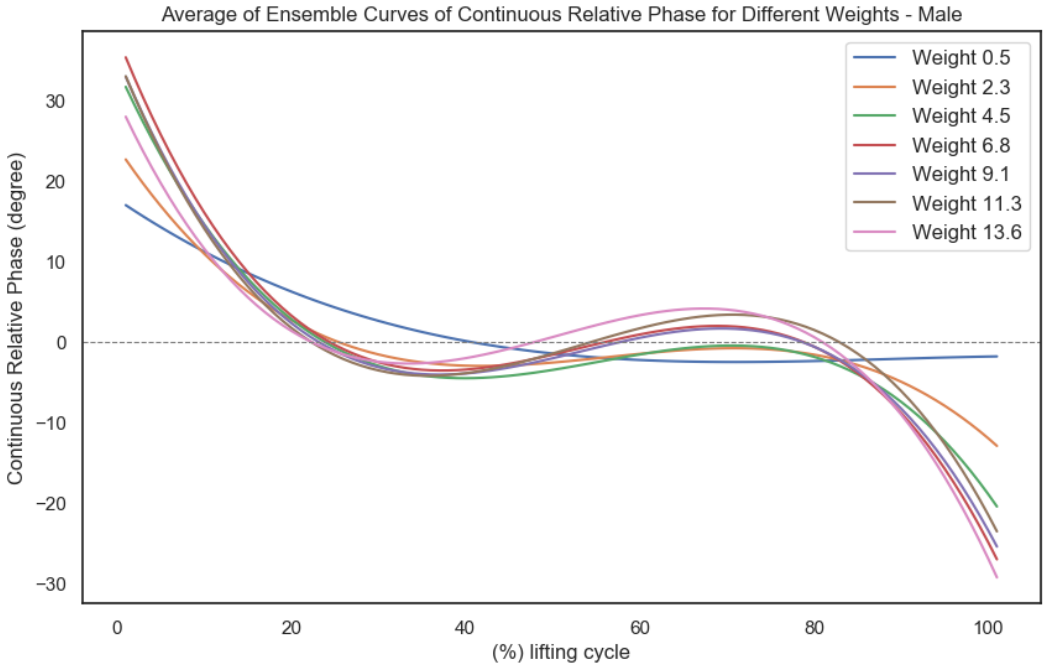

Figure 3.19: Average of ensemble curves of continuous relative phase for (a) female and (b) male. (Note that * denotes a significant difference between two weights.)

3.3.4 Between-Subjects and Within-Subjects Variations

For peak angular velocities, the variation intra-subjects was smaller than inter-subject variation (Table B1, Table B2 in Appendix B). Though the inter-subject variation varied in magnitude for different combinations of lifting height and weight, this variability was due to the inherent randomness in the data and not attributed to changes of lifting weight and height. Similar to inter-subject variation, there was no systematic variability in intra-subject variation for different combinations of lifting height and weight. The inter-subject CVs of each peak angular velocity were not substantially different, suggesting that the relative variability was consistent across these variables. This consistency was also found in intra-subject variation. While for average angular velocities, the inter-subject variation of shoulder abduction and adduction velocities was much higher than those of other average velocities (Table B3, Table B4 in Appendix B).

3.4 Discussion

The aim of this study was to investigate the effects of lifting weight on upper limb kinematics. It was hypothesized that shoulder and elbow kinematics would change as the level of lifting weights varies. Strong evidence was found to confirm the changing of the lifting weight impacts the peak and average angular velocities of shoulder and elbow, and shoulder-elbow coordination .

Shoulder flexion and elbow flexion typically occurred during the box-raising phase, in which concentric muscle contractions are used to counter the weight of the box. Subjects tended to reduce their peak and average shoulder flexion velocities with increased lifting weight. This is because lifting heavier weight requires more muscle force. This increased force requirement may lead to slower muscle concentric contractions, which tends to result in slower shoulder flexion.

Another reason could be the coactivation of antagonist muscles increased with higher lifting weights (Yoon et al., 2012), which leads to slower and more controlled shoulder flexion. In Davis & Marras, 2000, they demonstrated that decreased trunk velocity was associated with increased lifting weight, which could be a protective motion pattern (Davis & Marras, 2000). For elbow flexion, peak and average velocities decreased with increased lifting weight, however, the average velocity was not significantly different when lifting heavier than 4.5 kg, and peak velocity was not significantly affected by lifting weight. This may be because the elbow is weaker than the shoulder, causing subjects to rely more on their shoulder than the elbow to raise boxes heavier than 4.5 kg. Consequently, the main joint responsible for movement shifts from elbow to shoulder. Shoulder extension and elbow extension typically occurred during the box-placing phase, in which eccentric muscle contractions are responsible to lower or release the box. Shoulder average extension velocity significantly decreased at weight 11.3 and 13.6 kg for female and at 13.6 kg for male. The elbow average extension velocity was also significantly decreased at weight 11.3 and 13.6 kg. An explanation for this decreasing is placing heavier weights requires more control and stability to ensure proper form and prevent injury. To maintain control and stability, subjects tended to intentionally slow down the movement during heavy placements, reducing upper limb extension. In this study, the results indicated that there were gender-related differences in average shoulder extension velocity when lifting less than 9.1 kg, with higher velocity observed for females. It seemed that female might adopt different lifting strategies that prioritize velocity, especially when the weight is relatively light or moderate compared to their maximal capacity. The average shoulder extension velocity differences between female and male were no longer significant when lifting weights were heavier than 9.1 kg. This may be because females were closer to their maximal capacity and seemed to adapt their

kinematics by reducing velocities in response to increased weight. According to Stålhammar et al., 1989, females rated the acceptable loads as on average 8.8 kg, males on average 19 kg, in a lowering-lifting test. If this explains the kinematic adaptation in female, it would be expected that female's velocity would be lower than male's as lifting weight further increases. Moreover, our results showed that subjects did not change shoulder average external and internal rotation velocities if varying weight 4.5 – 11.3 kg. However, shoulder peak and average external rotation velocities of female were significantly different from male's during the box-raising phase. In a review conducted by Côté, 2012, it was reported that there may be indeed gender differences in movement strategies during upper limb tasks (Côté, 2012). Martinez et al., 2019 reported gender-related difference in upper limb kinematics during above shoulder lifting task. Previous studies have reported that some lifting kinematics were different between female and male, e.g., trunk motion, hip motion, knee angle (Davis et al., 2003; Lindbeck & Kjellberg, 2001; Martinez et al., 2019, 2020; Plamondon et al., 2017). Although a direct comparison with this study was not possible as different joints, these previous studies supported the findings obtained in this study that kinematic patterns of a lift task may be gender related.

Our results indicated that the shoulder-elbow coordination, described by MARP, significantly decreased when lifting weight was heavier than 9.1 kg. With the increased lifting weight, shoulder flexion/extension and elbow flexion/extension did not occur synchronously, and the out-of-phase magnitude was lifting weight dependent. No significant gender difference was found in the current study. Our finding was generally consistent with those in Martinez et al., 2019, who found that gender difference in upper limb coordination was not apparent when the lifting was lower than subject's shoulder height (Martinez et al., 2019). DP was used to measure the variability of the coordination relationship. Our results showed that the variability of

shoulder-elbow coordination for male subjects did not change significantly as lifting weight increased, while the relative phase fluctuations of female subjects increased significantly at weights heavier than 9.1 kg. This may be because female subjects were closer to their maximal capacity, which corresponds on average to 48%-61% of male's maximum (Plamondon et al., 2014, 2017). Other studies investigating lifting weight effect on variability of joint coordination focused on lower limb and trunk. For example, increased variability of knee-shoulder coordination was found 0%-30% maximum lifting capacity (MLC) for males (Scholz, 1993), and that of knee-hip and ankle-hip coordination at 30%-75% MLC (Scholz, 1993).

It was expected that the dependent variables would be less varied within subject than between subjects. The higher inter-subject variability could be a reflection of differences in individual characteristics such as age, anthropometry and gender. Another possible source was individual physical fitness such as muscular strength and flexibility which affect how the body moves and responds to physical demands. There was higher inconsistency between subjects in shoulder coronal average velocity. This was probably shoulder abduction/adduction involves a more complex movement pattern that requires shoulder stabilization and involvement of scapula rotation. Another reason may be shoulder abduction/adduction involves larger muscle groups and coordinating these muscles effectively can introduce variability.

3.5 Limitations

A few limitations should be noted. First, this study only investigated symmetric, two-handed lifting. The highest lifting height examined in the study was at elbow level, while higher height, such as shoulder height or overhead height, wasn't studied. Second, individuals with larger (BMI > 27.0) or smaller (BMI < 18.9) body size were underrepresented because they could not wear the tight suit required for accurate Xsens data collection. Third, we used

Bonferroni correction for the post-hoc analysis. But Bonferroni correction is known to be very conservative, which can increase Type II error rates, potentially overlooking significant effects (Cabin & Mitchell, 2000). Alternative methods, such as Holm method (Holm, 1979) or false discovery rate (FDR) (Benjamini & Hochberg, 1995), are less conservative and may potentially identify additional significant effects that the Bonferroni method may not detect.

3.6 Conclusion

The effects of lifting weight on upper extremity kinematics were explored during a laboratory study of a lifting task. This study found that lifting weight level had statistically significant effects on upper extremity kinematics, including peak angular velocity, average angular velocity and shoulder-elbow coordination. Other studies have reported significant effects of lifting weight on the kinematics of body segments and joints (Davis & Marras, 2000; Norasi et al., 2019; Plamondon et al., 2017; Song & Qu, 2014). Taken together, these findings serve as a foundation for subsequent studies using lifting kinematic variables to predict lifting weight.

3.7 References

Benjamini, Y., & Hochberg, Y. (1995). Controlling the False Discovery Rate: A Practical and Powerful Approach to Multiple Testing. *Journal of the Royal Statistical Society Series B: Statistical Methodology*, *57*(1), 289–300. https://doi.org/10.1111/j.2517-6161.1995.tb02031.x

Cabin, R. J., & Mitchell, R. J. (2000). To Bonferroni or Not to Bonferroni: When and How Are the Questions. *Bulletin of the Ecological Society of America*, *81*(3), 246–248.

Côté, J. N. (2012). A critical review on physical factors and functional characteristics that may explain a sex/gender difference in work-related neck/shoulder disorders. *Ergonomics*, *55*(2), 173–182. https://doi.org/10.1080/00140139.2011.586061

Davis, K. G., Jorgensen, M. J., & Marras, W. S. (2000). An investigation of perceived exertion via whole body exertion and direct muscle force indicators during the determination of the maximum acceptable weight of lift. *Ergonomics*, *43*(2), 143–159. https://doi.org/10.1080/001401300184521

Davis, K. G., & Marras, W. S. (2000). Assessment of the Relationship between Box Weight and Trunk Kinematics: Does a Reduction in Box Weight Necessarily Correspond to a Decrease in Spinal Loading? *Human Factors: The Journal of the Human Factors and Ergonomics Society*, *42*(2), 195–208. https://doi.org/10.1518/001872000779656499

Davis, K. G., Splittstoesser, R. E., & Marras, W. S. (2003). Kinematic contribution and synchronization of the trunk, hip, and knee during free-dynamic lifting. *Occupational Ergonomics*, *3*(2), 99–108. https://doi.org/10.3233/OER-2003-3202

El-Gohary, M., & McNames, J. (2012). Shoulder and Elbow Joint Angle Tracking With Inertial Sensors. *IEEE Transactions on Biomedical Engineering*, *59*(9), 2635–2641. https://doi.org/10.1109/TBME.2012.2208750

Grood, E. S., & Suntay, W. J. (1983). A Joint Coordinate System for the Clinical Description of Three-Dimensional Motions: Application to the Knee. *Journal of Biomechanical Engineering*, *105*(2), 136–144. https://doi.org/10.1115/1.3138397

Hamill, J., van Emmerik, R. E. A., Heiderscheit, B. C., & Li, L. (1999). A dynamical systems approach to lower extremity running injuries. *Clinical Biomechanics*, *14*(5), 297–308. https://doi.org/10.1016/S0268-0033(98)90092-4

Holm, S. (1979). A Simple Sequentially Rejective Multiple Test Procedure. *Scandinavian Journal of Statistics*, *6*(2), 65–70.

Kjellberg, K., Lindbeck, L., & Hagberg, M. (1998). Method and performance: Two elements of work technique. *Ergonomics*, *41*(6), 798–816. https://doi.org/10.1080/001401398186658

Lee, R. Y. W., Laprade, J., & Fung, E. H. K. (2003). A real-time gyroscopic system for three-dimensional measurement of lumbar spine motion. *Medical Engineering & Physics*, *25*(10), 817–824. https://doi.org/10.1016/S1350-4533(03)00115-2

Lee, T.-H. (2015). The effects of load magnitude and lifting speed on the kinematic data of load and human posture. *International Journal of Occupational Safety and Ergonomics*, *21*(1), 55–61. https://doi.org/10.1080/10803548.2015.1017956

Li, K., & Zhang, X. (2009). Can Relative Strength Between the Back and Knees Differentiate Lifting Strategy? *Human Factors: The Journal of the Human Factors and Ergonomics Society*, *51*(6), 785–796. https://doi.org/10.1177/0018720809360801

Lindbeck, L., & Kjellberg, K. (2001). Gender differences in lifting technique. *Ergonomics*, *44*(2), 202–214. https://doi.org/10.1080/00140130120142

Marras, W. S., Davis, K. G., & Jorgensen, M. (2003). Gender influences on spine loads during complex lifting. *The Spine Journal*, *3*(2), 93–99. https://doi.org/10.1016/S1529-9430(02)00570-3

Martinez, R., Assila, N., Goubault, E., & Begon, M. (2020). Sex differences in upper limb musculoskeletal biomechanics during a lifting task. *Applied Ergonomics*, *86*, 103106. https://doi.org/10.1016/j.apergo.2020.103106

Martinez, R., Bouffard, J., Michaud, B., Plamondon, A., Côté, J. N., & Begon, M. (2019). Sex differences in upper limb 3D joint contributions during a lifting task. *Ergonomics*, *62*(5), 682–693. https://doi.org/10.1080/00140139.2019.1571245

Norasi, H., Koenig, J., & Mirka, G. A. (2019). The effects of load weight and load starting height on variability of lifting kinematics and kinetics. *International Journal of Industrial Ergonomics*, *73*, 102830. https://doi.org/10.1016/j.ergon.2019.102830

Picerno, P., Cereatti, A., & Cappozzo, A. (2008). Joint kinematics estimate using wearable inertial and magnetic sensing modules. *Gait & Posture*, *28*(4), 588–595. https://doi.org/10.1016/j.gaitpost.2008.04.003

Plamondon, A., Larivière, C., Denis, D., Mecheri, H., & Nastasia, I. (2017). Difference between male and female workers lifting the same relative load when palletizing boxes. *Applied Ergonomics*, *60*, 93–102. https://doi.org/10.1016/j.apergo.2016.10.014

Plamondon, A., Larivière, C., Denis, D., St-Vincent, M., & Delisle, A. (2014). Sex differences in lifting strategies during a repetitive palletizing task. *Applied Ergonomics*, *45*(6), 1558–1569. https://doi.org/10.1016/j.apergo.2014.05.005

Robert-Lachaine, X., Mecheri, H., Larue, C., & Plamondon, A. (2017). Validation of inertial measurement units with an optoelectronic system for whole-body motion analysis. *Medical & Biological Engineering & Computing*, *55*(4), 609–619. https://doi.org/10.1007/s11517-016-1537-2

Schall, M. C., Fethke, N. B., Chen, H., Oyama, S., & Douphrate, D. I. (2016). Accuracy and repeatability of an inertial measurement unit system for field-based occupational studies. *Ergonomics*, *59*(4), 591–602. https://doi.org/10.1080/00140139.2015.1079335

Scholz, J. P. (1993). Organizational principles for the coordination of lifting. *Human Movement Science*, *12*(5), 537–576. https://doi.org/10.1016/0167-9457(93)90004-9

Song, J., & Qu, X. (2014). Effects of age and its interaction with task parameters on lifting biomechanics. *Ergonomics*, *57*(5), 653–668. https://doi.org/10.1080/00140139.2014.897376

Stålhammar, H. R., Troup, J. D. G., & Leskinen, T. P. J. (1989). Rating of acceptable loads: Lifting with and without handles. *International Journal of Industrial Ergonomics*, *3*(3), 229–234. https://doi.org/10.1016/0169-8141(89)90022-X

Stergiou, N., Jensen, J. L., Bates, B. T., Scholten, S. D., & Tzetzis, G. (2001). A dynamical systems investigation of lower extremity coordination during running over obstacles. *Clinical Biomechanics*, *16*(3), 213–221. https://doi.org/10.1016/S0268-0033(00)00090-5

Yoon, J., Shiekhzadeh, A., & Nordin, M. (2012). The effect of load weight vs. Pace on muscle recruitment during lifting. *Applied Ergonomics*, *43*(6), 1044–1050. https://doi.org/10.1016/j.apergo.2012.03.004

Chapter 4

A Transformer-Based Model for Lifting Load Recognition

4.1 Introduction

Estimation of the loads experienced in activities, such as lifting and carrying, is useful in many circumstances. In ergonomics, monitoring hand-handled loads can help identify and prevent excessive exertion. Repetitive manual handling of excessive weight can pose immediate risks of injury or long-term MSDs to workers and is a significant ergonomic concern. For example, workers in retail and distribution center centers are often involved in handling a wide range of boxes and packages. By monitoring hand-handled weight, high-risk tasks related to excessive exertion can be identified, and appropriate interventions can be implemented. Human-robot collaboration systems may benefit from tracking the load weight being handled, enabling robots to provide additional assistance if a human worker encounters an object that exceeds their safe handling capacity. In addition, with weight estimation, wearable devices like exoskeletons can adjust the level of support provided to the user, which ensures that the device offers enough support to reduce strain without overburdening or restricting the user's natural movement.

Previous studies have demonstrated the feasibility of using data regarding human motion and posture (e.g., velocity, acceleration, displacement, angular rotations and angles) of to assess risks associated with manually handled activities (, such as carrying), by for predicting the weight of carried loads (Goršič et al., 2020; H. Lee et al., 2020; Lim & D'Souza, 2019; Yang et al., 2020). These studies leveraged fact that human movement and posture kinematic measures, such as gait parameters, segment displacement, joint angles, etc., change in response to the weight of the objects they are carrying (Caderby et al., 2013; Fowler et al., 2006; LaFiandra et al., 2003; Qu & Yeo, 2011). For instance, Yang et al., 2020 classified different load-carrying

levels (0 kg, 3.8 kg, 7.6 kg and 11.4 kg) using kinematics of lower body movement with a bidirectional long short-term memory (BiLSTM) model (Hochreiter & Schmidhuber, 1997; Schuster & Paliwal, 1997), and achieved an overall accuracy of 0.986, 0.864 and 0.746 for 2-level, 3-level and 4-level classification, respectively. H. Lee et al., 2020 explored the utilization of a model consisting of Convolutional Neural Network (CNN) and long short-term memory (-LSTM) modulesdel and kinematics derived specifically from ankles and waist to detect three levels of carried weight (0.2 kg, 13.6 kg and 24 kg) alongside two load-carrying postures (two-hand and one-shoulder). The two studies implemented LSTM network (Gers et al., 2002; Hochreiter & Schmidhuber, 1997), a type of Recurrent Neural Networks (RNNs) designed for processing sequential data, to predict load weights from time series kinematic data derived from carrying activities. This deep learning approach circumvents the necessity for manual feature engineering, directly extracting and learning relevant features from the temporal sequences of kinematic data. Concurrently, there are studies employing traditional machine learning techniques for the prediction of carried load weights. These methods require explicit engineering of features, necessitating the handcrafting of relevant features from raw data to effectively train and develop predictive models. Using statistical features parameters (e.g., mean and variance) extracted from time series joint angle data, Goršič et al., 2020 trained a multiple linear regression (REG) classifier to detect balanced and, unbalanced loads with a weight difference of < 9 kgs (or < 4.5 kgs), and unbalanced with a weight difference of > 9 kgs (or > 4.5 kgs) in carrying tasks. In Lim & D'Souza, 2019, a set of gait parameters was engineered based on domain-specific knowledge. A classifier, based on a random forest algorithm, was then developed to discern four carrying modes as well as two levels of carrying weight (e.g., 50% and 75% of the subject's

maximum acceptable weight of carry). In these studies, machine learning models were employed to recognize kinematic patterns and correlate them with the weight of the carried loads.

On the other hand, a limited number of studies have investigated the application of machine learning techniques, with input features describing human motion and posture, to identify different levels of loads being lifted lifting load weights. G. Zhou et al., 2022 investigated the application of both traditional machine learning and deep learning techniques for the purpose of identifying different levels of the NIOSH Lifting Index (LI) by solely altering the lifting load weight. Their results demonstrated that the LSTM-based deep learning approach, utilizing kinematic data from lifting activities, outperformed traditional machine learning methods, achieving an accuracy of 0.878 in binary classification tasks and 0.702 in three-level classification tasks. Y. Li et al., 2020 used a deep learning method, specifically 1D Convolutional Neural Network (CNN), to discern light (26.7 N – 53.4 N), medium (53.4 N – 106.8 N), and heavy lifting (106.8 N – 133.4 N) loads. However, the achieved accuracy of the model was low, standing between 0.397 and 0.551.

Despite the previous work in classifying various levels of lifting load weight, there remains a critical need for a model that achieves better-improved accuracy. In this study, we attempt to improve the accuracy of lifting weight recognition via a transformer-based model. Particularly, a BiLSTM-Transformer Encoder structure is proposed for lifting weight recognition. The Transformer encoder is a part of the Transformer (Vaswani et al., 2017) architecture. The Transformer model proposed by Vaswani et al. (Vaswani et al., 2017) was shown to outperform CNN s and RNNs (e.g., LSTMs) in tasks requiring understanding long-range dependencies in sequence data, such as natural language modeling, machine translation, and text summarization, and achieved state-of-the-art performance (Devlin et al., 2018; Liu &

Lapata, 2019; Radford et al., 2018; Vaswani et al., 2017). Transformers have also been used with sequence sensor data or video frames for human activity recognition (Shavit & Klein, 2021; Wensel et al., 2022). A transformer encoder takes an input sequence and considers all parts of the input sequence simultaneously, while BiLSTM processes sequential data in temporal order (Schuster & Paliwal, 1997). Integrating a Transformer Encoder with a BiLSTM layer may be potentially complementary. By combining the two components, we present a joint model for lifting weight classification. Our contribution is fourfold: 1) We proposed the BiLSTM-Transformer Encoder model structure. 2) Comparing with an LSTM model, we showed that the joint model can effectively improve the accuracy of LSTM models used in previous work on classifying lifting load weight. 3) To visualize important features in predictions, Integrated Gradients was employed. 4) We explored using data from both full-body and half-body sensor configurations for lifting weight recognition.

4.2 Methods

4.2.1 Participants, Simulated Lifting Task, and Data

The data used in the current study were obtained in the previous chapter of a prior study in which only the first three lifts of each combination of lifting weight and height were evaluated. Thus, details were only summarized here. A total of 18 gender-balanced participants from the local university and community completed the study. The participants moved a weighted box with the dimensions of 46.3 × 31.3 × 11.2 cm (length × width × height) from floor or knee height and placed it on a shelf at elbow height. The box weights evaluated in this study were in a range ranged between 0.5 and 13.8 kg. Participants were asked to perform each lifting using self-selected comfortable styles and speed. Each participant performed six lifting trials for each combination of lifting height and weight in random order. The whole-body motion of lifting

activity was captured using a commercial IMU system (MVN Awinda, Xsens Technologies B.V., Enschede, Netherlands), which were sampled at 60 Hz. Whole-body segment kinematics were used as inputs, including time-series three-dimensional acceleration and angular velocity of head, trunk, pelvis, shoulders, upper arms, forearms, hands, upper legs, lower legs and feet (Figure 4.1). Figure 4.1 showed the origins of these segments with the corresponding coordinate systems, which followed the Xsens guidelines (Xsens Technologies B.V., 2021). These 102 Kinematic data were used as input features in the machine learning models. In addition, previous studies have demonstrated that angular velocities and accelerations of trunk and hip changed with lifting weight levels (Davis & Marras, 2000; Song & Qu, 2014). In the previous chapter, analysis showed that the kinematics and coordination of shoulder and elbow were affected by the varying lifting weight. Building on these findings data, we also used three-dimensional acceleration and angular velocity from 8 segments including trunk, pelvis, upper arms, forearms, and upper legs. Each participant finished 126 lifts with different load levels. Data from one participant was removed due to equipment failure. In total, 2142 lifts were completed by the participants in the experiment. All lifts were categorized into 4 levels based on lifting weights defined as class 0: 0.5 kg, class 1: 2.3 ~ 4.5 kg, class 2: 6.8 ~ 9.1 kg, class 3: 11.3 ~ 13.6 kg. To reduce noise and variability in the sequence data, a 5-frame moving average window was applied to the accelerations and angular velocities. Different window sizes were experimented with, and a moving window spanning 5 frames resulted in optimal performance. To address the variability in lengths of the lifting sequence data, an interpolation technique was implemented to standardize the sequences to have the same lengths equal to 109 frames which was the median length of the data. Min-max normalization was applied within each individual sequence individually to scale the data to the range of [0, 1]. This sequence-wise scaling allowed the

model to learn from the pattern and progression of lifting actions at different lifting weights, mitigating the variability introduced by individual subject's characteristics.

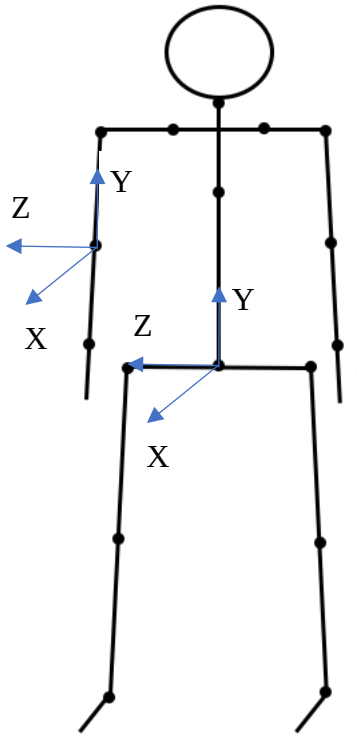

•: Segment Origin

Figure 4.1: Whole-body segments and examples of coordinates

4.2.2 Models

1. BiLSTM Model

A BiLSTM (Schuster & Paliwal, 1997) is an extension of LSTM (Hochreiter & Schmidhuber, 1997), which processes sequential data in both forward and backward directions. For a sequence of inputs $X = (x_1, x_2, \ldots, x_T)$ with length T, LSTM processes data step by step from the beginning of the sequence x_1 to the end x_T. At each time step, LSTM produces a cell state vector C_t , $C_t \in \mathbb{R}^H$, and hidden state vector h_t, $h_t \in \mathbb{R}^H$, based on the current input information and its previous states. Specifically, the cell state at time t, C_t, is obtained by

$$C_t = f_t \cdot C_{t-1} + i_t \cdot g_t ,$$

$$f_t = \sigma(W_f \cdot [h_{t-1}, x_t] + b_f),$$

$$i_t = \sigma(W_i \cdot [h_{t-1}, x_t] + b_i),$$

$$g_t = tanh(W_g \cdot [h_{t-1}, x_t] + b_g),$$

Where σ is the sigmoid function, *W* and *b* are the weights and biases. And the hidden state at time *t*, h_t, is obtained by

$$h_t = o_t \cdot tanh(C_t),$$

$$o_t = \sigma(W_o \cdot [h_{t-1}, x_t] + b_o),$$

Where *W* and *b* are the weights and biases.

For each LSTM layer *l* (*l = 1, 2, ..., L*), the hidden states $H_l = (h_1^l, h_2^l, \dots, h_T^l)$, $h_t^l \in \mathbb{R}^H$ are obtained and passed as input to the next layer where the sequence is processed from h_1^l to h_T^l. A BiLSTM consists of a forward LSTM and a backward LSTM that are run in parallel. Forward LSTM processes the input sequence from the start x_1 to the end x_T just like a standard LSTM, while Backward LSTM processes the input sequence from the end x_T to the start x_1. Each BiLSTM layer produces the hidden states $H_{forward}^l = (h_{forward,1}^l, h_{forward,2}^l, \dots, h_{forward,T}^l)$, $h_{forward,t}^l \in \mathbb{R}^H$ from the forward direction and the hidden states $H_{backward}^l = (h_{backward,1}^l, h_{backward,2}^l, \dots, h_{backward,T}^l)$, $h_{backward,t}^l \in \mathbb{R}^H$ from the backward direction. Before being passed to the next layer, the hidden states $H_{forward}^l$ and $H_{backward}^l$ are combined usually by concatenation, addition or a fully-connected layer. This study uses concatenation. The concatenated hidden states at BiLSTM layer *l*, $H_{BiLSTM}^l = (h_{BiLSTM,1}^l, h_{BiLSTM,2}^l, \dots, h_{BiLSTM,T}^l)$ where $h_{BiLSTM,t}^l \in \mathbb{R}^{2H}$, are then passed to the next layer. For the last BiLSTM layer *L*, only the concatenated hidden states from the final time step are used as input to a fully connected layer which is followed by a softmax layer for multi-class lifting weight recognition.

2. BiLSTM-Transformer Encoder Model

Originally developed for natural language processing (NLP), the transformer model consists of an encoder and decoder, which are based on the self-attention mechanism (Vaswani et al., 2017). The encoder takes an input sequence and maps it to a sequence of continuous representations that contain the combined information of the input sequence, while the decoder predicts an output sequence based on the encoder's output. We make use of the encoder architecture as shown in Figure 4.21. The encoder consists of a stack of blocks, with each block having a multi-head self-attention mechanism and a fully connected feed-forward network each of which is followed by a residual connection and layer normalization. The outputs of the encoder are aggregated into a single representation by mean pooling across all timesteps before being sent to the linear layers for classification. In (Vaswani et al., 2017), positional encoding is employed to capture the order of the sequence. However, we opted to use a BiLSTM layer to capture the sequential dependencies in the data. As shown in Figure 4.2, a BiLSTM layer is first used to process the data to learn the temporal patterns. The input sequence is fed into and processed by a forward and backward LSTM layer, and their outputs at each timestep are concatenated before being passed on to the encoder. For this joint model, if the number of hidden units from each LSTM layer is H, the BiLSTM layer outputs 2H-d vectors, and therefore the encoder takes 2H-d vectors as input.

4.2.3 Hyperparameter Optimization

Random search was used to find the best hyperparameters. For the BiLSTM model, a searching space was defined for each hyperparameter as follows:

1) learning rate: (10^{-5}, 10^{-2})
2) dropout rate: (0.1, 0.5)
3) batch size: [8, 16, 32, 64]

4) number of BiLSTM layers: (1, 5)

5) number of hidden units: [32, 64, 128, 256]

For the BiLSTM-Transformer Encoder model, we used the same searching space as BiLSTM for learning rate, dropout rate, batch size, and the number of hidden units for the single BiLSTM layer, while two additional hyperparameters were searched:

1) number of transformer encoder block: (1, 5)

2) number of attention head: [2, 4, 8]

The hyperparameter optimization process involved 50 trials, with each trial trained for up to 50 epochs. Early stopping was implemented when validation loss was not improved by a minimum of 0.001 with 3 epochs. The best 102-input BiLSTM model has 3 BiLSTM layers with 64-d hidden units at each direction for each layer. The model was trained with a learning rate of 0.0003 and batch size of 8. The dropout rate was 0.1. The 48-input BiLSTM model uses 5 BiLSTM layers with 64-d hidden units at each direction, which was trained with a learning rate of 0.0004, batch size of 8, and dropout rate of 0.15. In BiLSTM-Transformer Encoder models, the number of BiLSTM layer is one which is not a hyperparameter. The 102-input model is configured with the following architecture: 128-d hidden units at each direction for the BiLSTM layer, 3 transformer blocks with each having 8 attention heads, a learning rate of 0.0003, a dropout rate of 0.1, and a batch size of 8. The best configuration for the 48-input model is as follows: 64-d hidden units at each direction for the BiLSTM, 4 transformer blocks with each having 8 attention heads, a learning rate of 0.0003, a dropout rate of 0.11, and a batch size of 16. The models were trained by an Adam optimizer (Kingma & Ba, 2017) to minimize the Cross-Entropy loss function with L2 regularization.

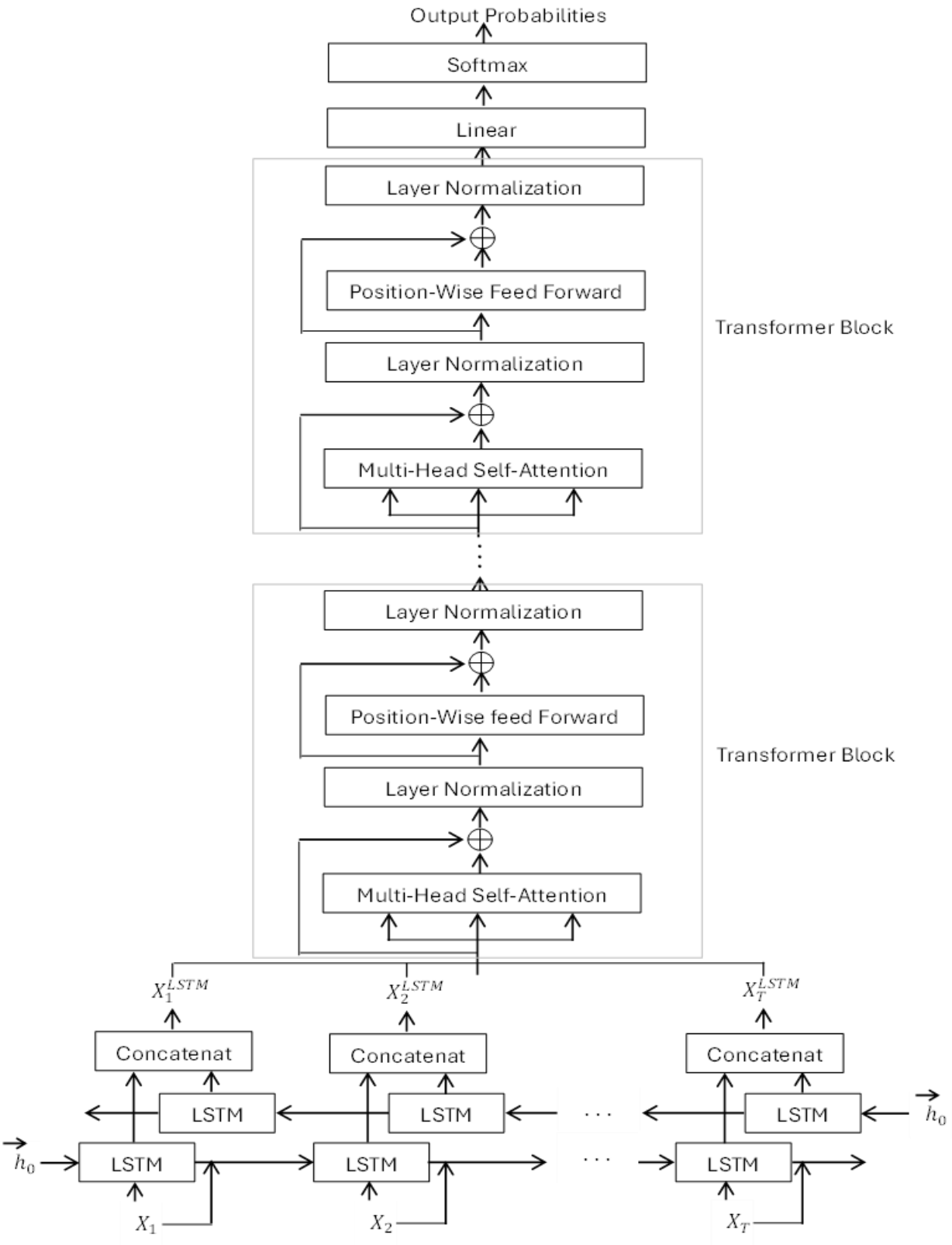

Figure 4.2: BiLSTM-Transformer Encoder model architecture

4.2.4 Model Evaluation

A 5-fold cross-validation method was used to train the model. Specifically, the data was randomly divided into 5 folds, and the first fold (about 20% data) was used for testing, with the remaining 4 folds (about 80% data) for training. This procedure was repeated 5 times; each time, a different subset of data was used as a test set. The performance metrics obtained from each fold were averaged to get the final performance metrics. For each fold, the performance metrics were calculated as follows:

$$\text{Accuracy} = \frac{Number\ of\ Correct\ Predictions}{Total\ Number\ of\ Predictions}$$

$$\text{Precision}_i = \frac{TP_i}{TP_i + FP_i} \text{ for class } i$$

$$\text{Recall}_i = \frac{TP_i}{TP_i + FN_i} \text{ for class } i$$

$$\text{F1} - \text{score}_i = 2 \times \frac{Precision_i \times Recall_i}{Precision_i + Recall_i} \text{ for class } i$$

$$\text{Precision}_{\text{weighted}} = \sum_{i=1}^{n} \frac{N_i}{N} Precision_i$$

$$\text{Recall}_{\text{weighted}} = \sum_{i=1}^{n} \frac{N_i}{N} Recall_i$$(Diego-Mas et al., 2017)

$$\text{F1-score}_{\text{weighted}} = \sum_{i=1}^{n} \frac{N_i}{N} F1 - score_i$$

where TP, FP, and FN are the numbers of true positives, false positives, and false negatives, respectively. For overall model performance, weighted precision, recall, and F1-score were also computed due to an imbalanced dataset where class 0 has about 50% fewer instances. The confusion matrix was computed by accumulating predictions and true labels from each fold. The models were trained with the PyTorch framework on an NVIDIA T4 GPU.

4.2.5 Model Explanation with Integrated Gradients

To explain the rationale behind the BiLSTM-Transformer Encoder model, Integrated Gradients (IG) method was applied to gain insights into how the model relied on individual features to make predictions. Introduced in Sundararajan et al., 2017, IG is used to explain a model's predictions in terms of individual features. This method typically generates feature-based maps that quantify the importance of each feature for a given prediction. The importance is represented by accumulated gradients of the model's output with respect to the inputs along a path from a baseline input to the actual input (Sundararajan et al., 2017). The baseline input is a reference point, providing no information. The integrated gradients of the *i*-th feature for an input *x* are computed as:

$$\text{IntegratedGrads}_i(x) ::= (x_i - x_i') \times \int_{\alpha=0}^{1} \frac{\partial F(x' + \alpha \times (x - x'))}{\partial x_i} d\alpha$$

Where *x* is an input, x' is a baseline, and α is an interpolation constant.

In this study, we used as the baseline zero accelerations and zero angular velocities. For each time-series input sequence, we computed the IG score at each time step for each feature. To understand the overall importance of each feature for the model's predictions, we further computed overall aggregated IG. We summed IG scores across all time steps for each input sequence, and then took the average across correctly classified sequences for each feature. We then took the absolute value and visualized the overall aggregated IG scores with a bar chart. We also visualized time-series aggregated IG scores, which were obtained by averaging across correctly classified sequences at each time step.

4.3 Results

The performance metrics of models using whole-body segment kinematics (102 features) and domain knowledge-selected Features (48 features) as inputs are presented in Table 4.1 and Table 4.2, respectively. The results showed varying performance across the models with

different numbers of input features. Overall, BiLSTM-Transformer Encoder had better performance than BiLSTM. Specifically, BiLSTM-Transformer Encoder with 102 features yielded the best performance, while BiLSTM model with 48 features performed slightly worse than the others. The BiLSTM model with 102 features and BiLSTM-Transformer Encoder with 48 features exhibited similar performance. The training time for BiLSTM-Transformer Encoder model and BiLSTM model using 102 features were 19 minutes and 44 minutes, respectively, while their training time using 48 features were 18 minutes and 40 minutes, respectively. As shown in Table 4.1 and 4.2, most performance metrics for L1 and L2 were relatively lower than those for L0 and L34. The confusion matrices of BiLSTM-Transformer Encoder and BiLSTM are presented in Figure 4.3 and Figure 4.4, respectively.

Table 4.1: Overall accuracy, precision, recall and F1-score values of lifting weight classification with whole-body segment kinematics.

Model	Lifting weight	Accuracy	Precision		Recall		F1-score	
			Weighted	Class *i*	Weighted	Class *i*	Weighted	Class *i*
BiLSTM	L0	0.779	0.777	0.92	0.779	0.90	0.775	0.91
	L1			0.78		0.86		0.82
	L2			0.72		0.59		0.65
	L3			0.75		0.83		0.79
BiLSTM-Transformer Encoder	L0	0.816	0.816	0.98	0.816	0.96	0.815	0.97
	L1			0.83		0.77		0.80
	L2			0.72		0.70		0.71
	L3			0.81		0.91		0.86

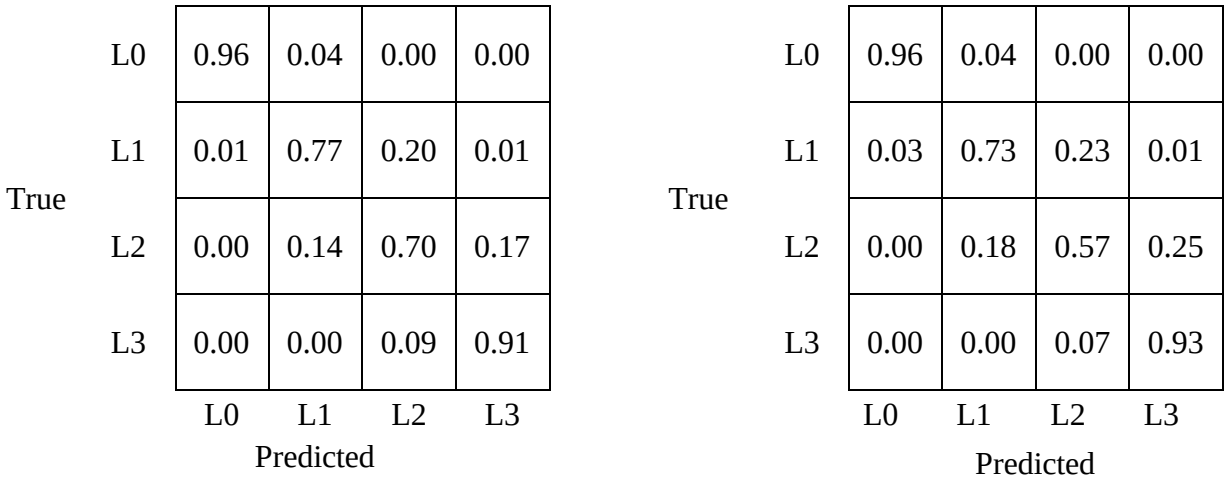

(a) whole-body segment kinematics (b) domain knowledge-selected Features

Figure 4.3: Confusion matrices of BiLSTM-Transformer Encoder with (a) whole-body segment kinematics and (b) domain knowledge-selected features

Table 4.2: Overall accuracy, precision, recall and F1-score values of lifting weight classification with domain knowledge-selected features.

Model	Lifting weight	Accuracy	Precision		Recall		F1-score	
			Weighted	Class *i*	Weighted	Class *i*	Weighted	Class *i*
BiLSTM	L0	0.751	0.750	0.86	0.751	0.94	0.748	0.90
	L1			0.70		0.78		0.74
	L2			0.66		0.59		0.63
	L3			0.84		0.78		0.81
BiLSTM-Transformer Encoder	L0	0.769	0.766	0.94	0.769	0.96	0.764	0.95
	L1			0.78		0.73		0.76
	L2			0.67		0.57		0.62
	L3			0.75		0.93		0.83

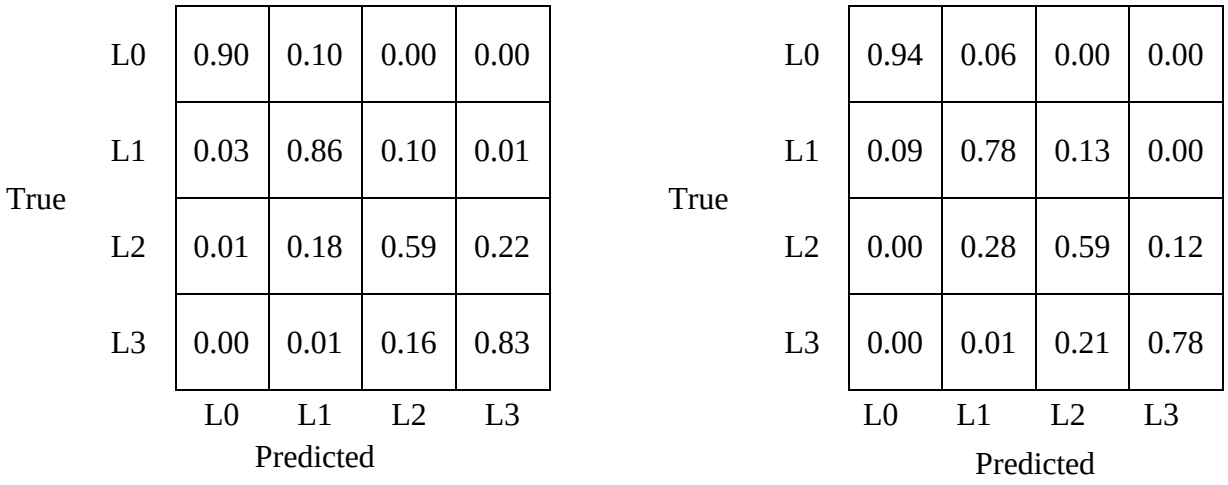

Figure 4.4: Confusion matrices of BiLSTM with (a) whole-body segment kinematics and (b) domain knowledge-selected features

To understand how the BiLSTM-Transformer Encoder model generally relied on each feature when using whole-body segment kinematics as inputs, the overall aggregated IG scores across all correctly classified sequences in the test data were computed for each of the 102 features. The top eight most important features were shown in Figure 4.5 (a) and highlighted on a skeleton model to provide a clearer visualization (Figure 4.5 (b)). The three most important features that had the highest overall aggregated IG score were pelvis acceleration on the x-axis, left shoulder acceleration on the x-axis, and right shoulder acceleration on the x-axis. The time-series aggregated IG scores of each feature at each time step were also computed to understand how the model relied on input features over time when making predictions. For clarity and illustration purposes, we provided a heatmap for each class visualizing the time-series aggregated IG scores for the eight most important features identified by the overall aggregated IG (Figure 4.6 – 4.9). From the heatmaps, we observed the time-series aggregated IG scores of the features changed significantly over three distinct periods. These periods corresponded d to the three main phases of lifting: the initial lift phase, the mid-lift phase, and the final place phase.

This observed trend in the selected features' IG score is representative of the overall pattern seen across all features, indicating that the model identified main lifting phases when making predictions. Focusing on selected features, during the initial lift, high positive IG scores were observed for shoulder and head accelerations at class L4 ($\geqslant$11.3 kg) (Figure 4.9), while their IG scores were highly negative for lighter loads (Figure 4.6 - Figure 4.7). However, for accelerations of the pelvis and upper legs, the opposite trend was observed in the plots: high negative IG scores at class L4 (Figure 4.9) and high positive IG scores for lighter loads (Figure 4.6 - Figure 4.7). In the mid-lift phase, shoulder accelerations showed high IG scores. Specifically, shoulder accelerations had high positive IG scores when lifting lighter weights (Figures 4.6 and 4.7), while they had high negative scores when lifting $\geqslant$11.3 kg. In the final place phase, the IG scores of these features mostly remained similar as those in the initial lift phase. Except for the lightest weight (0.5 kg) (Figure 4.6), the right shoulder acceleration shifted from highly negative in the initial lift to highly positive IG scores, and the right upper leg acceleration shifted from highly positive to highly negative IG scores. Moreover, we also observed high IG scores for angular velocities of left upper arm external/internal rotation and left upper leg abduction/adduction (Figure 4.6 - Figure 4.9).

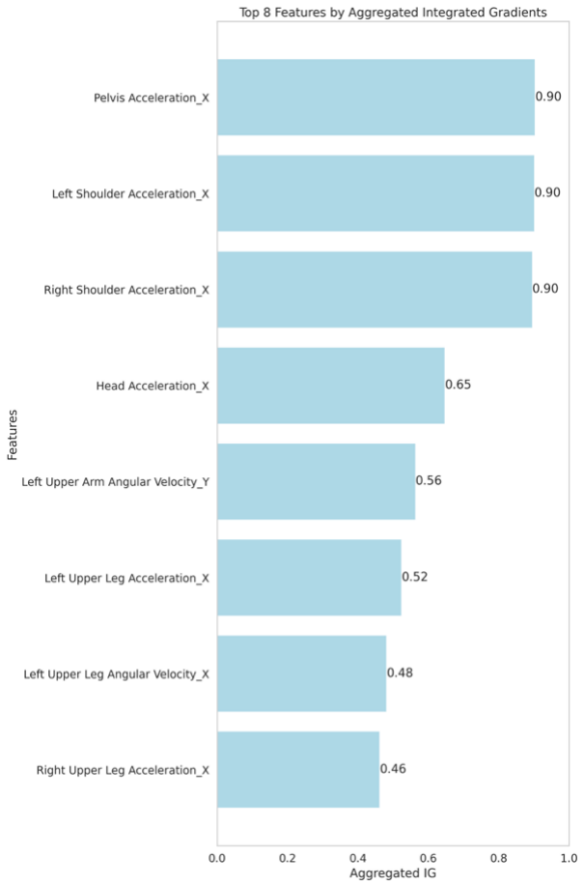

(a) top 8 important features

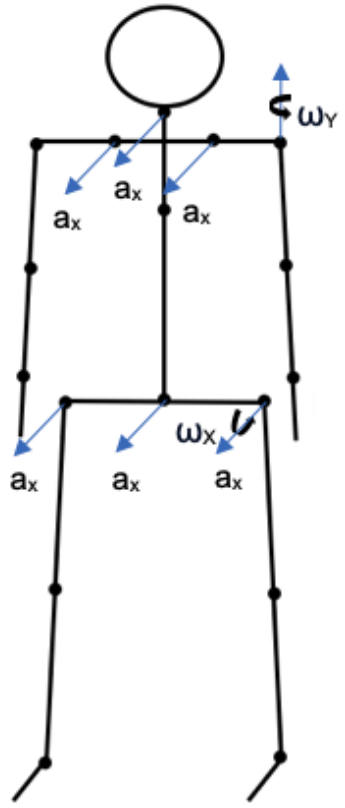

(b) skeletal model with top 8 important features

Figure 4.5: Top 8 important features measured by aggregated IG in (a) top 8 important features and (b) skeletal model with top 8 important features, using BiLSTM-Transformer Encoder with whole-body segment kinematics as input features

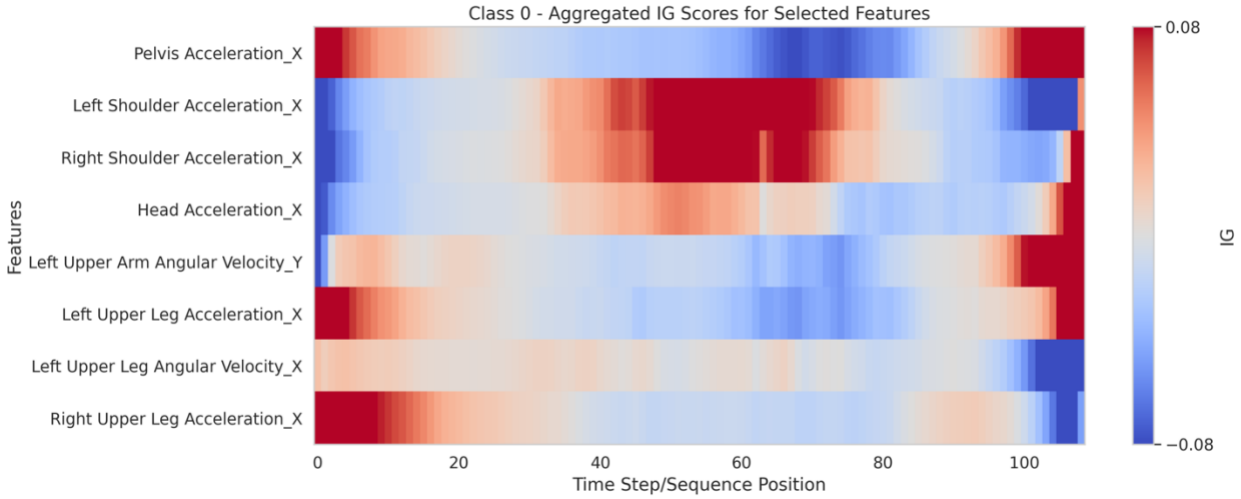

Figure 4.6: Visualizing time-series aggregated IG for class 0

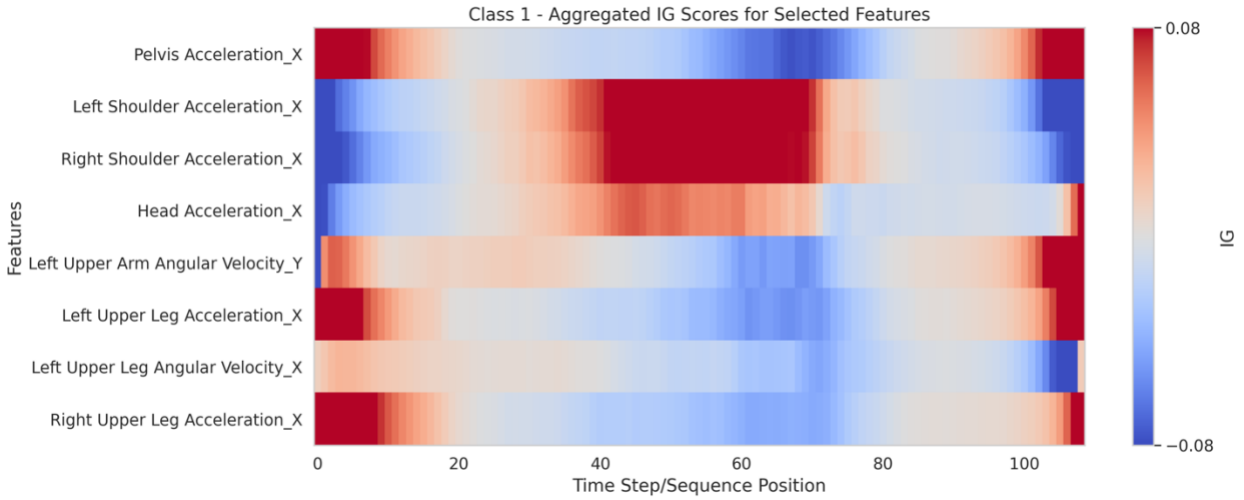

Figure 4.7: Visualizing time-series aggregated IG scores for class 1

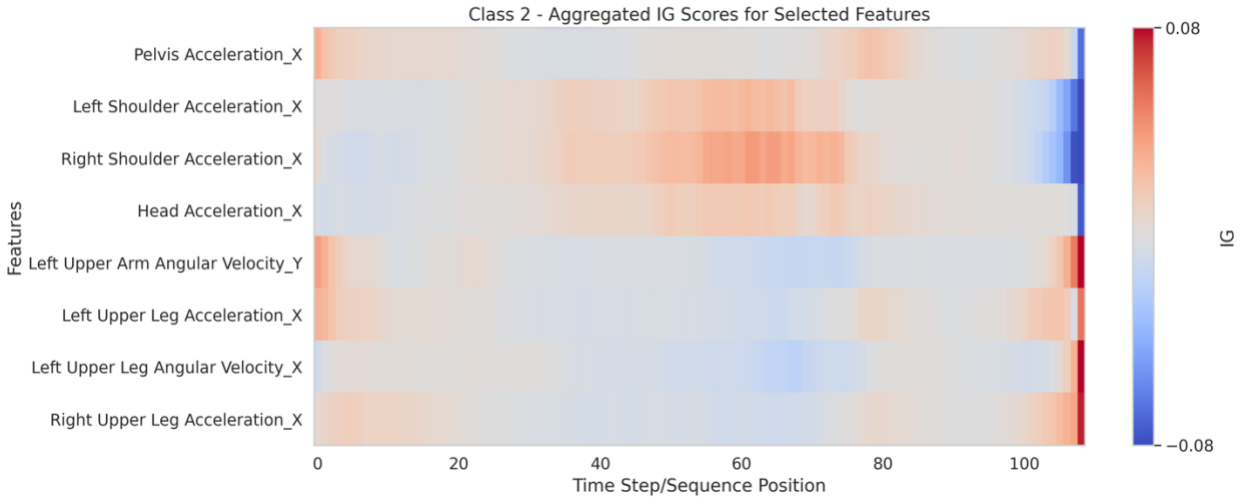

Figure 4.8: Visualizing time-series aggregated IG scores for class 2

Figure 4.9: Visualizing time-series aggregated IG scores for class 3

4.4 Discussion

Accurate lifting weight recognition estimation has the potential to impact benefit many fields, such as improving ergonomics, enhancing human-robot collaboration, and advancing the effectiveness of wearable devices. Previous studies employed LSTM-based models with human motion data for hand-handled load recognition, demonstrating superior performance compared to other machine learning methods. Extending the groundwork laid by these previous works, we developed a new transformer-based model, BiLSTM-Transformer Encoder, aimed at improving the accuracy of lifting weight recognition. In our study, we employed both the BiLSTM model and the BiLSTM-Transformer Encoder model, experimenting with different input configurations such as whole-body segment lifting kinematics (102 input features) and domain knowledge-selected segment lifting kinematics (48 input features). Our results demonstrated that the BiLSTM-Transformer Encoder outperformed BiLSTM, achieving an overall accuracy of 0.816 with whole-body segment kinematics. The precision, recall, and F1-score of each class were also computed for all combinations of models and input configurations (Table 4.1 and 4.2), and were consistently better for L0 (0.5 kg) and L3 (11.3 ~ 13.6 kg) compared to the middle classes (e.g., L1: 2.3 ~ 4.5 kg and L2: 6.8 ~ 9.1 kg). Specifically, the confusion matrices revealed that 2.3 ~ 4.5 kgL1 was misclassified as 6.8 ~ 9.1 kg L2 in 10% ~ 23% of the instances, and vice versa, with 6.8 ~ 9.1 kg L2 being misclassified as 2.3 ~ 4.5 kg L1 in 14% ~ 28% of the instances (Figure 4.3 and 4.4). Additionally, 6.8 ~ 9.1 kg L2 was misclassified as 11.3 ~ 13.6 kg L3 in 12% ~ 25% of the instances (Figures 4.3 and 4.4). This may be because lifting less than 0.5 kg and more than 11.3 kg had more distinct lifting kinematic characteristics that set them apart, leading to better performance metrics. In contrast, the middle classes (e.g., lifting 2.3 ~ 4.5 kg and 6.8 ~ 9.1 kg) have more overlap in lifting kinematic characteristics, making them harder to

distinguish. For example, in the previous chapter, we have shown that upper limb lifting kinematics, such as angular velocities, didn't have a significant difference when varying lifting weight between 4.5 kg and 11.3 kg. It is important to note that previous studies have shown some kinematics of lifting between 4.5 kg and 11.3 kg can be very similar, contributing to the difficulty in distinguishing between these lifting weight levels. This is a known challenge and not a unique shortcoming of our model. Moreover, with our model, there was a significant improvement in the performance metrics of distinguishing L1 and L2 by incorporating more (e.g., whole-body) kinematics as input.

IG was used to gain insights into how the BiLSTM-Transformer Encoder model makes predictions. The overall aggregated IG results demonstrated that specific kinematic features, such as shoulder acceleration, pelvis acceleration and upper leg acceleration, were crucial for accurate lifting weight recognition. This aligns with our expectations based on the nature of lifting tasks during which shoulders control the movement of lifting (Constant, 1989), and pelvis and upper legs that form the hip joint provide stability and strength during lifting (Nordin & Frankel, 2012). This highlights the model's ability to capture important body segments for lifting. We also obtained time-series aggregated IG scores for each feature. The changes of the time-series aggregated IG scores over the three phases indicated the influence of each feature varied between phases. This indicated that our model has the ability to understand the temporal dynamics of the lifting process, and process and identify important features during different phases. For instance, the IG scores revealed that during the initial lift, the model identified positive high contributions from shoulders and head accelerations to predicting lifting $\geqslant$11.3 kg, but they contributed negatively, though highly, to predicting lighter weights. This implied that in the initiation phase, a higher magnitude of shoulder and head accelerations increased the

likelihood of predicting heavier weights; however, it reduced that of predicting lighter weights. Additionally, the model identified higher magnitude accelerations of the pelvis and upper legs as reducing the likelihood of predicting ⩾11.3 kg but increasing the likelihood of predicting lighter loads. This alignment aligns well with our knowledge of lifting biomechanics. In the initial phase, with heavier weight, individuals tended to bring the load to the body as quickly as possible to reduce the moment arm on shoulders, which optimized energy use and maximized body stability. Furthermore, in order to lift the weight off the place shoulder, muscles have to generate more force to overcome the inertia of the weight. Higher shoulder accelerations lead to not only rapid recruitment of larger, fast-twitch motor units but also an increased number of motor units (Desmedt & Godaux, 1978; Henneman et al., 1965), so shoulder muscles can generate higher force to meet the increased force demand. In the meantime, the pelvis and upper legs naturally reduce their accelerations to maintain body stability and prevent toppling. In contrast, higher shoulder accelerations decreased the likelihood of predicting ⩾11.3 kg in the mid-lift phase when the load is elevated. This is because, when lifting heavy weight, decreased shoulder accelerations help maintain body balance and stabilize the load, preventing, for instance, unnecessary forward and backward movement. However, when lifting light weights, the body can afford faster shoulder movement without compromising stability and control. In the final placement, the influences of these features (e.g., accelerations of shoulders, pelvis, and upper legs) on predicting each level of weight were largely consistent with those in the initial lift phase. For instance, when lifting ⩾11.3 kg, increased shoulder acceleration contributed positively to predictions, while increased hip and upper leg accelerations had negative contributions to predictions. These were as expected because increased shoulder acceleration helps generate more force to control the lowering of the load, and decreased hip and upper leg

accelerations allow the body to maintain stability and balance. It is noteworthy that when lifting 0.5 kg, the roles of shoulder and upper leg accelerations on the right side diverged from theirs in the initiation phase and phase and were opposite to those on the left side. This asymmetry can occur because most individuals are right-hand dominant, which can lead to asymmetries in body movement when lifting a very light load like 0.5 kg. This asymmetry was captured by the model. Overall, the ability of the model to focus on different features during different phases of the lifting process highlights its nuanced understanding of the biomechanics involved.

4.5 Conclusion

In this study, a BiLSTM-Transformer Encoder model which incorporates a BiLSTM layer into transformer encoder layers was proposed to improve the accuracy of lifting weight recognition. The results showed consistent improvements in identifying lifting weight at 0.5 kg, 2.3 ~ 4.5 kg, 6.8 ~ 9.1 kg, and 11.3 ~ 13.6 kg, which have a 2.3 kg difference. The model identified key kinematic features that vary with lifting weight, such as shoulder acceleration, pelvis acceleration and upper leg acceleration. The model's capability to detect a 2.3 kg difference suggests that it has learned the subtle change in lifting kinematics corresponding to a 2.3 kg difference in lifting weight. These kinematic changes will be more pronounced and easier to detect as the weight difference increases, which makes the model suitable for applying to ergonomic assessment methods that require the consideration of different levels of weight, such as Rapid Upper Limb Assessment (RULA) (McAtamney & Nigel Corlett, 1993), Rapid Entire Body Assessment (REBA) (Hignett & McAtamney, 2000), and Ovako Working Posture Analysis System (OWAS) (Karhu et al., 1977). In REBA, the weight of the handled loads is classified into weight < 5kg, 5 kg< weight < 10 kg, and weight >10kg. RULA considers weight < 2kg, 2 kg < weight < 10 kg, and weight > 10 kg. OWAS considers a 10 kg difference of weight:

weight $\leqslant$ 10 kg , 10 kg < weight $\leqslant$ 20 kg, weight > 20 kg. In the future, this model can be integrated with posture recognition model to automate ergonomic assessment using methods including RULA, REBA and OWAS.

4.6 References

Caderby, T., Dalleau, G., Leroyer, P., Bonazzi, B., Chane-Teng, D., & Do, M.-C. (2013). Does an additional load modify the Anticipatory Postural Adjustments in gait initiation? *Gait & Posture*, *37*(1), 144–146. https://doi.org/10.1016/j.gaitpost.2012.06.012

Constant, C. R. (1989). Historical background, anatomy and shoulder function. *Baillière's Clinical Rheumatology*, *3*(3), 429–435. https://doi.org/10.1016/S0950-3579(89)80002-0

Davis, K. G., & Marras, W. S. (2000). Assessment of the Relationship between Box Weight and Trunk Kinematics: Does a Reduction in Box Weight Necessarily Correspond to a Decrease in Spinal Loading? *Human Factors: The Journal of the Human Factors and Ergonomics Society*, *42*(2), 195–208. https://doi.org/10.1518/001872000779656499

Desmedt, J. E., & Godaux, E. (1978). Ballistic contractions in fast or slow human muscles; discharge patterns of single motor units. *The Journal of Physiology*, *285*(1), 185–196. https://doi.org/10.1113/jphysiol.1978.sp012566

Devlin, J., Chang, M.-W., Lee, K., & Toutanova, K. (2018). *BERT: Pre-training of Deep Bidirectional Transformers for Language Understanding* (Version 2). arXiv. https://doi.org/10.48550/ARXIV.1810.04805

Fowler, N. E., Rodacki, A. L. F., & Rodacki, C. D. (2006). Changes in stature and spine kinematics during a loaded walking task. *Gait & Posture*, *23*(2), 133–141. https://doi.org/10.1016/j.gaitpost.2004.12.006

Gers, F. A., Schraudolph, N. N., & Schmidhuber, J. (2002). Learning precise timing with LSTM recurrent networks. *Journal of Machine Learning Research*, *3*(1), 115–143.

Goršič, M., Dai, B., & Novak, D. (2020). Load Position and Weight Classification during Carrying Gait Using Wearable Inertial and Electromyographic Sensors. *Sensors*, *20*(17), 4963. https://doi.org/10.3390/s20174963

Henneman, E., Somjen, G., & Carpenter, D. O. (1965). FUNCTIONAL SIGNIFICANCE OF CELL SIZE IN SPINAL MOTONEURONS. *Journal of Neurophysiology*, *28*(3), 560–580. https://doi.org/10.1152/jn.1965.28.3.560

Hignett, S., & McAtamney, L. (2000). Rapid Entire Body Assessment (REBA). *Applied Ergonomics*, *31*(2), 201–205. https://doi.org/10.1016/S0003-6870(99)00039-3

Hochreiter, S., & Schmidhuber, J. (1997). Long Short-Term Memory. *Neural Computation*, *9*(8), 1735–1780. https://doi.org/10.1162/neco.1997.9.8.1735

Karhu, O., Kansi, P., & Kuorinka, I. (1977). Correcting working postures in industry: A practical method for analysis. *Applied Ergonomics*, *8*(4), 199–201. https://doi.org/10.1016/0003-6870(77)90164-8

Kingma, D. P., & Ba, J. (2017). *Adam: A Method for Stochastic Optimization* (arXiv:1412.6980). arXiv. http://arxiv.org/abs/1412.6980

LaFiandra, M., Wagenaar, R. C., Holt, K. G., & Obusek, J. P. (2003). How do load carriage and walking speed influence trunk coordination and stride parameters? *Journal of Biomechanics*, *36*(1), 87–95. https://doi.org/10.1016/S0021-9290(02)00243-9

Lee, H., Yang, K., Kim, N., & Ahn, C. R. (2020). Detecting excessive load-carrying tasks using a deep learning network with a Gramian Angular Field. *Automation in Construction*, *120*, 103390. https://doi.org/10.1016/j.autcon.2020.103390

Li, Y., Greene, R. L., Mu, F., Hu, Y. H., & Radwin, R. G. (2020). Towards Video-Based Automatic Lifting Load Prediction. *Proceedings of the Human Factors and Ergonomics Society Annual Meeting*, *64*(1), 962–963. https://doi.org/10.1177/1071181320641230

Lim, S., & D'Souza, C. (2019). Statistical prediction of load carriage mode and magnitude from inertial sensor derived gait kinematics. *Applied Ergonomics*, *76*, 1–11. https://doi.org/10.1016/j.apergo.2018.11.007

Liu, Y., & Lapata, M. (2019). *Text Summarization with Pretrained Encoders* (Version 2). arXiv. https://doi.org/10.48550/ARXIV.1908.08345

McAtamney, L., & Nigel Corlett, E. (1993). RULA: A survey method for the investigation of work-related upper limb disorders. *Applied Ergonomics*, *24*(2), 91–99. https://doi.org/10.1016/0003-6870(93)90080-S

Nordin, M., & Frankel, V. (2012). *Basic biomechanics of the musculoskeletal system (4th ed.)* (Fourth). Wolters Kluwer Health – Lippincott Williams & Wilkins.

Qu, X., & Yeo, J. C. (2011). Effects of load carriage and fatigue on gait characteristics. *Journal of Biomechanics*, *44*(7), 1259–1263. https://doi.org/10.1016/j.jbiomech.2011.02.016

Radford, A., Narasimhan, K., Salimans, T., & Sutskever, I. (2018). *Improving language understanding by generative pre-training*. https://cdn.openai.com/research-covers/language-unsupervised/language_understanding_paper.pdf

Schuster, M., & Paliwal, K. K. (1997). Bidirectional recurrent neural networks. *IEEE Transactions on Signal Processing*, *45*(11), 2673–2681. https://doi.org/10.1109/78.650093

Shavit, Y., & Klein, I. (2021). Boosting Inertial-Based Human Activity Recognition With Transformers. *IEEE Access*, *9*, 53540–53547. https://doi.org/10.1109/ACCESS.2021.3070646

Song, J., & Qu, X. (2014). Effects of age and its interaction with task parameters on lifting biomechanics. *Ergonomics*, *57*(5), 653–668. https://doi.org/10.1080/00140139.2014.897376

Sundararajan, M., Taly, A., & Yan, Q. (2017). *Axiomatic Attribution for Deep Networks* (Version 2). arXiv. https://doi.org/10.48550/ARXIV.1703.01365

Vaswani, A., Shazeer, N., Parmar, N., Uszkoreit, J., Jones, L., Gomez, A. N., Kaiser, L., & Polosukhin, I. (2017). *Attention Is All You Need* (Version 7). arXiv. https://doi.org/10.48550/ARXIV.1706.03762

Wensel, J., Ullah, H., & Munir, A. (2022). *ViT-ReT: Vision and Recurrent Transformer Neural Networks for Human Activity Recognition in Videos* (Version 2). arXiv. https://doi.org/10.48550/ARXIV.2208.07929

Xsens Technologies B.V. (2021). *Xsens MVN User Manual*.

Yang, K., Ahn, C. R., & Kim, H. (2020). Deep learning-based classification of work-related physical load levels in construction. *Advanced Engineering Informatics*, *45*, 101104. https://doi.org/10.1016/j.aei.2020.101104

Zhou, G., Aggarwal, V., Yin, M., & Yu, D. (2022). A Computer Vision Approach for Estimating Lifting Load Contributors to Injury Risk. *IEEE Transactions on Human-Machine Systems*, *52*(2), 207–219. https://doi.org/10.1109/THMS.2022.3148339

Chapter 5

A Video-Based Pipeline for Lifting Load Recognition

5.1 Introduction

Low back pain is the fifth most common reason for visiting a doctor in the USA (Atlas & Deyo 2001). Annually, the prevalence of low back pain in the general US adult population is 10–30%.1 According to findings from Punnett et al., 2005, 37% of low back pain may be due to work-related risk factors. Previous studies show that manual lifting tasks are frequently associated with low back pain (Cheng et al., 1998; Cole & Grimshaw, 2003; de Looze et al., 1998).

Manual lifting tasks often require workers to lift variable, heavy loads. Several studies have revealed that higher lifting weights increase muscle activity and may sometimes increase spinal loads (Davis et al., 2000; Marras & Mirka, 1990; Marras & Sommerich, 1991). In ergonomics risk assessment, the amount of weight being lifted is one of the important variables related to the lifting task that needs to be measured or assessed. Ergonomists usually go out into the field to measure weight within the workplace using a scale, obtain it through worker estimates, or obtain information from product brochures and other sources. However, these approaches are cumbersome and time-consuming. Previous studies have shown that changes in the lifting weight have an impact on the variance in the lifter's kinematics (Norasi et al., 2019; Plamondon et al., 2017; Song & Qu, 2014). The current surge of human pose estimation techniques, which attempt to extract human joint positions from images, has made it possible to extract lifting kinematic features from data collected by cameras. These extracted kinematics have been used for ergonomic assessment to identify posture-based risks(Kim et al., 2021; Van Crombrugge et al., 2022b; Yu, Yang, Li, et al., 2019). In the previous chapter, we leveraged data

from wearable IMU sensors for lifting weight recognition using a transformer-based model. We demonstrated that kinematic features representing lifting biomechanics can identify different levels of lifting weight with reasonable accuracy. However, IMU sensors rely on direct measurements from sensors attached to the worker's body, which may not be feasible in long-time applications due to their intrusiveness and potential disturbance. The aim of this chapter was to develop a video-based method for lifting weight recognition.

5.2 Methods

5.2.1 Participants, Simulated Lifting Task, and Data

The data in the current chapter were obtained in the third chapter. Thus, we only summarized details here. A total of 18 participants (9 females and 9 males) from the local university and community completed the study. In the experiment, the participants lifted a weighted box with the dimensions of 46.3 × 31.3 × 11.2 cm (length × width × height) from the floor or knee height and placed it on a shelf at elbow height. The box weights evaluated in this study were in a range between 0.5 and 13.8 kg. Participants were asked to perform each lifting using self-selected comfortable styles and speed. Each participant performed six lifting trials for each combination of lifting height and weight in random order. All the trials were recorded by two synchronized RGB cameras from the right side (90°) and left frontal 60° positions (Figure 5.1). The cameras recorded at 60 frames per second with 1920×1080 resolution. In this study, only videos captured by the frontal 60° angle were used.

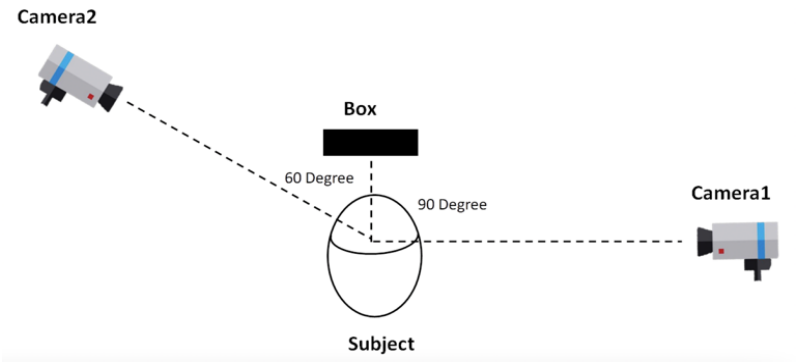

Figure 5.1 Two cameras were used to record lifting

5.2.2 Feature Extraction

MediaPipe Pose, an open-source framework developed by Google, was used to estimate 2D keypoint coordinates. The pose model provides 2D pose estimation of 33 landmarks (Figure 5.2) from images (Bazarevsky et al., 2020). Each landmark consists of a vector representing the relative position in an image. MediaPipe pose also outputs Z-axis coordinate representing the depth of a keypoint relative to the midpoint of the hips. We extracted 12 2D landmarks with their relative depths at z-axis, including right/left shoulder, right/left elbow, right/left wrist, right/left hip, right/left knee and right/left ankle. Lifting trajectories and velocities of the 12 keypoints were computed and taken as input features for lifting weight recognition. For keypoint i (i = 1, 2, …, 12), the displacement, $\boldsymbol{d}_{i,t}$, at time T = t is calculated by

$$\boldsymbol{d}_{i,t} = \boldsymbol{p}_{i,t} - \boldsymbol{p}_{i,t-1}$$

Where $\boldsymbol{p}_{i,t}$ is the position of joint i at time t.

The velocity of keypoint i, $\boldsymbol{v}_{i,t}$, at time t is calculated by

$$\boldsymbol{v}_{i,t} = \frac{\boldsymbol{d}_{i,t}}{\Delta T}$$

Joint angles of elbows, shoulders, hips and knees were also calculated by vectors that form the joints. Since MediaPipe doesn't extract keypoints related to the trunk, we calculated shoulder and hip angles as the angle between Hip-Shoulder vector and Shoulder-Elbow vector, and the angle between Hip-Knee vector and Knee-Ankle vector, respectively. For joint i (i = 1, 2, …, 8) defined by vectors $\boldsymbol{v}_j$ and $\boldsymbol{v}_k$, its joint angle $\boldsymbol{\theta}_{i,t}$ at time t is calculated by

$$\boldsymbol{\theta}_{i,t} = arccos\left(\frac{\boldsymbol{v}_{j,t} \cdot \boldsymbol{v}_{k,t}}{\|\boldsymbol{v}_{j,t}\| \|\boldsymbol{v}_{k,t}\|}\right),$$

Where $v_{j,t}$, $v_{k,t}$ are v_j and v_k at time t, respectively.

These extracted features were time-series sequences with different lengths. To ensure the sequences have equal lengths, post-padding was implemented, in which all sequences were padded with zeros at the end based on the maximum sequence length. Sequence-wise Min-max normalization was applied to scale the data to the range of [0, 1].

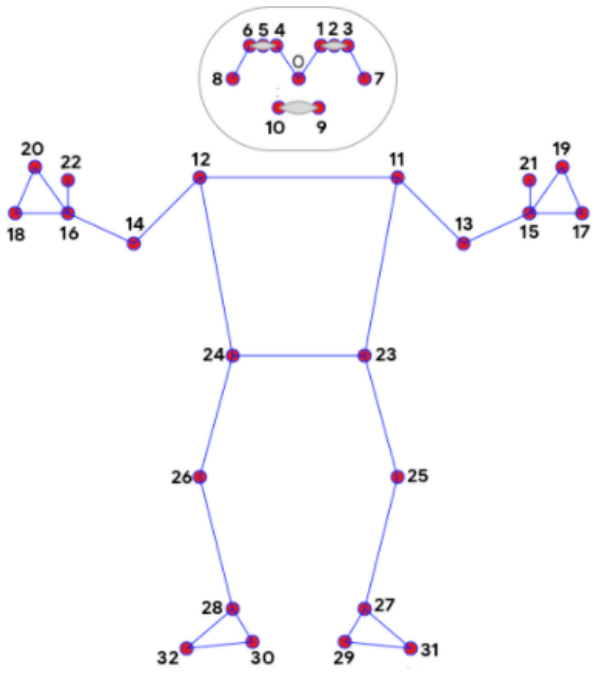

0. nose
1. left_eye_inner
2. left_eye
3. left_eye_outer
4. right_eye_inner
5. right_eye
6. right_eye_outer
7. left_ear
8. right_ear
9. mouth_left
10. mouth_right
11. left_shoulder
12. right_shoulder
13. left_elbow
14. right_elbow
15. left_wrist
16. right_wrist
17. left_pinky
18. right_pinky
19. left_index
20. right_index
21. left_thumb
22. right_thumb
23. left_hip
24. right_hip
25. left_knee
26. right_knee
27. left_ankle
28. right_ankle
29. left_heel
30. right_heel
31. left_foot_index
32. right_foot_index

Figure 5.2 33 Pose landmarks (*MediaPipe Pose*)

5.2.3 Lifting Weight Recognition

A BiLSTM-Transformer Encoder model was trained and used in the stage. The model took 60 time-series features as input representing lifting biomechanics, and output the level of lifting weight. It consists of BiLSTM layers and transformer encoder blocks. The numbers of BiLSTM layers and transformer encoder blocks were hyperparameters to tune. We used 3 BiLSTM layers with 128-d hidden state at each direction. The number of transformer encoder blocks was 2 with 8 attention heads and 256-d hidden state. An Adam optimizer is applied to minimize the Cross-Entropy loss function. The network was trained using a batch size of 32 for 100 epochs on NVIDIA T4 GPU.

5.2.4 Model Evaluation

A leave-one-out cross validation method was used to train the model. Specifically, data from 17 subjects was used for training, with the data from the remaining 1 subject for testing. This procedure was repeated until 18 times; Each time, a different fold of data was used as a test set. The performance metrics obtained from each fold were averaged to get the final performance metrics. For each fold, the performance metrics were calculated as follows:

Accuracy = $\frac{Number\ of\ Correct\ Predictions}{Total\ Number\ of\ Predictions}$

Precision $_{\text{weighted}}$ = $\sum_{i=1}^{n} \frac{N_i}{N}\ Precision_i$, where $Precision_i = \frac{TP_i}{TP_i+FP_i}$ for class i

Recall $_{\text{weighted}}$ = $\sum_{i=1}^{n} \frac{N_i}{N}\ Recall_i$, where $Recall_i = \frac{TP_i}{TP_i+FN_i}$ for class i

F1-score $_{\text{weighted}}$ = $\sum_{i=1}^{n} \frac{N_i}{N}\ F1-score_i$,

where $F1-score_i = 2 \times \frac{Precision_i \times Recall_i}{Precision_i + Recall_i}$ for class i

where TP, FP, and FN are the numbers of true positives, false positives, and false negatives, respectively. For overall model performance, weighted precision, recall and F1-score

were also computed. Confusion matrix was computed by accumulating the predictions and true labels from each fold.

5.3 Results

The performance metrics of the lifting weight recognition model were presented in Table 5.1, and the confusion matrices were shown in Figure 5.3. The overall accuracy was 0.766, and the percentage of actual L1 and L2 the model correctly classified were relatively lower than those for L0 and L3.

Table 5.1: Overall accuracy, precision, recall and F1-score values of lifting weight classification

Model	Accuracy	Precision	Recall	F1-score
BiLSTM-Transformer Encoder	0.714	0.773	0.723	0.720

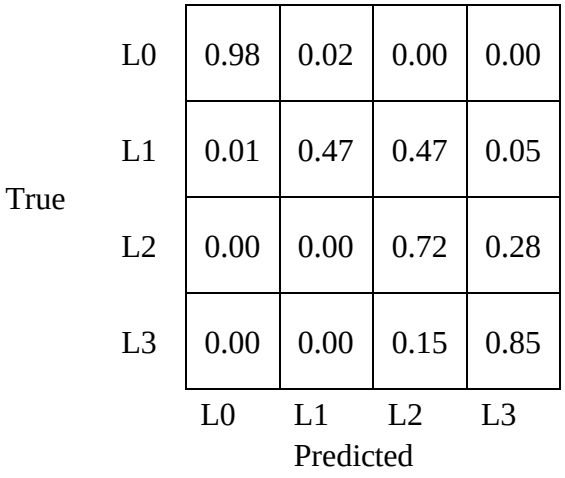

Figure 5.3: Confusion matrices of BiLSTM-Transformer Encoder model

5.4 Discussion

The current study aimed at examining the potential use of camera data to estimate the level of lifting weight. We used a validated human pose estimation framework that can estimate

keypoints from videos. Keypoints trajectories were calculated from the estimated positions and velocities were further calculated. These extracted features were then fed into a BiLSTM-Transformer Encoder classifier for lifting weight recognition. The overall accuracy, precision, recall and F1-score were 0.766, 0.779, 0.766 and 0.768, respectively. While it was worse than using BiLSTM-Transformer Encoder with whole-body kinematics, the performance was comparable to BiLSTM model using IMU data in the previous chapter. In general data derived from IMU sensors are more accurate due to their direct measurement, while features from camera data are indirect and sensitive to recording environment such as occlusions. The performance metrics were worse for middle classes (e.g., L1: 2.3 ~ 4.5 kg and L2: 6.8 ~ 9.1 kg) compared to L0 (0.5 kg) and L3 (11.3 ~ 13.6 kg), which was consistent with the result from the previous chapter.

5.5 Conclusion

In this work, we explore the feasibility of using BiLSTM-Transformer Encoder model with videos. The result showed that it was comparable to BiLSTM model with IMU data. Both IMU data and videos with BiLSTM-Transformer Encoder model consistently performed worse in recognizing 2.3 ~ 4.5 kg and 6.8 ~ 9.1 kg. The underperformance can be attributed to the intrinsic kinematic similarity between lifting 4.5 kg and 11.3 kg. Future work should possibly integrate additional data sources to improve the accuracy in distinguishing between such lifting weight levels.

5.6 References

Atlas, S. J., & Deyo, R. A. (2001). Evaluating and managing acute low back pain in the primary care setting. *Journal of General Internal Medicine*, *16*(2), 120–131. https://doi.org/10.1111/j.1525-1497.2001.91141.x

Bazarevsky, V., Grishchenko, I., Raveendran, K., Zhu, T., Zhang, F., & Grundmann, M. (2020). *BlazePose: On-device Real-time Body Pose tracking* (Version 1). arXiv. https://doi.org/10.48550/ARXIV.2006.10204

Cheng, C.-K., Chen, H.-H., Kuo, H.-H., Lee, C.-L., Chen, W.-J., & Liu, C.-L. (1998). A three-dimensional mathematical model for predicting spinal joint force distribution during manual liftings. *Clinical Biomechanics*, *13*(1), S59–S64. https://doi.org/10.1016/S0268-0033(97)00077-6

Davis, K. G., Jorgensen, M. J., & Marras, W. S. (2000). An investigation of perceived exertion via whole body exertion and direct muscle force indicators during the determination of the maximum acceptable weight of lift. *Ergonomics*, *43*(2), 143–159. https://doi.org/10.1080/001401300184521

de Looze, M. P., Dolan, P., Kingma, I., & Baten, C. T. M. (1998). Does an asymmetric straddle-legged lifting movement reduce the low-back load? *Human Movement Science*, *17*(2), 243–259. https://doi.org/10.1016/S0167-9457(97)00032-8

Kim, W., Sung, J., Saakes, D., Huang, C., & Xiong, S. (2021). Ergonomic postural assessment using a new open-source human pose estimation technology (OpenPose). *International Journal of Industrial Ergonomics*, *84*, 103164. https://doi.org/10.1016/j.ergon.2021.103164

Marras, W. S., & Mirka, G. A. (1990). Muscle activities during asymmetric trunk angular accelerations. *Journal of Orthopaedic Research*, *8*(6), 824–832. https://doi.org/10.1002/jor.1100080607

Marras, W. S., & Sommerich, C. M. (1991). A Three-Dimensional Motion Model of Loads on the Lumbar Spine: II. Model Validation. *Human Factors: The Journal of the Human Factors and Ergonomics Society*, *33*(2), 139–149. https://doi.org/10.1177/001872089103300202

MediaPipe Pose. (n.d.). Retrieved May 23, 2023, from https://github.com/google-ai-edge/mediapipe/blob/master/docs/solutions/pose.md

Norasi, H., Koenig, J., & Mirka, G. (2018). Effect of Load Weight and Starting Height on the Variability of Trunk Kinematics. *Proceedings of the Human Factors and Ergonomics Society Annual Meeting*, *62*(1), 905–909. https://doi.org/10.1177/1541931218621208

Plamondon, A., Larivière, C., Denis, D., Mecheri, H., & Nastasia, I. (2017). Difference between male and female workers lifting the same relative load when palletizing boxes. *Applied Ergonomics*, *60*, 93–102. https://doi.org/10.1016/j.apergo.2016.10.014

Punnett, L., Prüss-Ütün, A., Nelson, D. I., Fingerhut, M. A., Leigh, J., Tak, S., & Phillips, S. (2005). Estimating the global burden of low back pain attributable to combined occupational exposures. *American Journal of Industrial Medicine*, *48*(6), 459–469. https://doi.org/10.1002/ajim.20232

Song, J., & Qu, X. (2014). Effects of age and its interaction with task parameters on lifting biomechanics. *Ergonomics*, *57*(5), 653–668. https://doi.org/10.1080/00140139.2014.897376

Van Crombrugge, I., Sels, S., Ribbens, B., Steenackers, G., Penne, R., & Vanlanduit, S. (2022). Accuracy Assessment of Joint Angles Estimated from 2D and 3D Camera Measurements. *Sensors*, *22*(5), 1729. https://doi.org/10.3390/s22051729

Yu, Y., Yang, X., Li, H., Luo, X., Guo, H., & Fang, Q. (2019). Joint-Level Vision-Based Ergonomic Assessment Tool for Construction Workers. *Journal of Construction Engineering and Management*, *145*(5), 04019025. https://doi.org/10.1061/(ASCE)CO.1943-7862.0001647

Chapter 6

Conclusions and Limitations

This dissertation seeks to develop methods that simplify lifting weight recognition by leveraging kinematics and advanced machine learning models. By thoroughly investigating effects of lifting weight on the upper body joint kinematics and coordination, we showed that lifting weight level had statistically significant effects on upper extremity kinematics such as velocities and shoulder-elbow coordination. This research, along with previous studies, provides a robust basis for developing more effective lifting weight recognition methods with lifting kinematics. Building on this foundation, a machine learning model was developed and evaluated. This model was evaluated on IMU data. The results showed substantial improvements over existing lifting weight recognition models. Specifically, this model successfully recognized lifting between $\leqslant$0.5 kg, 2.3 ~ 4.5 kg, 6.8 ~ 9.1 kg, and $\geqslant$11.3 kg with an accuracy of 0.816. Moreover, to explain the rationale behind the BiLSTM-Transformer Encoder model, Integrated Gradients (IG) was applied to gain insights into how the model relied on individual features to make predictions. The results indicated that our model captured the temporal dependencies, and identified three lifting phases such as the initial lift phase, mid-lift phase and final place phase. It also showed the model's ability of focusing on different features during different phases of the lifting process, highlighting its nuanced understanding of the biomechanics involved. Additionally, the dissertation investigated the application of the developed machine learning model to videos for lifting weight recognition. The results showed that the BiLSTM-Transformer Encoder model applied to videos achieved comparable performance comparing to using IMU data, effectively recognizing multi-level lifting weight. In conclusion, this research demonstrated the potential for improved accuracy in lifting weight recognition tasks. The proposed method and

findings in this research pave the way for future innovations and developments in lifting weight recognition tasks.

While these advancements are notable, a few limitations should be addressed in future research. The investigation on lifting weight effects on lifting kinematics was limited by the types of lifting. For instance, this study only investigated symmetric, two-handed lifting. The highest lifting height examined in the study was at elbow level, while higher lifting heights, such as shoulder height or overhead height, were not included. Besides, individuals with larger (BMI > 27.0) or smaller (BMI < 18.9) body sizes were underrepresented because they could not wear the tight suit required for accurate Xsens data collection. Future research should cover a broader range of lifting types and population. The model's performance and its application to kinematic data, while promising, didn't provide precise lifting weight information and, therefore, not ideal for contexts that require continuous weight values. Future research should explore different approaches such as adding additional data sources.

In summary, while this research makes significant improvement in simplifying and improving lifting weight recognition tasks, ongoing research is needed to address these limitations and further improve the accuracy and applicability of lifting weight recognition model in diverse environments.

Bibliography

Abobakr, A., Nahavandi, D., Hossny, M., Iskander, J., Attia, M., Nahavandi, S., & Smets, M. (2019). RGB-D ergonomic assessment system of adopted working postures. *Applied Ergonomics*, *80*, 75–88. https://doi.org/10.1016/j.apergo.2019.05.004

Antwi-Afari, M. F., Li, H., Umer, W., Yu, Y., & Xing, X. (2020). Construction Activity Recognition and Ergonomic Risk Assessment Using a Wearable Insole Pressure System. *Journal of Construction Engineering and Management*, *146*(7). https://doi.org/10.1061/(ASCE)CO.1943-7862.0001849

Azari, D. P., Hu, Y. H., Miller, B. L., Le, B. V., & Radwin, R. G. (2019). Using Surgeon Hand Motions to Predict Surgical Maneuvers. *Human Factors*, *61*(8), 1326–1339. https://doi.org/10.1177/0018720819838901

Battini, D., Berti, N., Finco, S., Guidolin, M., Reggiani, M., & Tagliapietra, L. (2022). WEM-Platform: A real-time platform for full-body ergonomic assessment and feedback in manufacturing and logistics systems. *Computers and Industrial Engineering*, *164*. https://doi.org/10.1016/j.cie.2021.107881

Bazarevsky, V., Grishchenko, I., Raveendran, K., Zhu, T., Zhang, F., & Grundmann, M. (2020). *BlazePose: On-device Real-time Body Pose tracking* (Version 1). arXiv. https://doi.org/10.48550/ARXIV.2006.10204

Benjamini, Y., & Hochberg, Y. (1995). Controlling the False Discovery Rate: A Practical and Powerful Approach to Multiple Testing. *Journal of the Royal Statistical Society Series B: Statistical Methodology*, *57*(1), 289–300. https://doi.org/10.1111/j.2517-6161.1995.tb02031.x

Bortolini, M., Faccio, M., Gamberi, M., & Pilati, F. (2020). Motion Analysis System (MAS) for production and ergonomics assessment in the manufacturing processes. *Computers and Industrial Engineering, 139*. https://doi.org/10.1016/j.cie.2018.10.046

Cabin, R. J., & Mitchell, R. J. (2000). To Bonferroni or Not to Bonferroni: When and How Are the Questions. *Bulletin of the Ecological Society of America*, *81*(3), 246–248.

Caderby, T., Dalleau, G., Leroyer, P., Bonazzi, B., Chane-Teng, D., & Do, M.-C. (2013). Does an additional load modify the Anticipatory Postural Adjustments in gait initiation? *Gait & Posture*, *37*(1), 144–146. https://doi.org/10.1016/j.gaitpost.2012.06.012

Cao, Z., Hidalgo, G., Simon, T., Wei, S.-E., & Sheikh, Y. (2018). *OpenPose: Realtime Multi-Person 2D Pose Estimation using Part Affinity Fields* (Version 2). arXiv. https://doi.org/10.48550/ARXIV.1812.08008

Chen, C.-H., Hu, Y. H., Yen, T. Y., & Radwin, R. G. (2013). Automated video exposure assessment of repetitive hand activity level for a load transfer task. *Human Factors*, *55*(2), 298–308. https://doi.org/10.1177/0018720812458121

Chen, H. (2017). *The effects of movement speeds and magnetic disturbance on inertial measurement unit accuracy: The implications of sensor fusion algorithms in occupational ergonomics applications*. Iowa Research Online.

Cheng, C.-K., Chen, H.-H., Kuo, H.-H., Lee, C.-L., Chen, W.-J., & Liu, C.-L. (1998). A three-dimensional mathematical model for predicting spinal joint force distribution during manual liftings. *Clinical Biomechanics*, *13*(1), S59–S64. https://doi.org/10.1016/S0268-0033(97)00077-6

Cole, M. H., & Grimshaw, P. N. (2003). Low back pain and lifting: A review of epidemiology and aetiology. *Work*, *21*(2), 173–184.

Conforti, I., Mileti, I., Del Prete, Z., & Palermo, E. (2020). Measuring Biomechanical Risk in Lifting Load Tasks Through Wearable System and Machine-Learning Approach. *Sensors (Basel, Switzerland)*, *20*(6). https://doi.org/10.3390/s20061557

Constant, C. R. (1989). Historical background, anatomy and shoulder function. *Baillière's Clinical Rheumatology*, *3*(3), 429–435. https://doi.org/10.1016/S0950-3579(89)80002-0

Côté, J. N. (2012). A critical review on physical factors and functional characteristics that may explain a sex/gender difference in work-related neck/shoulder disorders. *Ergonomics*, *55*(2), 173–182. https://doi.org/10.1080/00140139.2011.586061

David, G. C. (2005). Ergonomic methods for assessing exposure to risk factors for work-related musculoskeletal disorders. *Occupational Medicine*, *55*(3), 190–199. https://doi.org/10.1093/occmed/kqi082

Davis, K. G., Jorgensen, M. J., & Marras, W. S. (2000). An investigation of perceived exertion via whole body exertion and direct muscle force indicators during the determination of the maximum acceptable weight of lift. *Ergonomics*, *43*(2), 143–159. https://doi.org/10.1080/001401300184521

Davis, K. G., & Marras, W. S. (2000). Assessment of the Relationship between Box Weight and Trunk Kinematics: Does a Reduction in Box Weight Necessarily Correspond to a Decrease in Spinal Loading? *Human Factors: The Journal of the Human Factors and Ergonomics Society*, *42*(2), 195–208. https://doi.org/10.1518/001872000779656499

Davis, K. G., Splittstoesser, R. E., & Marras, W. S. (2003). Kinematic contribution and synchronization of the trunk, hip, and knee during free-dynamic lifting. *Occupational Ergonomics*, *3*(2), 99–108. https://doi.org/10.3233/OER-2003-3202

de Looze, M. P., Dolan, P., Kingma, I., & Baten, C. T. M. (1998). Does an asymmetric straddle-legged lifting movement reduce the low-back load? *Human Movement Science*, *17*(2), 243–259. https://doi.org/10.1016/S0167-9457(97)00032-8

Desmedt, J. E., & Godaux, E. (1978). Ballistic contractions in fast or slow human muscles; discharge patterns of single motor units. *The Journal of Physiology*, *285*(1), 185–196. https://doi.org/10.1113/jphysiol.1978.sp012566

Devlin, J., Chang, M.-W., Lee, K., & Toutanova, K. (2018). *BERT: Pre-training of Deep Bidirectional Transformers for Language Understanding* (Version 2). arXiv. https://doi.org/10.48550/ARXIV.1810.04805

Diego-Mas, J.-A., Alcaide-Marzal, J., & Poveda-Bautista, R. (2017). Errors Using Observational Methods for Ergonomics Assessment in Real Practice. *Human Factors: The Journal of the Human Factors and Ergonomics Society*, *59*(8), 1173–1187. https://doi.org/10.1177/0018720817723496

Donisi, L., Cesarelli, G., Coccia, A., Panigazzi, M., Capodaglio, E. M., & Daddio, G. (2021). Work-related risk assessment according to the revised niosh lifting equation: A preliminary study using a wearable inertial sensor and machine learning. *Sensors*, *21*(8). http://dx.doi.org/10.3390/s21082593

E. Rocha-Ibarra, M. -I. Oros-Flores, D. -L. Almanza-Ojeda, G. -A. Lugo-Bustillo, A. Rosales-Castellanos, M. -A. Ibarra-Manzano, & J. C. Gomez. (2021). Kinect Validation of Ergonomics in Human Pick and Place Activities Through Lateral Automatic Posture Detection. *IEEE Access*, *9*, 109067–109079. https://doi.org/10.1109/ACCESS.2021.3101964

El-Gohary, M., & McNames, J. (2012). Shoulder and Elbow Joint Angle Tracking With Inertial Sensors. *IEEE Transactions on Biomedical Engineering*, *59*(9), 2635–2641. https://doi.org/10.1109/TBME.2012.2208750

EU-OSHA. (2019). *Work-related musculoskeletal disorders: Prevalence, costs and demographics in the EU European*. European Agency for Safety and Health at Work (EU-OSHA). https://osha.europa.eu/sites/default/files/Work-related_MSDs_prevalence_costs_and_demographics_in_the_EU_report.pdf

Fowler, N. E., Rodacki, A. L. F., & Rodacki, C. D. (2006). Changes in stature and spine kinematics during a loaded walking task. *Gait & Posture*, *23*(2), 133–141. https://doi.org/10.1016/j.gaitpost.2004.12.006

Fung, E. H. K. (2003). A real-time gyroscopic system for three-dimensional measurement of lumbar spine motion. *Medical Engineering & Physics*, *25*(10), 817–824. https://doi.org/10.1016/S1350-4533(03)00115-2

G. Zhou, V. Aggarwal, M. Yin, & D. Yu. (2022). A Computer Vision Approach for Estimating Lifting Load Contributors to Injury Risk. *IEEE Transactions on Human-Machine Systems*, *52*(2), 207–219. https://doi.org/10.1109/THMS.2022.3148339

Gallagher, S., & Schall Jr., M. C. (2017). Musculoskeletal disorders as a fatigue failure process: Evidence, implications and research needs. *Ergonomics*, *60*(2), 255–269. https://doi.org/10.1080/00140139.2016.1208848

Gers, F. A., Schraudolph, N. N., & Schmidhuber, J. (2002). Learning precise timing with LSTM recurrent networks. *Journal of Machine Learning Research*, *3*(1), 115–143.

Gong, J., Caldas, C. H., & Gordon, C. (2011). Learning and classifying actions of construction workers and equipment using Bag-of-Video-Feature-Words and Bayesian network

models. *Advanced Engineering Informatics*, *25*(4), 771–782. https://doi.org/10.1016/j.aei.2011.06.002

Goršič, M., Dai, B., & Novak, D. (2020). Load Position and Weight Classification during Carrying Gait Using Wearable Inertial and Electromyographic Sensors. *Sensors*, *20*(17), 4963. https://doi.org/10.3390/s20174963

Greene, R. L., Azari, D. P., Hu, Y. H., & Radwin, R. G. (2017). Visualizing stressful aspects of repetitive motion tasks and opportunities for ergonomic improvements using computer vision. *Applied Ergonomics*, *65*, 461–472. https://doi.org/10.1016/j.apergo.2017.02.020

Greene, R. L., Hu, Y. H., Difranco, N., Wang, X., Lu, M.-L., Bao, S., Lin, J.-H., & Radwin, R. G. (2019). Predicting Sagittal Plane Lifting Postures From Image Bounding Box Dimensions. *Human Factors*, *61*(1), 64–77. https://doi.org/10.1177/0018720818791367

Grood, E. S., & Suntay, W. J. (1983). A Joint Coordinate System for the Clinical Description of Three-Dimensional Motions: Application to the Knee. *Journal of Biomechanical Engineering*, *105*(2), 136–144. https://doi.org/10.1115/1.3138397

H. Jeong & W. Park. (2021). Developing and Evaluating a Mixed Sensor Smart Chair System for Real-Time Posture Classification: Combining Pressure and Distance Sensors. *IEEE Journal of Biomedical and Health Informatics*, *25*(5), 1805–1813. https://doi.org/10.1109/JBHI.2020.3030096

Hamill, J., van Emmerik, R. E. A., Heiderscheit, B. C., & Li, L. (1999). A dynamical systems approach to lower extremity running injuries. *Clinical Biomechanics*, *14*(5), 297–308. https://doi.org/10.1016/S0268-0033(98)90092-4

He, K., Zhang, X., Ren, S., & Sun, J. (2015). *Deep Residual Learning for Image Recognition* (Version 1). arXiv. https://doi.org/10.48550/ARXIV.1512.03385

Henneman, E., Somjen, G., & Carpenter, D. O. (1965). FUNCTIONAL SIGNIFICANCE OF CELL SIZE IN SPINAL MOTONEURONS. *Journal of Neurophysiology*, *28*(3), 560–580. https://doi.org/10.1152/jn.1965.28.3.560

Hignett, S., & McAtamney, L. (2000). Rapid Entire Body Assessment (REBA). *Applied Ergonomics*, *31*(2), 201–205. https://doi.org/10.1016/S0003-6870(99)00039-3

Hochreiter, S., & Schmidhuber, J. (1997). Long Short-Term Memory. *Neural Computation*, *9*(8), 1735–1780. https://doi.org/10.1162/neco.1997.9.8.1735

Holm, S. (1979). A Simple Sequentially Rejective Multiple Test Procedure. *Scandinavian Journal of Statistics*, *6*(2), 65–70.

Karhu, O., Kansi, P., & Kuorinka, I. (1977). Correcting working postures in industry: A practical method for analysis. *Applied Ergonomics*, *8*(4), 199–201. https://doi.org/10.1016/0003-6870(77)90164-8

Kim, W., Sung, J., Saakes, D., Huang, C., & Xiong, S. (2021). Ergonomic postural assessment using a new open-source human pose estimation technology (OpenPose). *International Journal of Industrial Ergonomics*, *84*. https://doi.org/10.1016/j.ergon.2021.103164

Kingma, D. P., & Ba, J. (2017). *Adam: A Method for Stochastic Optimization* (arXiv:1412.6980). arXiv. http://arxiv.org/abs/1412.6980

Kjellberg, K., Lindbeck, L., & Hagberg, M. (1998). Method and performance: Two elements of work technique. *Ergonomics*, *41*(6), 798–816. https://doi.org/10.1080/001401398186658

Kruger, J., & Nguyen, T. D. (2015). Automated vision-based live ergonomics analysis in assembly operations. *CIRP Annals*, *64*(1), 9–12. https://doi.org/10.1016/j.cirp.2015.04.046

LaFiandra, M., Wagenaar, R. C., Holt, K. G., & Obusek, J. P. (2003). How do load carriage and walking speed influence trunk coordination and stride parameters? *Journal of Biomechanics*, *36*(1), 87–95. https://doi.org/10.1016/S0021-9290(02)00243-9

Lamooki, S. R., Hajifar, S., Kang, J., Sun, H., Megahed, F. M., & Cavuoto, L. A. (2022). A data analytic end-to-end framework for the automated quantification of ergonomic risk factors across multiple tasks using a single wearable sensor. *Applied Ergonomics*, *102*. https://doi.org/10.1016/j.apergo.2022.103732

Lee, H., Yang, K., Kim, N., & Ahn, C. R. (2020). Detecting excessive load-carrying tasks using a deep learning network with a Gramian Angular Field. *Automation in Construction*, *120*, 103390. https://doi.org/10.1016/j.autcon.2020.103390

Lee, S., Liu, L., Radwin, R., & Li, J. (2021). Machine Learning in Manufacturing Ergonomics: Recent Advances, Challenges, and Opportunities. *IEEE Robotics and Automation Letters*, *6*(3), 5745–5752. https://doi.org/10.1109/LRA.2021.3084881

Lee, T.-H. (2015). The effects of load magnitude and lifting speed on the kinematic data of load and human posture. *International Journal of Occupational Safety and Ergonomics*, *21*(1), 55–61. https://doi.org/10.1080/10803548.2015.1017956

Li, K., & Zhang, X. (2009). Can Relative Strength Between the Back and Knees Differentiate Lifting Strategy? *Human Factors: The Journal of the Human Factors and Ergonomics Society*, *51*(6), 785–796. https://doi.org/10.1177/0018720809360801

Li, Y., Greene, R. L., Mu, F., Hu, Y. H., & Radwin, R. G. (2020). Towards Video-Based Automatic Lifting Load Prediction. *Proceedings of the Human Factors and Ergonomics Society Annual Meeting*, *64*(1), 962–963. https://doi.org/10.1177/1071181320641230

Li, Z., Zhang, R., Lee, C.-H., & Lee, Y.-C. (2020). An Evaluation of Posture Recognition Based on Intelligent Rapid Entire Body Assessment System for Determining Musculoskeletal Disorders. *Sensors (Basel, Switzerland)*, *20*(16). https://doi.org/10.3390/s20164414

Liberty Mutual. (2021). *Liberty Mutual Workplace Safety Index 2021*. https://business.libertymutual.com/wp-content/uploads/2021/06/2021_WSI_1000_R2.pdf

Lim, S., & D'Souza, C. (2019). Statistical prediction of load carriage mode and magnitude from inertial sensor derived gait kinematics. *Applied Ergonomics*, *76*, 1–11. https://doi.org/10.1016/j.apergo.2018.11.007

Lin, P.-C., Chen, Y.-J., Chen, W.-S., & Lee, Y.-J. (2022). Automatic real-time occupational posture evaluation and select corresponding ergonomic assessments. *Scientific Reports*, *12*(1), 2139. https://doi.org/10.1038/s41598-022-05812-9

Lindbeck, L., & Kjellberg, K. (2001). Gender differences in lifting technique. *Ergonomics*, *44*(2), 202–214. https://doi.org/10.1080/00140130120142

Liu, Y., & Lapata, M. (2019). *Text Summarization with Pretrained Encoders* (Version 2). arXiv. https://doi.org/10.48550/ARXIV.1908.08345

Looze, M. P., Dolan, P., Kingma, I., & Baten, C. T. M. (1998). Does an asymmetric straddle-legged lifting movement reduce the low-back load? *Human Movement Science, 17*, 243–259.

Lorenzini, M., Kim, W., De Momi, E., & Ajoudani, A. (2018). A Synergistic Approach to the Real-Time Estimation of the Feet Ground Reaction Forces and Centers of Pressure in Humans With Application to Human–Robot Collaboration. *IEEE Robotics and Automation Letters*, *3*(4), 3654–3661. https://doi.org/10.1109/LRA.2018.2855802

Malaise, A., Maurice, P., Colas, F., & Ivaldi, S. (2019). Activity Recognition for Ergonomics Assessment of Industrial Tasks With Automatic Feature Selection. *IEEE Robotics and Automation Letters*, *4*(2), 1132–1139. https://doi.org/10.1109/LRA.2019.2894389

Manghisi, V. M., Uva, A. E., Fiorentino, M., Bevilacqua, V., Trotta, G. F., & Monno, G. (2017). Real time RULA assessment using Kinect v2 sensor. *Applied Ergonomics*, *65*((Manghisi V.M., vitomodesto.manghisi@poliba.it; Uva A.E.; Fiorentino M.; Bevilacqua V.; Trotta G.F.; Monno G.) Polytechnic Institute of Bari, Italy), 481–491. https://doi.org/10.1016/j.apergo.2017.02.015

Marras, W. S., Davis, K. G., & Jorgensen, M. (2003). Gender influences on spine loads during complex lifting. *The Spine Journal*, *3*(2), 93–99. https://doi.org/10.1016/S1529-9430(02)00570-3

Marras, W. S., & Mirka, G. A. (1990). Muscle activities during asymmetric trunk angular accelerations. *Journal of Orthopaedic Research*, *8*(6), 824–832. https://doi.org/10.1002/jor.1100080607

Marras, W. S., & Sommerich, C. M. (1991). A Three-Dimensional Motion Model of Loads on the Lumbar Spine: II. Model Validation. *Human Factors: The Journal of the Human Factors and Ergonomics Society*, *33*(2), 139–149. https://doi.org/10.1177/001872089103300202

Martinez, R., Assila, N., Goubault, E., & Begon, M. (2020). Sex differences in upper limb musculoskeletal biomechanics during a lifting task. *Applied Ergonomics*, *86*, 103106. https://doi.org/10.1016/j.apergo.2020.103106

Martinez, R., Bouffard, J., Michaud, B., Plamondon, A., Côté, J. N., & Begon, M. (2019). Sex differences in upper limb 3D joint contributions during a lifting task. *Ergonomics*, *62*(5), 682–693. https://doi.org/10.1080/00140139.2019.1571245

Maruyama, T., Ueshiba, T., Tada, M., Toda, H., Endo, Y., Domae, Y., Nakabo, Y., Mori, T., & Suita, K. (2021). Digital Twin-Driven Human Robot Collaboration Using a Digital Human. *Sensors*, *21*(24), 8266. https://doi.org/10.3390/s21248266

Matijevich, E. S., Volgyesi, P., & Zelik, K. E. (2021). A Promising Wearable Solution for the Practical and Accurate Monitoring of Low Back Loading in Manual Material Handling. *Sensors*, *21*(2), 340. https://doi.org/10.3390/s21020340

McAtamney, L., & Nigel Corlett, E. (1993). RULA: A survey method for the investigation of work-related upper limb disorders. *Applied Ergonomics*, *24*(2), 91–99. https://doi.org/10.1016/0003-6870(93)90080-S

MediaPipe Pose. (n.d.). Retrieved May 23, 2023, from https://github.com/google-ai-edge/mediapipe/blob/master/docs/solutions/pose.md

Messeri, C., Bicchi, A., Zanchettin, A. M., & Rocco, P. (2022). A Dynamic Task Allocation Strategy to Mitigate the Human Physical Fatigue in Collaborative Robotics. *IEEE Robotics and Automation Letters*, *7*(2), 2178–2185. https://doi.org/10.1109/LRA.2022.3143520

Nath, N. D., Chaspari, T., & Behzadan, A. H. (2018). Automated ergonomic risk monitoring using body-mounted sensors and machine learning. *Advanced Engineering Informatics*, *38*, 514–526. https://doi.org/10.1016/j.aei.2018.08.020

Newell, A., Yang, K., & Deng, J. (2016). Stacked Hourglass Networks for Human Pose Estimation. In B. Leibe, J. Matas, N. Sebe, & M. Welling (Eds.), *Computer Vision* –

ECCV 2016 (Vol. 9912, pp. 483–499). Springer International Publishing. https://doi.org/10.1007/978-3-319-46484-8_29

Norasi, H., Koenig, J., & Mirka, G. A. (2019). The effects of load weight and load starting height on variability of lifting kinematics and kinetics. *International Journal of Industrial Ergonomics*, *73*, 102830. https://doi.org/10.1016/j.ergon.2019.102830

Nordin, M., & Frankel, V. (2012). *Basic biomechanics of the musculoskeletal system (4th ed.)* (Fourth). Wolters Kluwer Health – Lippincott Williams & Wilkins.

Oyekan, J., Chen, Y., Turner, C., & Tiwari, A. (2021). Applying a fusion of wearable sensors and a cognitive inspired architecture to real-time ergonomics analysis of manual assembly tasks. *Journal of Manufacturing Systems*, *61*, 391–405. https://doi.org/10.1016/j.jmsy.2021.09.015

Pan, T., Wang, Z., & Fan, Y. (2022). Optimized convolutional pose machine for 2D hand pose estimation. *Journal of Visual Communication and Image Representation*, *83*, 103461. https://doi.org/10.1016/j.jvcir.2022.103461

Parsa, B., Samani, E. U., Hendrix, R., Devine, C., Singh, S. M., Devasia, S., & Banerjee, A. G. (2019). Toward Ergonomic Risk Prediction via Segmentation of Indoor Object Manipulation Actions Using Spatiotemporal Convolutional Networks. *IEEE Robotics and Automation Letters*, *4*(4), 3153–3160. https://doi.org/10.1109/LRA.2019.2925305

Peppoloni, L., Filippeschi, A., Ruffaldi, E., & Avizzano, C. A. (2016). A novel wearable system for the online assessment of risk for biomechanical load in repetitive efforts. *International Journal of Industrial Ergonomics*, *52*, 1–11. https://doi.org/10.1016/j.ergon.2015.07.002

Picerno, P., Cereatti, A., & Cappozzo, A. (2008). Joint kinematics estimate using wearable inertial and magnetic sensing modules. *Gait & Posture*, *28*(4), 588–595. https://doi.org/10.1016/j.gaitpost.2008.04.003

Plamondon, A., Larivière, C., Denis, D., Mecheri, H., & Nastasia, I. (2017). Difference between male and female workers lifting the same relative load when palletizing boxes. *Applied Ergonomics*, *60*, 93–102. https://doi.org/10.1016/j.apergo.2016.10.014

Plamondon, A., Larivière, C., Denis, D., St-Vincent, M., & Delisle, A. (2014). Sex differences in lifting strategies during a repetitive palletizing task. *Applied Ergonomics*, *45*(6), 1558–1569. https://doi.org/10.1016/j.apergo.2014.05.005

Plantard, P., Auvinet, E., Pierres, A.-S. L., & Multon, F. (2015). Pose estimation with a Kinect for ergonomic studies: Evaluation of the accuracy using a virtual mannequin. *Sensors (Basel, Switzerland)*, *15*(1), 1785–1803. https://doi.org/10.3390/s150101785

Plantard, P., Shum, H. P. H., Le Pierres, A.-S., & Multon, F. (2017). Validation of an ergonomic assessment method using Kinect data in real workplace conditions. *Applied Ergonomics*, *65*, 562–569. https://doi.org/10.1016/j.apergo.2016.10.015

Punnett, L., Prüss-Ütün, A., Nelson, D. I., Fingerhut, M. A., Leigh, J., Tak, S., & Phillips, S. (2005). Estimating the global burden of low back pain attributable to combined occupational exposures. *American Journal of Industrial Medicine*, *48*(6), 459–469. https://doi.org/10.1002/ajim.20232

Qu, X., & Yeo, J. C. (2011). Effects of load carriage and fatigue on gait characteristics. *Journal of Biomechanics*, *44*(7), 1259–1263. https://doi.org/10.1016/j.jbiomech.2011.02.016

Radford, A., Narasimhan, K., Salimans, T., & Sutskever, I. (2018). *Improving language understanding by generative pre-training*. https://cdn.openai.com/research-covers/language-unsupervised/language_understanding_paper.pdf

Ray, S. J., & Teizer, J. (2012). Real-time construction worker posture analysis for ergonomics training. *Advanced Engineering Informatics*, *26*(2), 439–455. https://doi.org/10.1016/j.aei.2012.02.011

Robert-Lachaine, X., Mecheri, H., Larue, C., & Plamondon, A. (2017). Validation of inertial measurement units with an optoelectronic system for whole-body motion analysis. *Medical & Biological Engineering & Computing*, *55*(4), 609–619. https://doi.org/10.1007/s11517-016-1537-2

Roberts, D., Torres Calderon, W., Tang, S., & Golparvar-Fard, M. (2020). Vision-Based Construction Worker Activity Analysis Informed by Body Posture. *Journal of Computing in Civil Engineering*, *34*(4). https://doi.org/10.1061/(ASCE)CP.1943-5487.0000898

Sarafianos, N., Boteanu, B., Ionescu, B., & Kakadiaris, I. A. (2016). 3D Human pose estimation: A review of the literature and analysis of covariates. *Computer Vision and Image Understanding*, *152*, 1–20. https://doi.org/10.1016/j.cviu.2016.09.002

Schall, M. C., Fethke, N. B., Chen, H., Oyama, S., & Douphrate, D. I. (2016). Accuracy and repeatability of an inertial measurement unit system for field-based occupational studies. *Ergonomics*, *59*(4), 591–602. https://doi.org/10.1080/00140139.2015.1079335

Scholz, J. P. (1993). Organizational principles for the coordination of lifting. *Human Movement Science*, *12*(5), 537–576. https://doi.org/10.1016/0167-9457(93)90004-9

Schuster, M., & Paliwal, K. K. (1997). Bidirectional recurrent neural networks. *IEEE Transactions on Signal Processing*, *45*(11), 2673–2681. https://doi.org/10.1109/78.650093

Seo, J., & Lee, S. (2021). Automated postural ergonomic risk assessment using vision-based posture classification. *Automation in Construction*, *128*. https://doi.org/10.1016/j.autcon.2021.103725

Shavit, Y., & Klein, I. (2021). Boosting Inertial-Based Human Activity Recognition With Transformers. *IEEE Access*, *9*, 53540–53547. https://doi.org/10.1109/ACCESS.2021.3070646

Song, J., & Qu, X. (2014). Effects of age and its interaction with task parameters on lifting biomechanics. *Ergonomics*, *57*(5), 653–668. https://doi.org/10.1080/00140139.2014.897376

Spector, J. T., Lieblich, M., Bao, S., McQuade, K., & Hughes, M. (2014). Automation of workplace lifting hazard assessment for musculoskeletal injury prevention. *Annals of Occupational and Environmental Medicine*, *26*(1). https://doi.org/10.1186/2052-4374-26-15

Stålhammar, H. R., Troup, J. D. G., & Leskinen, T. P. J. (1989). Rating of acceptable loads: Lifting with and without handles. *International Journal of Industrial Ergonomics*, *3*(3), 229–234. https://doi.org/10.1016/0169-8141(89)90022-X

Stergiou, N., Jensen, J. L., Bates, B. T., Scholten, S. D., & Tzetzis, G. (2001). A dynamical systems investigation of lower extremity coordination during running over obstacles. *Clinical Biomechanics*, *16*(3), 213–221. https://doi.org/10.1016/S0268-0033(00)00090-5

Sundararajan, M., Taly, A., & Yan, Q. (2017). *Axiomatic Attribution for Deep Networks* (Version 2). arXiv. https://doi.org/10.48550/ARXIV.1703.01365

Toshev, A., & Szegedy, C. (2014). DeepPose: Human Pose Estimation via Deep Neural Networks. *2014 IEEE Conference on Computer Vision and Pattern Recognition*, 1653–1660. https://doi.org/10.1109/CVPR.2014.214

U.S. Bureau of Labor Statistics. (2020, May 1). *Occupational injuries and illnesses resulting in musculoskeletal disorders (MSDs)*. https://www.bls.gov/iif/factsheets/msds.htm

Van Crombrugge, I., Sels, S., Ribbens, B., Steenackers, G., Penne, R., & Vanlanduit, S. (2022a). Accuracy Assessment of Joint Angles Estimated from 2D and 3D Camera Measurements. *Sensors*, *22*(5), 1729. https://doi.org/10.3390/s22051729

Van Crombrugge, I., Sels, S., Ribbens, B., Steenackers, G., Penne, R., & Vanlanduit, S. (2022b). Accuracy Assessment of Joint Angles Estimated from 2D and 3D Camera Measurements. *Sensors (Basel, Switzerland)*, *22*(5). https://doi.org/10.3390/s22051729

Vaswani, A., Shazeer, N., Parmar, N., Uszkoreit, J., Jones, L., Gomez, A. N., Kaiser, L., & Polosukhin, I. (2017). *Attention Is All You Need* (Version 7). arXiv. https://doi.org/10.48550/ARXIV.1706.03762

Vianello, L., Gomes, W., Stulp, F., Aubry, A., Maurice, P., & Ivaldi, S. (2022). Latent Ergonomics Maps: Real-Time Visualization of Estimated Ergonomics of Human Movements. *Sensors*, *22*(11), 3981. https://doi.org/10.3390/s22113981

Wei, S.-E., Ramakrishna, V., Kanade, T., & Sheikh, Y. (2016). Convolutional Pose Machines. *2016 IEEE Conference on Computer Vision and Pattern Recognition (CVPR)*, 4724–4732. https://doi.org/10.1109/CVPR.2016.511

Wensel, J., Ullah, H., & Munir, A. (2022). *ViT-ReT: Vision and Recurrent Transformer Neural Networks for Human Activity Recognition in Videos* (Version 2). arXiv. https://doi.org/10.48550/ARXIV.2208.07929

Wu, Y., Kirillov, A., Massa, F., Lo, W.-Y., & Girshick, R. (2019). *Detectron2*. https://github.com/facebookresearch/detectron2

Xsens Technologies B.V. (2021). *Xsens MVN User Manual*.

Yan, X., Li, H., Li, A. R., & Zhang, H. (2017). Wearable IMU-based real-time motion warning system for construction workers' musculoskeletal disorders prevention. *Automation in Construction, 74*, 2–11. https://doi.org/10.1016/j.autcon.2016.11.007

Yang, K., Ahn, C. R., & Kim, H. (2020). Deep learning-based classification of work-related physical load levels in construction. *Advanced Engineering Informatics*, *45*, 101104. https://doi.org/10.1016/j.aei.2020.101104

Yoon, J., Shiekhzadeh, A., & Nordin, M. (2012). The effect of load weight vs. Pace on muscle recruitment during lifting. *Applied Ergonomics, 43*(6), 1044–1050. https://doi.org/10.1016/j.apergo.2012.03.004

Yu, Y., Li, H., Umer, W., Dong, C., Yang, X., Skitmore, M., & Wong, A. Y. L. (2019). Automatic Biomechanical Workload Estimation for Construction Workers by Computer Vision and Smart Insoles. *Journal of Computing in Civil Engineering*, *33*(3). https://doi.org/10.1061/(ASCE)CP.1943-5487.0000827

Yu, Y., Li, H., Yang, X., Kong, L., Luo, X., & Wong, A. Y. L. (2019). An automatic and non-invasive physical fatigue assessment method for construction workers. *Automation in Construction, 103*, 1–12. https://doi.org/10.1016/j.autcon.2019.02.020

Yu, Y., Yang, X., Li, H., Luo, X., Guo, H., & Fang, Q. (2019). Joint-level vision-based ergonomic assessment tool for construction workers. *Journal of Construction Engineering and Management, 145*(5). https://doi.org/10.1061/(ASCE)CO.1943-7862.0001647

Zhao, J., Obonyo, E., & G. Bilén, S. (2021). Wearable Inertial Measurement Unit Sensing System for Musculoskeletal Disorders Prevention in Construction. *Sensors*, *21*(4), 1324. https://doi.org/10.3390/s21041324

Zhao, J., Obonyo, E., & G Bilén, S. (2021). Wearable Inertial Measurement Unit Sensing System for Musculoskeletal Disorders Prevention in Construction. *Sensors (Basel, Switzerland)*, *21*(4). https://doi.org/10.3390/s21041324

Zhou, X., Huang, Q., Sun, X., Xue, X., & Wei, Y. (2017). Towards 3D Human Pose Estimation in the Wild: A Weakly-Supervised Approach. *2017 IEEE International Conference on Computer Vision (ICCV)*, 398–407. https://doi.org/10.1109/ICCV.2017.51

Appendices

Appendix A

Figure A1: Lifting a weighted box (a) from floor to knee (b) from floor to elbow (c) from knee to elbow.

(a) Lifting from floor to knee

(b) Lifting from floor to elbow

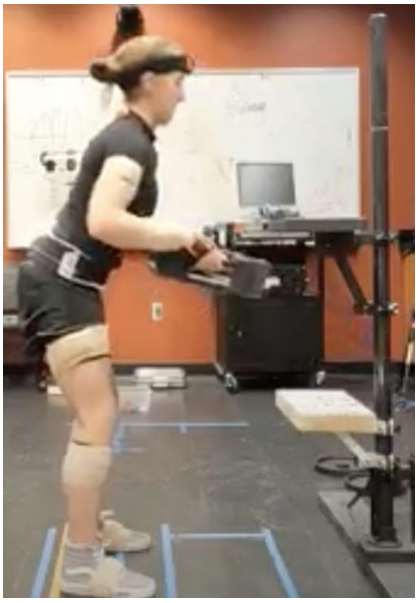

(c) Lifting from knee to elbow

Figure A2: Positions of IMU sensors on subjects.

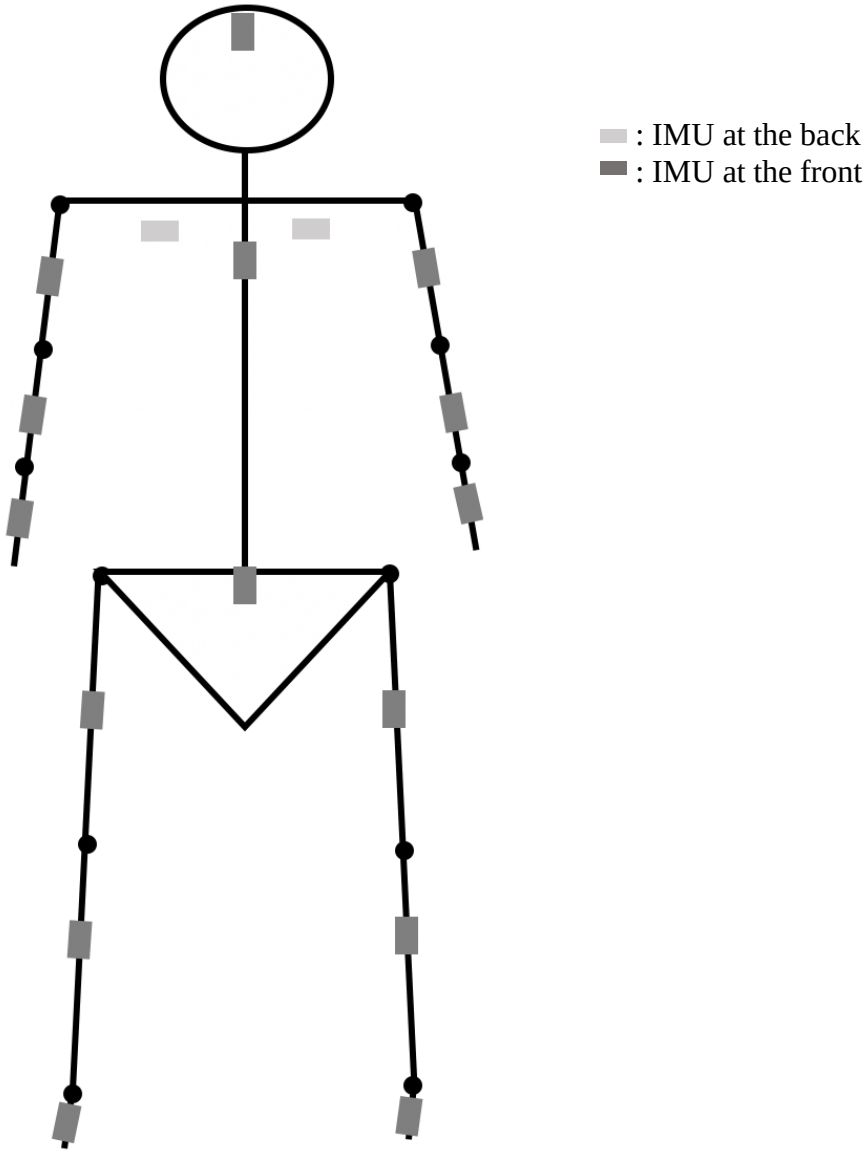

Appendix B

Table B1: Inter-subject CVs and intra-subject CVs of peak angular velocities during the lifting phase.

CV (%)	Height	Weight (kg)	Abduction Peak Angular Velocity of Shoulder	External Rotation Peak Angular Velocity of Shoulder	Flextion Peak Angular Velocity of Shoulder	Flextion Peak Angular Velocity of Elbow
Inter	Floor-Elbow	0.5	14.14	14.38	12.54	8.75
		2.3	14.24	13.96	11.54	9.85
		4.5	12.99	12.57	11.87	9.86
		6.8	11.09	10.71	11.99	11.08
		9.1	12.19	13.15	12.52	10.67
		11.3	12.29	11.26	12.58	12.99
		13.6	12.49	12.59	14.37	13.05
	Floor-Knee	0.5	12.36	12.59	9.40	11.44
		2.3	16.65	16.12	12.97	16.23
		4.5	15.92	15.61	13.91	15.24
		6.8	13.31	13.20	11.50	12.03
		9.1	15.21	15.56	11.09	12.58
		11.3	11.72	14.03	12.89	12.23
		13.6	12.04	12.65	12.42	11.57
	Knee-Elbow	0.5	13.90	16.99	11.56	9.28
		2.3	12.37	14.61	12.03	5.42
		4.5	12.40	10.79	11.76	8.12
		6.8	11.74	11.69	12.44	8.93
		9.1	12.07	10.14	10.32	9.08
		11.3	13.38	12.04	14.54	10.44
		13.6	13.45	12.36	12.28	12.28
Intra	Floor-Elbow	0.5	6.93	6.23	9.16	7.57
		2.3	5.93	6.11	8.72	6.69
		4.5	6.21	6.31	7.59	7.24
		6.8	6.90	6.27	8.21	6.76
		9.1	5.32	4.19	7.45	6.59
		11.3	6.67	7.00	7.80	7.98
		13.6	6.65	7.29	6.84	6.32
	Floor-Knee	0.5	10.41	9.08	10.30	11.11
		2.3	7.47	6.92	8.55	8.30
		4.5	7.73	7.41	8.89	6.45
		6.8	6.42	5.98	8.38	6.82
		9.1	7.37	6.52	7.13	7.55
		11.3	7.62	8.51	9.86	7.49
		13.6	9.48	8.79	10.87	6.30
	Knee-Elbow	0.5	9.28	7.49	7.62	6.21
		2.3	6.60	8.43	9.14	6.27
		4.5	5.29	6.78	7.69	6.65
		6.8	8.59	7.29	7.49	7.96
		9.1	6.02	7.14	7.40	7.73
		11.3	9.77	7.48	7.80	8.22
		13.6	8.77	7.34	9.73	7.41

Table B2: Inter-subject CVs and intra-subject CVs of peak angular velocities during the placement phase.

CV (%)	Height	Weight (kg)	Adduction Peak Angular Velocity of Shoulder	Internal Rotation Peak Angular Velocity of Shoulder	Extension Peak Angular Velocity of Shoulder	Extension Peak Angular Velocity of Elbow
Inter	Floor-Elbow	0.5	14.52	14.07	12.16	9.64
		2.3	12.41	12.75	12.99	5.14
		4.5	15.68	14.47	11.44	6.93
		6.8	17.09	14.53	14.87	7.39
		9.1	14.08	15.56	12.67	7.51
		11.3	12.14	11.60	11.73	9.21
		13.6	25.35	23.54	19.86	10.78
	Floor-Knee	0.5	12.01	11.40	9.68	10.93
		2.3	9.48	11.66	9.09	10.69
		4.5	11.73	10.97	10.47	10.23
		6.8	10.04	10.22	8.38	8.36
		9.1	13.86	14.35	13.75	8.02
		11.3	16.23	17.79	15.39	11.40
		13.6	14.23	15.82	13.95	11.06
	Knee-Elbow	0.5	12.15	11.65	11.85	7.69
		2.3	10.70	10.90	9.86	6.38
		4.5	12.44	11.53	9.64	7.64
		6.8	11.93	13.07	10.90	9.91
		9.1	11.32	9.37	9.69	8.39
		11.3	12.48	10.74	11.67	9.09
		13.6	13.06	13.39	14.37	12.98
Intra	Floor-Elbow	0.5	8.87	9.10	10.17	8.93
		2.3	5.71	6.23	7.09	6.21
		4.5	5.10	6.22	7.18	8.24
		6.8	7.59	6.07	7.66	7.18
		9.1	7.55	6.39	8.93	6.41
		11.3	8.39	7.73	8.21	7.15
		13.6	9.52	10.26	10.13	8.87
	Floor-Knee	0.5	7.43	7.98	8.53	9.01
		2.3	7.73	6.85	7.90	6.18
		4.5	7.02	7.42	5.86	6.88
		6.8	6.17	6.61	7.35	6.83
		9.1	5.12	4.54	4.48	6.76
		11.3	7.31	7.36	8.37	6.55
		13.6	8.82	8.51	8.80	7.32
	Knee-Elbow	0.5	7.06	8.47	10.25	5.71
		2.3	6.02	6.55	8.01	6.62
		4.5	5.64	4.74	6.31	5.90
		6.8	5.39	6.45	5.47	6.65
		9.1	6.78	5.85	7.21	6.83
		11.3	7.66	8.49	9.82	6.58
		13.6	6.97	6.65	8.87	6.89

Table B3: Inter-subject CVs and intra-subject CVs of average angular velocities during the lift phase.

CV (%)	Height	Weight (kg)	Abduction Average Angular Velocity of Shoulder	External Rotation Average Angular Velocity of	Flextion Average Angular Velocity of Shoulder	Flextion Average Angular Velocity of Elbow
Inter	Floor-Elbow	0.5	38.94	14.47	11.51	8.58
		2.3	27.69	12.62	12.27	8.30
		4.5	26.13	14.47	14.86	8.08
		6.8	30.67	13.80	14.40	9.62
		9.1	28.61	15.47	15.99	10.58
		11.3	24.59	13.12	14.48	9.19
		13.6	32.63	13.86	15.89	10.41
	Floor-Knee	0.5	43.24	12.35	11.45	12.56
		2.3	75.35	17.09	15.06	19.34
		4.5	50.28	18.37	15.16	18.76
		6.8	31.42	18.37	15.29	16.92
		9.1	37.30	20.85	18.72	17.48
		11.3	29.03	20.88	17.62	17.29
		13.6	26.89	20.71	20.52	16.15
	Knee-Elbow	0.5	32.65	17.75	11.58	10.40
		2.3	28.91	14.19	11.81	9.34
		4.5	33.70	16.33	13.00	11.64
		6.8	28.11	15.79	12.83	10.58
		9.1	31.97	15.69	13.75	10.53
		11.3	32.06	17.03	13.38	10.73
		13.6	33.38	15.31	14.34	11.38
Intra	Floor-Elbow	0.5	15.75	7.14	8.05	8.13
		2.3	11.03	5.20	5.80	6.05
		4.5	7.40	6.05	6.81	6.44
		6.8	8.71	6.10	5.97	5.36
		9.1	11.63	5.43	6.04	5.96
		11.3	11.25	6.93	7.49	6.71
		13.6	10.51	7.47	6.86	6.10
	Floor-Knee	0.5	20.68	11.20	11.45	13.93
		2.3	11.44	8.14	7.15	9.60
		4.5	10.87	9.40	8.68	9.28
		6.8	12.18	7.71	7.03	8.85
		9.1	13.51	8.09	7.29	7.59
		11.3	13.64	7.22	8.16	8.72
		13.6	15.36	11.55	12.17	8.66
	Knee-Elbow	0.5	17.52	7.40	7.42	6.89
		2.3	12.83	6.75	6.64	7.14
		4.5	16.90	5.73	5.18	5.23
		6.8	15.37	7.76	7.51	7.38
		9.1	16.47	7.39	6.52	6.72
		11.3	18.70	8.03	8.46	7.13
		13.6	23.01	9.44	8.19	8.80

Table B4: Inter-subject CVs and intra-subject CVs of average angular velocities during the placement phase.

CV (%)	Height	Weight (kg)	Adduction Average Angular Velocity of Shoulder	Internal Rotation Average Angular Velocity of	Extension Average Angular Velocity of Shoulder	Extension Average Angular Velocity of Elbow
Inter	Floor-Elbow	0.5	35.58	14.36	10.55	13.40
		2.3	24.25	11.31	7.02	9.77
		4.5	25.65	12.42	9.43	11.24
		6.8	28.92	14.11	11.29	11.20
		9.1	21.33	14.04	9.55	9.13
		11.3	21.47	13.52	11.70	10.49
		13.6	25.91	17.62	15.54	14.19
	Floor-Knee	0.5	29.85	12.98	11.62	13.49
		2.3	54.25	14.09	10.38	20.91
		4.5	39.87	13.05	8.94	18.64
		6.8	26.05	14.16	11.45	16.49
		9.1	35.91	15.28	12.81	17.19
		11.3	34.37	15.65	9.33	16.52
		13.6	34.72	14.33	10.36	16.59
	Knee-Elbow	0.5	26.24	11.99	6.66	12.53
		2.3	22.37	11.80	10.71	10.91
		4.5	25.86	13.51	10.02	10.57
		6.8	25.17	14.61	12.34	12.47
		9.1	25.17	12.03	11.01	10.29
		11.3	26.78	19.58	15.56	12.53
		13.6	30.42	15.74	13.16	13.64
Intra	Floor-Elbow	0.5	14.76	10.31	10.22	9.48
		2.3	14.64	7.86	8.14	9.46
		4.5	14.30	7.81	7.45	7.17
		6.8	11.43	7.02	6.84	6.99
		9.1	17.75	6.27	6.28	6.80
		11.3	12.29	8.57	8.27	7.80
		13.6	13.40	8.09	7.80	9.00
	Floor-Knee	0.5	21.83	10.79	11.80	13.36
		2.3	32.44	9.35	9.26	11.55
		4.5	28.77	7.82	8.54	9.10
		6.8	15.05	6.70	6.53	9.28
		9.1	19.01	6.77	8.08	7.85
		11.3	29.54	7.66	7.87	9.37
		13.6	20.51	10.24	9.91	9.32
	Knee-Elbow	0.5	12.17	9.99	9.45	9.15
		2.3	14.78	7.77	7.82	7.07
		4.5	12.92	6.57	6.32	6.57
		6.8	13.18	6.51	6.02	6.92
		9.1	10.47	6.79	7.49	7.05
		11.3	9.63	7.87	9.24	8.80
		13.6	14.10	6.11	5.91	6.25